Melt-blowing of polymers for porous and functional air filters

by

Sahar Kalani

A thesis

presented to the University of Waterloo

in fulfillment of the

thesis requirement for the degree of

Master of Applied Science

in

Chemical Engineering

Waterloo, Ontario, Canada, 2024

© Sahar Kalani 2024

Author’s Declaration

I hereby declare that I am the sole author of this thesis. This is a true copy of the thesis, including any required final revisions, as accepted by my examiners.

I understand that my thesis may be made electronically available to the public.

Abstract

This thesis develops innovative, high-performance, melt-blown nonwoven materials for air filtration. The first chapter presents a two-step process to create nano-porous, compostable PLA nonwovens with high porosity for particulate capture. First, PLA is melt-blended with polyethylene glycol (PEG) of varying molecular weights to enhance melt flow index (MFI), producing blends with MFI values ranging from 56 g/10 min to 238 g/10 min. These blends are processed into microfibers, with diameters from 1.05 to 2.64 μm, using a twin-screw extruder. The second step involves boiling water etching to remove PEG and form nanopores (50–200 nm), achieving approximately 85% particulate capture efficiency for 0.3 μm NaCl particles. This eco-friendly method shows potential for air and water filtration and battery separators.

The second chapter addresses the limitations of conventional face masks, which lack antibacterial or antiviral properties. To improve mask functionality, advanced melt-blown filters are created using polypropylene (PP) and Rose bengal (RB), a photosensitizer. The study investigates the impact of processing temperature on fiber morphology, filtration efficiency, and antibacterial properties. The optimized filters show superior antibacterial performance, particulate filtration efficiency, and breathability, offering significant improvements for personal protective equipment (PPE), with enhanced antimicrobial protection and durability.

Acknowledgements

I would like to express my gratitude to Professor Tizazu Mekonnen for his support and mentorship. I also want to thank my husband, Dr. Reza Kohandani, for always being there with his love and support. My heartfelt thanks to my parents for their encouragement and sacrifices, helping me reach my goals. I also extend my appreciation to all my former teachers and mentors for believing in my potential.

Table of Contents

Author's Declaration ii

Abstract iii

Acknowledgements iv

List of Figures viii

List of Tables xii

List of Abbreviations xiii

Chapter 1 Introduction 1

1.1 Motivation 1

1.2 Research objectives 1

1.3 Thesis outlines 2

Chapter 2 Literature review 4

2.1 Introduction 4

2.2 Introducing and Analyzing Major Fabrication Techniques of Porous Nonwovens 9

2.2.1 Electrospinning 10

2.2.2 Solution Blowing 16

2.2.3 Melt-blowing 20

2.2.4 Comparative Analysis of the Fabrication Methods 23

2.2.5 Sustainability 27

2.3 Nonwovens as Air Filters 36

2.3.1 Properties of Melt-blown Nonwovens 37

2.3.2 Melt-blown Nonwovens as Air Filters 38

2.3.3 Melt-blowing Process 39
2.4 Case Study 50
2.4.1 Fabrication Method 50
2.4.2 Performance of Transparent Air Filters 51
2.4.3 Conclusion and Future Direction of the Case Study 53
2.5 Conclusion and Future Direction 55
Chapter 3 Nano-porous melt-blown poly (lactic acid) fiber mat air filters for high efficiency particulate capture 57
3.1 Introduction 58
3.2 Materials and processing methods 61
3.2.1 Materials 61
3.2.2 Melt blending and injection molding 61
3.2.3 Melt-blowing 62
3.2.4 Etching process 63
3.2.5 Characterizations 63
3.3 Results and Discussion 68
3.3.1 Compatibility analysis 68
3.3.2 Fourier transform infrared spectroscopy (FTIR) 69
3.3.3 Thermal properties 71
3.3.4 Physio-chemical properties 75
3.3.5 Fiber morphology 81
3.3.6 Air filtration performance and pressure drop 85

3.4 Conclusions 89

Chapter 4 Towards scalable antimicrobial air filters: rose bengal/polypropylene melt- blown nonwoven filters 90

4.1 Introduction 90

4.2 Materials and Processing methods 93

4.2.1 Materials 93

4.2.2 Melt-blown processing 93

4.2.3 Characterization 94

4.3 Results and discussion 100

4.3.1 Parallel Plate Rheology and Melt flow index (MFI) 100

4.3.2 FTIR-DSC 103

4.3.3 Fiber morphology 104

4.3.4 Mechanical properties 106

4.3.5 Air Filtration 107

4.3.6 Antibacterial properties 108

4.4 Conclusion 115

Chapter 5 Concluding Marks 116

References 119

Appendix A 158

Appendix B 159

List of Figures

Figure 2-1 Porous nonwovens using in surgical masks and HEPA filters for air filtration..... 6

Figure 2-2 Morphological comparison of three nonwoven fabrication methods at 50 micrometers scale bars with PVDF as the main substrate (a) solution blowing. Adapted from ref. [20] with permission from Journal of Applied Polymer. Copyright © 2005; (b) melt-blowing. Adapted from ref. [21] with permission from Sage Journals. Copyright © 2003; (c) electrospinning [22] 8

Figure 2-3 Sustainability and ecosystem benefits of PLA, a compostable corn-based polymer with environmentally friendly properties. 9

Figure 2-4 Electrospinning process for fabrication of nanofibers [37]..... 11

Figure 2-5 Solution blowing process schematic. Adapted from ref. [48] with permission from Springer Nature. Copyright © 2022..... 17

Figure 2-6 Schematic of the fiber attenuation after exiting the die in Melt-blowing process [72] 21

Figure 2-7 Contribution of marine and landfill compostable polymers, such as PHA, in surgical masks to reducing environmental pollution across marine and terrestrial ecosystem 30

Figure 2-8 Marine compostable PHA used in surgical masks, offering a sustainable solution to reduce marine pollution 31

Figure 3-1 ATR-FTIR Spectras of nonwovens; (a) PLA/PEG 400-10%, (b) PLA/PEG 2000-10%, (c) PLA/PEG 4000-10%, prior and after etching of PEG content..... 70

Figure 3-2 (a) GPC for the PLA L040 from Totalenergies corbion, (b) Before etching PEG DSC for the first heating cycle of PLA, PEG 400-5%, PEG 400-10%, PEG 2000-5%, PEG

2000-10%, PEG 4000-5%, PEG 4000-10% nonwoven samples, (c) After etching PEG. As well as (d) model fitting for the changes within the blends TG. 74
Figure 3-3 (a) TGA prior to etching PEG, (b) Derivative of weight loss prior etching PEG, (c) TGA after etching PEG, (d) Derivative of weight loss after etching PEG. 75
Figure 3-4 (a) MFI for PLA and the various PLA PEG blends, (b) Shear viscosity from capillary rheometry for PLA and the various PLA PEG blends, (c) Shear Stress from capillary rheometry for PLA and the various PLA PEG blends, and (d) Complex viscosity from dynamic rheometry for PLA and the various PLA PEG blends. 78
Figure 3-5 (a) Storage modulus curve (G'), from parallel plate, for PLA and its various PEG blends, (b) Loss modulus curve (G"), from parallel plate, for PLA and its various PEG blends, (c) Torque rheometer curves for PLA and its various PEG blends while melt blending, and (d) PLA blending schematic with PEG and different MW contents [262]. 79
Figure 3-6 SEM images and fiber distributions of non-etched samples (a) Pristine PLA; (b) PLA/PEG 400-5%; (c) PLA/PEG 400-10%; (d) PLA/PEG 2000-5%; (e) PLA/PEG 2000-10%; (f) PLA/PEG 4000-5%; (g) PLA/PEG 4000-10%. 82
Figure 3-7 Post-etching SEM images and fiber distributions of (a) PLA/PEG 400-5%, (b) PLA/PEG 400-10%, (c) PLA/PEG 2000-5%, (d) PLA/PEG 2000-10%, (e) PLA/PEG 4000-5%, and (g) PLA/PEG 4000-10%. 84
Figure 3-8 The effect of PEG etching process on PLA/PEG 400-10% fibers causing PEG removal from the substrate and resulting in creating nanopores within a single fiber strand. SEM image of PLA/PEG 400-10% (a) Perior etching off the PEG; (b) After etching the PEG. 85

Figure 3-9 Schematics of (a) bulk non-woven mats capturing microparticles, (b) porous non-woven mats capturing microparticles, (c) schematic representation of air filter testing system, (d) particle filtration efficiency of nonwoven mats, and (e) pressure drop. 87
Figure 3-10 Post etching SEM images and histograms of (a) PLA/PEG 400-10% (c) PLA/PEG 2000-10%. 88
Figure 4-1 Melt-blown nonwovens fabricated at different nozzle temperatures (a) Pristine PP at 210 °C, (b) PP/RB at 210 °C, (c) PP/RB at 220 °C, (d) PP/RB at 240 °C. 95
Figure 4-2 Parallel plate rheological analysis (a) complex viscosity as a function of frequency for Pristine PP and PP/RB (b) MFI of the Pristine PP and PP/RB 100
Figure 4-3 (a) TGA (b) DTGA of the PP and PP/RB nonwovens processed at 210°C, 220°C, 240°C 103
Figure 4-4 (a) FTIR and (b) DSC of the PP and PP/RB nonwovens 104
Figure 4-5 Analysis of fiber morphology and histograms of melt-blown nonwovens for (a) Pristine PP, (b) PP/RB@210°C, (c) PP/RB@220°C, (d) PP/RB@240°C..... 105
Figure 4-6 Mechanical properties of the PP and PP/RB@210, PP/RB@220, PP/RB@240 nonwovens (a) Tensile strength (b) Elongation at break (c) Elastic modulus 107
Figure 4-7 (a) Particulate filtration efficiency (b) pressure drop of PP, PP/RB@210°C, @220°C, @240°C nonwovens 108
Figure 4-8 Schematic illustrations of the mechanism of action of Rose Bengal (RB), a photosensitizer, for its antibacterial action under light. RB molecules get activated to their excited states under illumination by visible light or near-IR spectral region. The RB molecules

in their excited states (active) then work via two different types of mechanisms to kill the susceptible bacteria [312]. 110

Figure 4-9 Turbidity measurement of bacterial culture media withdrawn after 24 hours in cuvettes forecasting bacterial growth or cessation of growth due to treatment with samples i) PP, ii) PP/RB@210°C, iii) PP/RB@220°C and iv) ii) PP/RB@240°C for a) *Bacillus subtilis* (Gram-positive) and c) *Escherichia coli*. The data of OD-600 are plotted showing the growth trends for all the experimental nonwoven PP/RB samples on b) *B. subtilis* and d) *E. coli*. . 112

Figure 4-10 Bacterial colony growth tests in agar plates seeded from the bacterial culture media withdrawn from the elute collected after 24 h of contact with fresh diluted culture of each bacterium with the fabrics. The CFU counts on the agar plates (i—iv: PP, PP/RB@210°C, PP/RB@220°C, and PP/RB@240°C respectively) are shown indicating potential antibacterial activities of the RB-modified melt-blown fabrics in a) For Bacillus subtilis (Gram-positive), and in b) For Escherichia coli. c) The corresponding results from the CFU data are plotted showing the antibacterial efficacies for all the experimental fabric samples on both bacteria. 114

List of Tables

Table 2-1 Comparative summary of fiber fabrication methods for air filtration. 9

Table 2-2 Melt processable and Compostable Polymers 34

Table 2-3 Melt Processable and Antimicrobial Materials Incorporated into Fibers 43

Table 3-1 Formulation breakdown for the processed blends 62

Table 3-2 Solubility parameters and mixing enthalpies of PLA and PEG variants 69

Table 3-3 Thermal properties of PLA and the PLA+PEG blends obtained from DSC. 72

Table 3-4 Calculated K and n values for PLA and its PEG blends at 190 °C. 80

Table 4-1 Melt-blown process parameters for the fabrication of PP/RB nonwovens. 94

List of Abbreviations

AGS X	Shimadzu AGS X Series Universal Testing Machine
ASTM	American Society for Testing and Materials
ATR FTIR	Attenuated Total Reflectance Fourier Transform Infrared Spectroscopy
B subtilis	Bacillus subtilis (Gram-positive bacterium)
BSC	Biosafety Cabinet
C H	Carbon-Hydrogen
C=C	Carbon-Carbon Double Bond
°C	Celsius
CFU	Colony Forming Unit (a measure of viable bacterial cells)
DI	Deionized
DMF	Dimethylformamide
dp	Pressure Drop
DSC	Differential Scanning Calorimetry
E coli	Escherichia coli (Gram-negative bacterium)
EELS	Electron Energy Loss Spectroscopy
FESEM	Field Emission Scanning Electron Microscopy
FDA	U.S. Food and Drug Administration
FTIR	Fourier Transform Infrared Spectroscopy
G’	Storage Modulus
G”	Loss Modulus

g/10 min	Grams per 10 Minutes
GPC	Gel Permeation Chromatography
HF	Heat of Fusion
HVAC	Heating Ventilation and Air Conditioning
Hz	Hertz (unit of frequency)
K	Consistency of the Polymer Melt
L min	Liters per minute
LB	Lysogeny Broth
log τ	Logarithmic Shear Stress
log γ	Logarithmic Shear Rate
MFI	Melt Flow Index
min	Minutes
Mn	Number-Average Molecular Weight
MPPS	Most Penetrating Particle Size (refers to the particle size that the filter is least efficient at capturing)
MW	Molecular Weight
NaCl	Sodium chloride
N95	A standard for respiratory protective devices
n	Non-Newtonian Index
NI	National Instruments
OD	Optical Density

OM	Optical Microscopy
PAN	Polyacrylonitrile
PBA	Polybutyrate Adipate
PBAT	Polybutylene Adipate Terephthalate
PBS	Phosphate-Buffered Saline
PBS	Polybutylene Succinate
PCL	Polycaprolactone
PE	Polyethylene
PEG	Polyethylene glycol
PFE	Particulate Filtration Efficiency
PHAs	Polyhydroxyalkanoates
PHB	Polyhydroxybutyrate
PHBV	Polyhydroxybutyrate-co-Valerate
PLA	Poly(lactic acid)
PM	Particulate Matter
PM0.1	Ultrafine Particulate Matter
PM2.5	Fine Particulate Matter
PPE	Personal Protective Equipment
PP	Polypropylene
PS	Photosensitizer
PS	Polystyrene

PVA	Polyvinyl Alcohol
PVP	Polyvinylpyrrolidone
Q	Figure of Merit
RB	Rose Bengal
Rheomix	Torque Mixer (HAAKE PolyLab QC)
RHEO	Rheometer
ROS	Reactive Oxygen Species
RPM	Revolutions per minute
RT	Room Temperature
SCFM	Standard Cubic Feet per Minute
SDG	Sustainable Development Goals
SEM	Scanning Electron Microscopy
SMS	Spunbond Meltblown Spunbond (a nonwoven structure)
SMPs	Shape Memory Polymers
TCC	Cold Crystallization Temperature
TEM	Transmission Electron Microscopy
TENGs	Triboelectric Nanogenerators
TG	Glass Transition Temperature
TGA	Thermogravimetric Analysis
TM	Melting Temperature
UTM	Universal Testing Machine

UV	Ultraviolet
VOC	Volatile Organic Compounds
wMW	Weight Average Molecular Weight
XPS	X-ray Photoelectron Spectroscopy
µm	Micrometer
µm	Micrometer
UN	United Nations

Chapter 1
Introduction

1.1 Motivation

The COVID-19 pandemic has highlighted critical public health challenges, from widespread morbidity and mortality to the heightened demand for effective personal protective equipment (PPE). Concurrently, air pollution and the transmission of airborne pathogens continue to pose significant threats, particularly in high-risk settings such as hospitals, public spaces, and industrial environments. Conventional air filtration systems, though generally effective at capturing particulate matter, often fall short in neutralizing harmful microorganisms like bacteria and viruses and sometimes struggle with inadequate particle filtration. These shortcomings have driven the demand for high-performance, multifunctional filters.

Filters with enhanced porosity offer superior particulate capture and airflow efficiency, addressing key limitations of traditional systems. When combined with antimicrobial agents, such as Rose Bengal (RB), these advanced filters gain the ability to deactivate pathogens, significantly improving their functionality. This work focuses on developing next-generation filtration systems by integrating innovative material designs and fabrication techniques to achieve high porosity and robust antimicrobial performance, meeting the demands of modern public health and environmental challenges.

1.2 Research objectives

The primary objective of this thesis is to develop and characterize advanced air filtration systems. The first study focuses on the development of porous nonwoven mats made from PLA and PEG. By incorporating PEG of varying molecular weights into PLA through melt blending

and melt-blowing, this research aims to investigate how the PEG component influences the structural and functional properties of the filters. The porous structure, achieved through a water-etching process that removes the sacrificial PEG, is evaluated for its potential in air filtration.

The second study explores the integration of Rose Bengal, a well-known photosensitizer, into PP nonwoven fibers to create antimicrobial air filters. By optimizing fabrication conditions, such as processing temperature and fiber morphology, the research aims to ensure uniform RB incorporation without compromising the filter's structural integrity. The antimicrobial properties of these filters are evaluated in conjunction with their particulate filtration efficiency, providing insights into their performance and potential applications in environments with high biological risks.

1.3 Thesis outlines

The structure of this thesis is organized as follows: Chapter 2 provides a comprehensive overview of porous structures for air filtration applications, with a focus on their fabrication methods and sustainability. It highlights melt-blowing as an effective technique for producing nonwovens, which are crucial for air filter applications, and explores their environmental impact and potential for sustainable solutions. Chapter 3 explores the design and fabrication of highly porous, compostable networks for use in air filtration. It focuses on the porous network properties, fabrication phases, and performance characteristics that make these networks suitable for advanced air filtrations. Chapter 4 presents a research study on production methods for antibacterial melt-blown nonwovens. The focus is on optimizing the production process for

large-scale manufacturing while maintaining high filtration efficiency and antimicrobial properties, ensuring their effectiveness in medical and high-risk environments.

Chapter 2
Literature review

2.1 Introduction

Filters with high filtration efficiency are crucial because they can capture a greater percentage of harmful particles, such as dust, pollen, bacteria, and viruses, from the air [1]. This is especially important in protecting human health, reducing the spread of airborne diseases, and maintaining cleaner air in sensitive environments like hospitals and cleanrooms [2]. High particulate filtration efficiency (PFE) filters effectively capture harmful particulate matter (PM), including fine particles (PM2.5) and ultrafine particles (PM0.1), which are known to cause respiratory issues and other health problems [1]. High filtration efficiency also contributes to better indoor air quality, which is essential for respiratory health, particularly for people with allergies or asthma [1]. Furthermore, these filters are vital in industrial and environmental applications where strict air purity standards must be met to ensure safety and compliance [1]. Several factors influence the filtration efficiency of air filters, including the fiber diameter, pore size, and material composition [2]. Finer fibers and smaller pores typically result in higher filtration efficiency, as they create a more surface area for particles to pass through [2]. However, increasing the efficiency often comes at the cost of increased airflow resistance [3], which can negatively affect energy consumption [4].

In real-world applications, such as High-Efficiency Particulate Air (HEPA) filters used in air purifiers and N95 masks, achieving a balance between high efficiency and acceptable airflow is crucial [5]. These filters are designed to capture particles as small as 0.3 microns, ensuring

protection against harmful pollutants and pathogens [5]. Energy consumption is a major consideration in air filtration systems, particularly in large-scale applications such as heating, ventilation, and air conditioning (HVAC) systems in buildings or industrial filtration setups [5]. As air passes through a filter, resistance to the airflow, known as pressure drop, causes the system to work harder, leading to higher energy consumption [5]. Increased pressure drop across air filters necessitates higher fan power consumption as the fan works harder to sustain the desired airflow, leading to higher overall energy consumption and diminished system efficiency [5]. Achieving a balance between filtration efficiency and pressure drop is crucial for optimizing filter performance. While nanofiber filters typically exhibit higher pressure drops due to their finer fiber diameters [6], they often achieve an improved figure of merit (Q), which considers both efficiency and pressure drop [5]. This makes them an effective choice for applications where the trade-off between pressure drop and filtration efficiency needs to be carefully managed. Techniques such as pleating or folding the filter material, as seen in HEPA filters [7], help reduce resistance, which lowers pressure drop and minimizes the energy demand [5].

In addition to removing airborne particles, high-performance air filters are increasingly being designed to have antibacterial and antimicrobial properties [8]. This is especially important in healthcare settings, public spaces, and other environments where the spread of bacteria and viruses poses a significant risk. Antibacterial filters can inhibit the growth of microorganisms on their surface, ensuring that they do not become breeding grounds for harmful pathogens. Several methods can be used to enhance the antibacterial properties of air filters. One common

technique is to incorporate antimicrobial agents, such as silver nanoparticles or copper ions, into the filter material [9]. These agents actively kill or inhibit the growth of bacteria and viruses on the filter's surface. Another approach is to modify the filter surface using plasma treatment or coating it with bioactive compounds that provide long-lasting antibacterial effects [10]. Recent advancements in air filtration technology have also introduced self-cleaning filters that are capable of killing bacteria and viruses without the need for external cleaning [11]. Such innovations are particularly valuable in settings where frequent filter replacement is impractical. Porous nonwoven materials or porous fibers are a proper choice for high-performance air filters **(Figure 2-1)** due to their ability to trap particles while maintaining airflow [12].

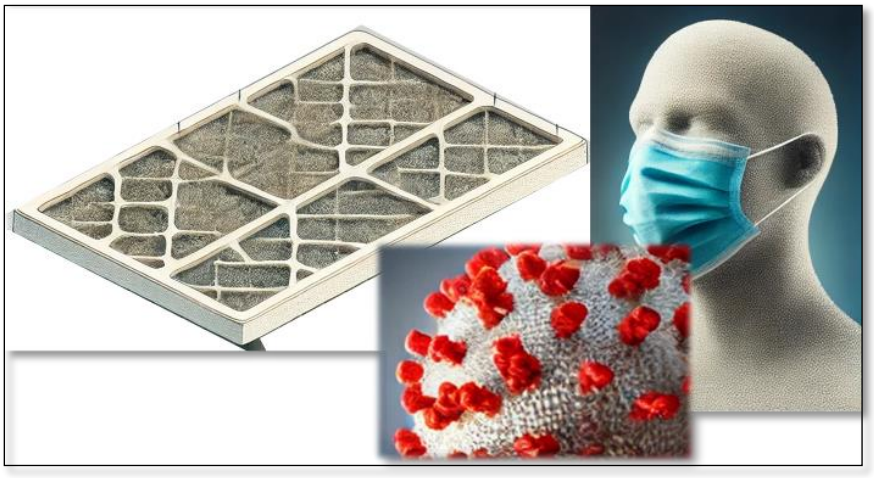


Figure 2-1 Porous nonwovens using in surgical masks and HEPA filters for air filtration. Generated through OpenAI's ChatGPT platform [13].

Three common methods for fabricating these materials are electrospinning, solution blowing and melt blowing, each with distinct advantages and limitations. Electrospinning is a process

that uses an electrical charge to draw ultrafine fibers from a liquid polymer solution. These fibers, typically in the nanometer range, form a nonwoven mat with a high surface area and very fine pore structure [14]. The key advantage of electrospinning is its ability to produce exceptionally fine fibers making it ideal for applications where high filtration efficiency is required. However, electrospinning is relatively slow and costly, limiting its scalability for large-scale production [15].

Solution blow spinning is another method used to fabricate porous materials, in which a polymer solution is extruded through a nozzle and blown by a high-velocity gas stream, resulting in fiber formation [16, 17]. Solution blowing can produce fibers with diameters comparable to those achieved by electrospinning but with greater scalability and without the need for high-voltage equipment. This method also allows a broader range of polymer solutions to be used, including those that are not suitable for melt blowing due to their high melting temperatures. Compared to electrospinning, solution blowing is more versatile and cost-effective, while still capable of producing fine fibers, making it suitable for a variety of filtration and biomedical applications [18]. However, the use of solvents in this process may present environmental and safety concerns, depending on the type of solvent required for the polymer solution [18].

Melt blowing on the other hand, is a process where molten polymer is extruded through small nozzles and blown by high-speed air jets to form fibers. Melt-blown fibers are generally larger than electrospun fibers, but the process is much faster and more scalable. Melt-blown materials are widely used in commercial applications, including N95 masks and industrial filters, due to

their cost-effectiveness and rapid production capability [19]. However, melt-blown filters may have less control over fiber size and pore structure compared to electrospun filters. The SEM images in **Figure 2-2 (a-c)** reveal visual differences in pore and fiber size uniformity, and also fiber density across the morphological scales of the three nonwoven samples produced by the three different fabrication methods including solution blowing, melt blowing and electrospinning respectively. The fiber size and pore size variations impact the performance characteristics of each sample, influencing factors like filtration efficiency and airflow resistance [20]. **Table 2-1** also shows a comparative analysis of the three fiber fabrication methods.

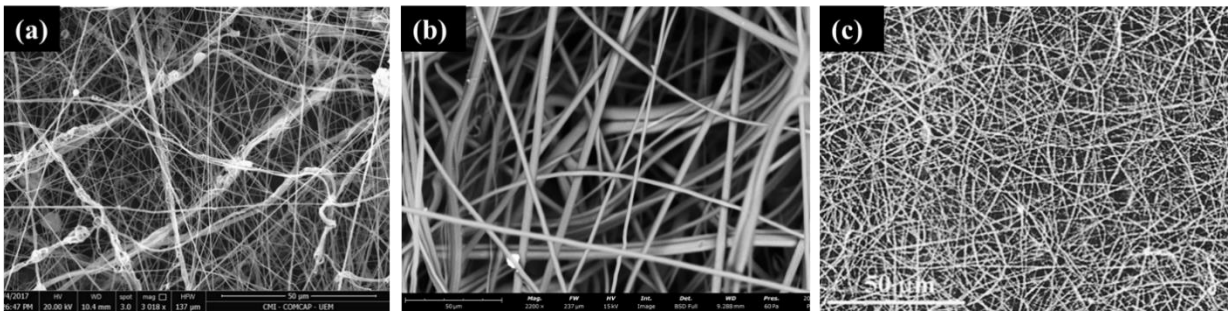


Figure 2-2 Morphological comparison of three nonwoven fabrication methods at 50 micrometers scale bars with PVDF as the main substrate (a) solution blowing. Adapted from ref. [21] with permission from Journal of Applied Polymer. Copyright © 2005; (b) melt-blowing. Adapted from ref. [22] with permission from Sage Journals. Copyright © 2003; (c) electrospinning [23]

Traditional filter materials, such as polypropylene (PP), are derived from fossil fuels and contribute to plastic waste [24]. In response, researchers and manufacturers are exploring

biodegradable and compostable alternatives, such as filters made from polylactic acid (PLA) **(Figure 2-3)**, a biopolymer derived from corn starch [25].

Table 2-1 Comparative summary of fiber fabrication methods for air filtration.

Fabrication Method	Fiber Diameter (nm)	Production Rate	Cost Efficiency	Environmental Impact	Applications
Electrospinning [26, 27]	100-500	Low	High	Moderate-toxic solvents	N95 masks, HEPA filters, advanced filtration
Solution Blowing [28]	200-1000	Medium	Moderate	Dependent on solvent	Biomedical, filtration, industrial filters
Melt-blowing [29, 30]	500-2000	High	Low	Low	Industrial filters, masks (N95), HVAC



Figure 2-3 Sustainability and ecosystem benefits of PLA, a compostable corn-based polymer with environmentally friendly properties. Generated through OpenAI's ChatGPT platform [13].

2.2 Introducing and Analyzing Major Fabrication Techniques of Porous Nonwovens

The production of micro- and nanofibers has garnered significant attention in recent years due to their porosity and exceptional properties and diverse applications in fields such as filtration,

biomedical engineering, and advanced materials [31–33]. In this section, common fabrication methods of porous nonwoven is explained in details.

2.2.1 Electrospinning

Electrospinning is a prominent technique for producing nanofibers, known for its capacity to create fibers with diameters ranging from a few nanometers to several micrometers [34]. The process involves applying a high-voltage electric field to a polymer solution, resulting in the formation of ultra-fine fibers [35]. Electrospinning is known for its ability to produce highly uniform nanofibers, and it allows for precise control over fiber diameter and morphology [36]. Despite being limited by a narrow range of compatible polymers, this method is highly adaptable for creating nanostructures suited for specialized applications, including biomedical, tissue engineering, scaffolds, and sensors [37].

2.2.1.1 Process Overview

The electrospinning process begins with the preparation of a polymer solution, which is typically dissolved in a suitable solvent. The solution is then loaded into a syringe equipped with a needle. Upon applying a high voltage between the needle and a collector [34], an electrostatic charge is induced at the tip of the needle, leading to the formation of a Taylor cone. As the electric field increases, the repulsive forces overcome the surface tension of the polymer solution, causing a continuous jet of polymer to be ejected from the cone. As the polymer jet travels toward the collector, it undergoes elongation and solvent evaporation, resulting in the formation of fine fibers [38]. The collector can take various forms, such as a flat plate or rotating drum, to influence the fiber orientation and morphology **(Figure 2-4)**. The

key parameters affecting fiber formation include voltage, flow rate, distance between the needle and collector, and environmental conditions like humidity and temperature [39, 40].

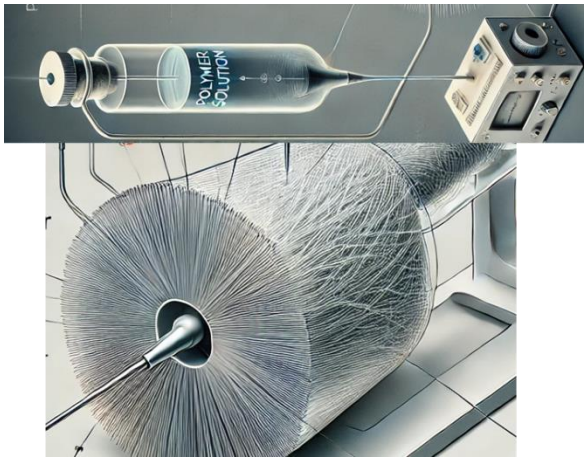


Figure 2-4 Electrospinning process for fabrication of nanofibers [38]. Generated through OpenAI's ChatGPT platform [13].

2.2.1.2 Advantages of Electrospinning

One of the primary advantages of electrospinning is its ability to produce fibers with high surface area-to-volume ratios, which enhances their performance in applications such as filtration, tissue engineering, and drug delivery [40]. Additionally, the technique allows for the incorporation of various additives, such as nanoparticles or bioactive agents, enabling the fabrication of multifunctional fibers tailored for specific applications [41, 42]. Moreover, electrospinning offers exceptional control over fiber diameter and morphology by adjusting processing parameters, facilitating the design of materials with desired characteristics. This flexibility makes electrospinning an attractive option for researchers seeking to develop advanced materials for cutting-edge applications [36].

2.2.1.3 Challenges and Limitations

Despite its advantages, electrospinning faces several challenges that hinder its widespread industrial adoption. The technique is often limited by low production throughput, which can be attributed to the continuous nature of the electrospinning process and the time required for solvent evaporation. Furthermore, the use of toxic solvents poses safety and environmental concerns, necessitating the exploration of greener alternatives [43]. Additionally, while electrospun fibers exhibit unique properties, they may suffer from issues related to uniformity and reproducibility. The influence of environmental factors, such as humidity and temperature, can significantly impact fiber morphology, complicating the scaling-up process [44].

2.2.1.4 Recent Developments and Modifications in Electrospinning

Recent advancements in electrospinning technology have focused on enhancing fiber production efficiency, improving material properties, and expanding the range of applications. In the following, various modifications to the traditional electrospinning setup and process have been explored to address the limitations of conventional methods and capitalize on the unique advantages of electrospun fibers.

Nanofiber Hybridization and Composite Materials

Recent studies have emphasized the development of hybrid and composite nanofibers by incorporating nanoparticles, graphene, or carbon nanotubes into the polymer matrix during the electrospinning process. Zhang et al. reported the successful incorporation of silver nanoparticles into polyvinyl alcohol (PVA) fibers, resulting in enhanced antibacterial properties and mechanical strength [45]. This approach not only enhances the mechanical

properties and conductivity of the fibers but also imparts additional functionalities, such as electromagnetic interference shielding. Composite electrospun fibers have shown promising results in applications spanning electronics, biomedical engineering, and environmental remediation, demonstrating the versatility of modified electrospun materials [46].

Co-electrospinning Techniques

Co-electrospinning has emerged as a promising modification, allowing for the simultaneous spinning of two or more polymer solutions. This technique facilitates the creation of core-shell or segmented fibers, enabling the encapsulation of active agents within the fiber core while maintaining a protective outer layer [47]. Researchers developed core-shell fibers using polycaprolactone (PCL) as the shell and an antibacterial agent as the core [48], achieving controlled release of the active agent. Such structures can enhance drug delivery systems, improve stability, and enable the controlled release of bioactive substances, making them ideal for various medical applications.

Solvent-Free and Green Electrospinning

In response to environmental concerns associated with toxic solvents, recent developments in electrospinning have shifted towards solvent-free and green electrospinning techniques [49]. Innovations such as melt electrospinning and electrospinning from water-based or biodegradable solvents are gaining traction. Scientists demonstrated the feasibility of melt electrospinning using PLA without the use of organic solvents, resulting in fibrous mats with desirable mechanical properties [50]. These methods not only reduce the environmental

footprint but also simplify the fiber production process, making it more sustainable and safer for industrial applications.

Process Optimization and Real-Time Monitoring

Advancements in process optimization have led to the development of automated electrospinning systems equipped with real-time monitoring capabilities. Researchers employed a feedback control system that adjusted voltage and flow rate in real time, improving fiber uniformity and production rates. This literature [51] has highlighted the use of machine learning algorithms to predict and optimize fiber characteristics based on processing parameters. It presents a closed-loop control system for electrospinning, integrating a high-speed camera, NI image processor, controller, signal amplifier, and high-voltage supplier. Using model predictive control, it regulates fiber diameter under disturbances, ensuring stability and consistency. The system improves the precision of micro electrical components and supports manufacturing complex structures like island-bridge microstructures for sensors and tissue engineering [51].

Electrospinning for 3D Structures

Recent explorations into 3D electrospinning techniques have expanded the versatility of electrospun fibers in creating complex structures. By modifying collector geometries and utilizing techniques such as multi-jet or rotary electrospinning, researchers can fabricate three-dimensional fibrous scaffolds with controlled architectures. A study by Liu et al. [52] demonstrated the creation of 3D fibrous scaffolds for tissue engineering, which significantly improved cell adhesion and proliferation compared to traditional 2D scaffolds. These 3D

structures are particularly advantageous in tissue engineering and regenerative medicine, providing a conducive environment for cell growth and differentiation.

Integration with other Fabrication Techniques

Integrating electrospinning with other fabrication techniques, such as additive manufacturing or surface modification processes, has been used for creating multifunctional materials [53]. Recent studies have reported the successful combination of electrospinning and 3D printing to produce composite scaffolds that leverage the unique properties of both techniques. Researchers integrated electrospun fibers into 3D-printed structures to enhance mechanical strength and bioactivity, resulting in materials suitable for bone tissue engineering. This hybrid approach enables the combination of the unique properties of electrospun fibers with the precision of other manufacturing techniques, allowing for the design of materials with enhanced functionalities tailored for specific applications [54].

Advances in Scalability and Production Techniques

To improve scalability, one promising approach is the use of multi-spinneret systems, which allow for parallel spinning of multiple fibers simultaneously [55]. Researchers demonstrated a multi-spinneret electrospinning system that achieved an output of over 500 grams per hour, showcasing the potential for high-volume production [56].

Additionally, the introduction of rotary electrospinning has gained traction as a scalable alternative to traditional electrospinning. This technique involves the use of a rotating drum as the collector, allowing for continuous fiber collection and increased production rates [57].

Moreover, researchers have explored the use of continuous-flow electrospinning systems, which enable uninterrupted fiber production by employing a feed mechanism that continuously supplies polymer solution to the spinning apparatus [58]. This approach has been shown to enhance production efficiency and reduce downtime associated with conventional batch processes.

Recent developments are broadening the scope of electrospun materials, making them increasingly relevant across various industries, including biomedical, environmental, and energy sectors. Electrospinning remains a powerful method for producing micro- and nanofibers with diverse applications, offering notable advantages in fiber properties and customization. However, challenges related to scalability and environmental impact persist, prompting continued research toward optimizing this technique and exploring complementary methods [59].

2.2.2 Solution Blowing

2.2.2.1 Process Overview

Solution blowing is an innovative fiber production technique that leverages the principles of air flow to create fine polymer fibers. The process begins with dissolving a polymer in a suitable solvent to form a viscous solution. This solution is then extruded through a spinneret, where a high-velocity air stream is applied to the emerging filament. The air stream helps in rapidly evaporating the solvent, stretching the polymer, and forming continuous fibers **(Figure 2-5)**. The resulting fibers can vary in diameter, typically from nanometers to micrometers, depending on the specific parameters of the solution and process. The flexibility of solution

blowing allows for precise control over fiber characteristics. Factors such as polymer concentration, solution viscosity, air temperature, and pressure can be manipulated to achieve desired fiber morphologies [60].

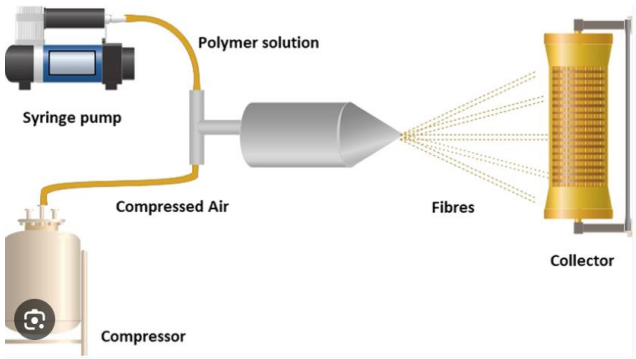


Figure 2-5 Solution blowing process schematic. Adapted from ref. [48] with permission from Springer Nature. Copyright © 2022.

2.2.2.2 Recent Developments and Modifications

Recent advancements in solution blowing technology have significantly enhanced its versatility and effectiveness in producing high-performance fibers. One notable area of development is the incorporation of bio-based additives into the polymer matrix. Research by Zhang et al. highlighted the use of cellulose nanocrystals as reinforcing agents in PLA fibers [61]. The study found that the addition of cellulose nanocrystals improved both the tensile strength and thermal stability of the resulting fibers, demonstrating that hybrid materials can enhance performance while promoting sustainability. Moreover, the optimization of process parameters has been a critical focus in recent research. Lee et al. [62] conducted a systematic investigation into how various conditions, such as air pressure and temperature, influence fiber formation. Their findings revealed that optimizing the solvent evaporation rate is crucial for

producing uniform nanofibers. This research underscores the importance of fine-tuning process parameters to achieve consistent fiber characteristics, which is vital for industrial applications. The exploration of hybrid techniques has also gained momentum, where solution blowing is combined with other fiber production methods. Liu et al. [63] introduced a novel approach that integrates solution blowing with electrospinning to create core-shell fibers. This method allows for the encapsulation of bioactive agents within a protective polymer shell, enhancing the functionality of the fibers. Such hybrid materials are particularly useful in biomedical applications, where controlled release and protective properties are desired. Environmental considerations have prompted researchers to explore the use of alternative, eco-friendly solvents in the solution blowing process. Researchers investigated the feasibility of using biodegradable solvents for solution blowing. This study [64] explores solution blow spinning for producing PCL fibers, focusing on reducing solvent toxicity for green and biomedical applications. Traditional chlorinated solvents such as chloroform, are replaced with less toxic alternatives: acetic acid, acetone, and their mixtures. Results show that acetone alone does not degrade PCL but cannot produce fibers independently, while acetic acid degrades PCL chains. The acetic acid/acetone mixture effectively produces PCL fibers, with the solvent ratio influencing fiber morphology and orientation. This green solvent system offers tailored fiber production for specific applications, advancing environmentally friendly solution blow spinning techniques. The results indicated that fibers produced with these solvents maintained desirable mechanical properties while significantly reducing the environmental impact associated with traditional organic solvents. Recent innovations have also focused on improving the scalability of solution blowing by developing new configurations and equipment

to enhance fiber production rates. [65]. For example, advancements in multi-nozzle setups enable simultaneous processing of multiple fibers, effectively increasing throughput [66].

2.2.2.3 Advantages and Disadvantages

Solution blowing presents several advantages that make it a compelling choice for fiber production. The ability to produce fibers with precise control over diameter and morphology allows for tailored material properties suitable for various applications. The process is generally more scalable than electrospinning, which has traditionally faced challenges in scaling up for industrial production. Additionally, solution blowing can utilize a wide range of polymer materials, including biodegradable options, providing versatility in material selection.

However, the process poses challenges, particularly due to the use of organic solvents, which raise significant environmental and health concerns. Although advancements are being made towards using green solvents, the need for proper handling and disposal of solvents remains a consideration [67]. Furthermore, achieving consistent fiber quality can be difficult, as minor variations in process parameters can lead to significant differences in fiber morphology. This necessitates careful monitoring and optimization during production.

2.2.2.4 Applications

In the biomedical field, solution-blown fibers have emerged as promising materials for various applications, including wound dressings and drug delivery systems [68]. The tunable properties of these fibers allow for customized designs that can enhance healing and therapeutic effects. For instance, research has demonstrated the successful use of solution-blown scaffolds [69] in tissue engineering, where their porous structure promotes cell adhesion and proliferation. This

study prepares a nylon 6 nanofibrous membrane using solution blowing and hot-pressing for nanofiltration applications. Hot-pressing parameters and areal densities were optimized, enhancing fiber morphology and membrane strength.

2.2.3 Melt-blowing

2.2.3.1 Process Overview

Melt blowing is a fiber production technique widely recognized for its efficiency in generating micro- and nanofibers. The process involves extruding molten polymer through nozzle with fine holes, where a high-velocity hot air stream rapidly cools and stretches the extruded fibers. This results in the formation of fine fibers that can be collected as a nonwoven fabric **(Figure 2-6)**. Melt-blown fibers typically exhibit diameters ranging from 1 to 10 micrometers, providing unique properties such as high surface area, low density, and excellent filtration capabilities [70]. The melt blowing process can accommodate various thermoplastic polymers, including PP, polyethylene (PE), and bio-based polymers, making it versatile for different applications [71]. The control of process parameters such as polymer flow rate, air temperature, and die configuration allows to produce fibers with tailored characteristics, suitable for diverse industries.

2.2.3.2 Recent Developments and Modifications

Researchers developed compostable nonwovens using PLA and its blends, achieving desirable mechanical properties while maintaining biodegradability. The fibers produced demonstrated significant potential for applications in packaging and hygiene products, highlighting an environmentally friendly alternative to traditional plastics [72].

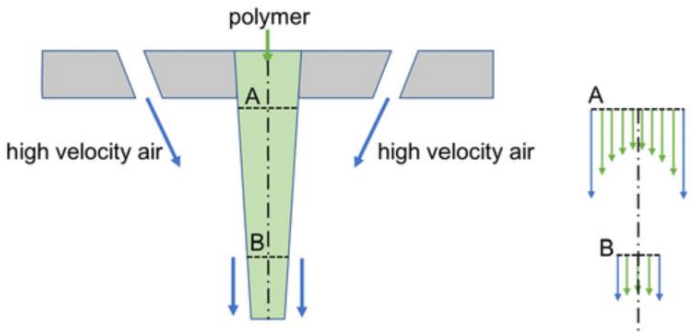


Figure 2-6 Schematic of the fiber attenuation after exiting the die in Melt-blowing process [73]

In addition to sustainability, the incorporation of antibacterial and antimicrobial agents into melt-blown fibers has garnered attention for applications in medical and protective textiles. Recent work by scientists investigated the addition of silver nanoparticles to melt-blown PP fibers, demonstrating effective antibacterial activity against common pathogens [42]. This modification enhances the utility of melt-blown nonwovens in medical applications, such as surgical masks and gowns, where hygiene is paramount. Moreover, the exploration of melt-blown scaffolds for biomedical applications has shown promising results. There is a recent study focused on creating three-dimensional (3D) melt-blown scaffolds from PCL for tissue engineering [74]. The scaffolds exhibited favorable biocompatibility and mechanical properties, making them suitable for cell culture and tissue regeneration applications. The automotive and textile industries are also leveraging the advantages of melt-blown technology. In automotive applications, melt-blown nonwovens are utilized for sound absorption and thermal insulation. Researchers demonstrated that melt-blown PP nonwovens could effectively reduce cabin noise while providing lightweight insulation, making them an attractive option

for automotive manufacturers seeking to enhance vehicle comfort and performance [75]. In the textile and fashion sectors, melt-blown fibers are increasingly incorporated into functional textiles that offer properties such as water repellency and breathability. Research on fabrics explored the use of melt-blown fibers in developing lightweight, breathable, and water-resistant textiles for activewear [76].

2.2.3.3 Advantages and Disadvantages

Melt blowing offers several advantages; the process is highly scalable, enabling the production of large quantities of fibers with relative ease [77]. The ability to use various thermoplastic polymers expands its application range, and the resulting fibers possess excellent filtration capabilities, making them ideal for hygiene products and filtration media. One significant limitation is the dependency on polymer characteristics and processing conditions, such as melt flow index, which can affect the uniformity and quality of the fibers [78]. Additionally, while melt-blown nonwovens exhibit desirable properties for many applications, their mechanical strength may not always match that of other fiber production methods, such as spun bonding [79]. The versatility of melt-blown fibers has led to their widespread use in numerous applications across various industries [80]. Melt-blown nonwovens are critical in producing personal protective equipment (PPE), such as face masks and gowns. Studies have shown that melt-blown fibers treated with silver nanoparticles demonstrate effective bacterial filtration efficiency, making them suitable for medical and surgical applications [81].

In the realm of filtration, melt-blown nonwovens serve as a primary component of HEPA filters used in various air purification applications. Their fine fiber structure allows for efficient

filtration of airborne particles [6]. Additionally, melt-blown layers in face masks significantly enhance their filtration capabilities, providing effective protection against airborne viruses and pollutants. Melt-blown nonwovens are also utilized in HVAC systems as filter media to capture airborne contaminants. Their high surface area and low resistance to airflow make them ideal for maintaining efficient air circulation while improving indoor air quality [82].

With growing concerns over plastic waste, melt-blown technology has been explored for developing compostable nonwovens. These materials can replace traditional plastics in packaging and hygiene products, contributing to sustainability goals and reducing environmental impact. Melt-blown nonwovens with fine fibers are widely recognized for their exceptional filtration capabilities, commonly used in air and liquid filtration applications [83], including HVAC systems, air purifiers, and water treatment filters.

2.2.4 Comparative Analysis of the Fabrication Methods

The choice of fiber production method significantly influences the functionality and application of the finished products. This analysis evaluates electrospinning, solution blowing, and melt blowing techniques across several critical factors: functionality of finished products, porosity of nonwovens, production rate, ease of processing, and material versatility.

2.2.4.1 Functionality of Finished Products

The functionality of finished products produced through these fiber fabrication techniques varies greatly. Electrospun fibers typically exhibit unique surface characteristics, high surface area-to-volume ratios, and finer diameters compared to fibers produced by other methods. These attributes enhance their performance in applications such as drug delivery systems,

where the release rate of therapeutic agents can be finely controlled. Kharaghani et al. demonstrated that electrospun PCL fibers loaded with curcumin exhibited a sustained release profile, showing significant potential for biomedical applications [84]. Similarly, Zhang et al. highlighted the use of electrospun nanofibers as scaffolds for tissue engineering, where their high porosity and surface area facilitate cell attachment and proliferation [85].

In contrast, melt-blown and solution-blown fibers are characterized by their bulkier structures, which lend themselves to applications where higher filtration efficiencies and durability are required, such as in PPE and industrial filters [86].

Furthermore, solution-blown fibers have gained traction in various sectors due to their unique properties. A recent study explored the potential of solution-blown nanofibers for use in energy storage applications, highlighting how their fine structures could enhance ionic conductivity and charge transfer rates [87]. This versatility emphasizes the critical role that each production method plays in defining the end-use functionality of nonwoven products.

2.2.4.2 Porosity

Porosity is a critical parameter that affects the performance of high functional nonwovens in various applications [88]. Electrospinning can achieve a high degree of porosity due to the extremely fine fibers produced, which enables the formation of interconnected voids and enhances permeability while maintaining structural integrity. Researchers reported that electrospun nanofibers with high porosity facilitated effective moisture wicking [89] and oxygen transport in wound dressings [90], making them highly effective for managing exudate in clinical settings. Melt-blown fibers typically exhibit lower porosity than electrospun fibers;

however, they possess a higher bulk density. Researchers demonstrated that by optimizing the air temperature and polymer feed rate in the melt blowing process, the porosity could be increased, leading to improved filtration performance in HVAC applications. Solution blowing offers a middle ground between electrospinning and melt blowing, producing fibers with customizable porosity levels that can be adjusted based on polymer concentration and solvent evaporation rate [91].

2.2.4.3 Production Rate

Production rate is a crucial factor influencing the industrial applicability of these fiber fabrication methods. Melt blowing is recognized for its high throughput capabilities, allowing for the rapid production of large volumes of nonwoven materials. The melt blowing process can produce meters of fabric per minute, making it ideal for applications requiring bulk quantities, such as hygiene products and industrial filters. Advances in melt blowing technology, such as the development of nozzles with customizable holes numbers have further enhanced production efficiency, enabling manufacturers to meet the increasing demand for nonwoven materials [92]. In comparison, electrospinning is limited by its relatively low production rate, often constrained by the need for precise control over fiber morphology. Recent research suggests that while traditional electrospinning setups yield fibers at rates suitable for niche applications, innovations like rotational electrospinning have shown promise in increasing throughput, potentially transforming the scalability of the technique for industrial use [93]. Solution blowing offers a balance between production rate and fiber quality, typically achieving higher throughput than electrospinning while still producing fibers with desirable

properties. However, the production rate may not reach the levels of melt blowing, making it a suitable option for applications where moderate quantities and specific fiber characteristics are required [94]. The dual capability of producing both fibers and films through solution blowing further broadens its applicability [95].

2.2.4.4 Ease of Processing

Melt blowing is often regarded as user-friendly, with straightforward equipment requirements and operational procedures. The process can accommodate a range of thermoplastic polymers without significant modifications, allowing for efficient scaling up from lab to production levels. The straightforward nature of the melt blowing process, combined with its high production rates, contributes to its widespread use in the manufacturing of nonwovens for various applications [96]. Electrospinning, while offering remarkable fiber properties, is more complex and requires careful control of multiple parameters, including voltage, distance between the spinneret and collector, and solution viscosity. The intricacy of the electrospinning setup can pose challenges for scaling up production, necessitating advanced equipment and process optimization to achieve consistent quality in larger batches [97]. Recent studies are investigating simplified electrospinning setups and alternative approaches, such as coaxial electrospinning, which can improve process control and fiber functionality while simplifying operations [98]. Solution blowing strikes a balance between the simplicity of melt blowing and the sophistication of electrospinning. It generally requires less stringent conditions than electrospinning and can be more easily adapted for different polymers and applications. This flexibility makes solution blowing an attractive option for researchers and manufacturers

seeking to explore innovative fiber applications without the extensive setup required for electrospinning [99].

2.2.4.5 Raw Material Versatility

Melt blowing and solution blowing techniques can process a wide range of thermoplastic polymers, including biodegradable and renewable materials, facilitating the development of sustainable nonwovens. Melt-blown nonwovens can be manufactured from various materials such as polypropylene, polyethylene, and even bio-based polymers like PLA, allowing manufacturers to tailor properties according to specific application needs [100].

Electrospinning is somewhat more limited in terms of material selection, as it primarily accommodates specific polymers that can form stable solutions or melts suitable for the process. However, advancements in electrospinning have expanded its material versatility, enabling the incorporation of polymers blended with nanoparticles or other additives to enhance fiber functionality. Recent research highlighted the incorporation of bioactive glass nanoparticles into electrospun fibers to improve osteo-conductivity in bone tissue engineering applications, showcasing the technique's potential for diverse materials [101].

2.2.5 Sustainability

The increasing global emphasis on environmental responsibility has led to a growing interest in sustainable practices within the fiber manufacturing sector. The production methods employed for micro and nanofibers must consider ecological impacts, particularly in the context of material selection, process efficiency, and waste management [102]. This section

delves into sustainable practices in fiber manufacturing, the development of polymer formulations, and essential safety and environmental considerations.

2.2.5.1 Sustainable Practices in Fiber Manufacturing

Sustainable practices in fiber manufacturing focus on minimizing the ecological footprint associated with production processes. This includes adopting renewable raw materials, improving energy efficiency, and reducing waste. One approach gaining traction is the use of bio-based and biodegradable polymers, such as PLA and polyhydroxyalkanoates (PHAs), which can significantly lower the carbon footprint compared to traditional petrochemical-derived polymers. Recent studies highlight the potential of PLA in various applications, including textiles and medical devices, due to its excellent mechanical properties and biodegradability [103]. In addition to material selection, optimizing manufacturing processes is crucial for sustainability. For instance, advancements in melt blowing technology have enabled higher energy efficiencies, allowing manufacturers to produce nonwovens at lower energy costs. Recent research illustrated that adjusting process parameters, such as air flow rates and temperatures, could lead to reductions in energy consumption while maintaining product quality [104].

Furthermore, a study showing waste management practices in solution blowing addresses Polystyrene (PS) waste management by recycling expanded PS into value-added hydrophobic fibers using an eco-friendly solution blow spinning process [105]. This sustainable approach repurposes low-density plastic waste, reducing environmental impact and promoting circular

economy principles. The resulting fibers show promising applications in oil-water separation, highlighting a practical pathway for waste reutilization and sustainability.

2.2.5.2 Compostable Formulations

Compostable materials break down into natural substances within a composting environment (landfill or marine environments) **(Figure 2-7)**, offering an eco-friendly alternative to traditional fibrous nonwoven materials. Recent research has explored various biopolymer blends, such as PLA combined with starch or natural fibers, to enhance mechanical properties while ensuring compostability [106]. Studies indicate that the incorporation of additives, such as plasticizers and modifiers, can improve the performance of compostable fibers. For example, adding plasticizers like glycerol to PLA formulations enhances flexibility and processability [107], making them suitable for applications in hygiene products and agricultural films. Furthermore, innovative approaches, such as using microbial enzymes to break down synthetic polymers, have shown promise in developing more efficient compostable formulations that can degrade within months [108]. Traditional nonwovens predominantly utilize petroleum-based polymers, such as PP, which significantly contribute to environmental pollution. In response, researchers are exploring biodegradable and compostable alternatives, including PHA, polybutylene adipate terephthalate (PBAT), polybutylene succinate (PBS), and polybutyrate adipate (PBA), as well as novel marine compostable polymers [109]. This shift towards sustainable materials has sparked increased interest in compostable melt-blown nonwovens, particularly for applications that commonly involve single-use products, such as PPE. **Table 2-2** shows a list of compostable and melt processable polymers.

A notable study by Wang et al. (2024) highlighted the feasibility of producing compostable melt-blown filters from PLA [110]. These filters not only achieved high filtration efficiency but also demonstrated the ability to degrade under composting conditions, thereby supporting sustainability initiatives in the medical and hygiene sectors. In the following some known compostable and biodegradable polymers will be discussed.

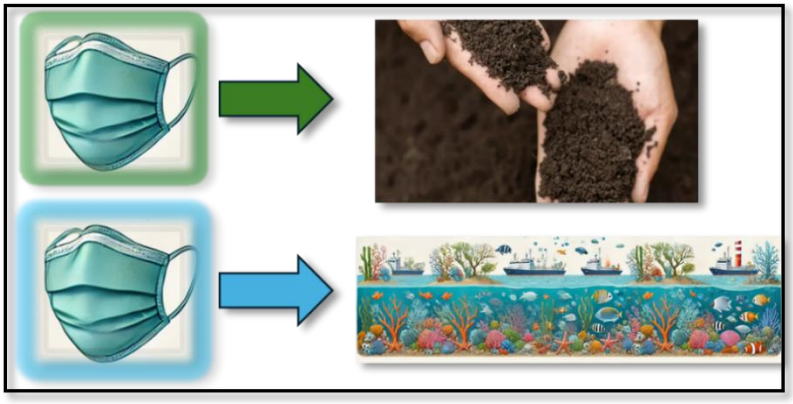


Figure 2-7 Contribution of marine and landfill compostable polymers, such as PHA, in surgical masks to reducing environmental pollution across marine and terrestrial ecosystem. Generated through OpenAI's ChatGPT platform [13].

Polyhydroxyalkanoates (PHAs)

PHA represents a family of polyesters produced via microbial fermentation and is considered one of the most promising biopolymers due to its complete biodegradability in natural environments, including marine ecosystems [111]. PHAs are known for their thermoplastic properties, making them suitable for melt-blown and spun bond nonwoven production [15]. Notably, PHAs, particularly polyhydroxybutyrate (PHB), have mechanical properties comparable to PP and PE, exhibiting a relatively high melting point (~175°C), crystallinity, and rigidity, which makes them suitable for creating strong, durable nonwoven fabrics [112].

However, PHAs are inherently brittle, posing a challenge in applications requiring flexibility [113]. To counteract this, copolymers such as polyhydroxybutyrate-co-valerate (PHBV) are often used to enhance flexibility without sacrificing biodegradability [15]. Importantly, PHAs also demonstrate marine compostability, degrading rapidly in the presence of marine microorganisms within months under optimal conditions [114]. This unique property makes PHA nonwovens highly attractive for products likely to end up in aquatic environments **(Figure 2-8)**, such as disposable wipes [115], biodegradable fishing gear [116], and packaging for foods [117]. Studies indicate that PHA nonwovens can fully degrade in marine environments, significantly reducing the impact of plastic pollution on marine ecosystems [118].



Figure 2-8 Marine compostable PHA used in surgical masks, offering a sustainable solution to reduce marine pollution. Generated through OpenAI's ChatGPT platform [13].

Poly(butylene adipate-co-terephthalate) (PBAT)

PBAT is a synthetic copolymer known for its excellent biodegradability, flexibility, and processability. It is derived from fossil resources but is fully compostable, breaking down under industrial composting conditions [119]. PBAT exhibits high elongation at break, making it highly flexible and tear-resistant, which is critical for nonwoven applications requiring durability, such as packaging materials and agricultural nonwovens [120]. The mechanical properties of PBAT can be tailored by blending it with other biodegradable polymers, such as PLA or starch-based materials, to improve strength while maintaining compostability [121]. While PBAT is primarily known for its industrial compostability, research has indicated that it can also biodegrade in marine environments, though at a slower rate compared to PHAs [122]. This makes PBAT nonwovens suitable for applications in coastal protection, agriculture [123] (e.g., erosion control mats), and marine packaging, where rapid biodegradation after use is crucial. However, the degradation rate in marine settings is contingent on specific environmental conditions, such as microbial activity [124].

Poly(butylene succinate) (PBS)

PBS is an aliphatic polyester synthesized from succinic acid and 1,4-butanediol, recognized for its biodegradability in composting conditions. PBS has a lower melting point (114°C) than PHAs and PBAT, facilitating processing through conventional nonwoven production methods like melt blowing [125]. It exhibits moderate mechanical properties, including good flexibility, tensile strength, and thermal stability [126]. While PBS is primarily compostable in industrial settings, ongoing research suggests that it may degrade in marine environments with sufficient

microbial action, albeit more slowly than PHAs or modified PBAT formulations [127]. PBS nonwovens are suitable for packaging, agricultural textiles, and hygiene products [128]. Their degradation rates are slower than those of PBAT in natural environments, making them more appropriate for applications requiring a longer service life, such as geotextiles and construction materials. The exploration of PBS blends and copolymers may further enhance its performance and degradation profiles [129].

Poly(butylene acrylate) (PBA)

PBA is another biodegradable polyester like PBAT, often blended with other polymers to optimize properties for nonwoven applications. PBA offers excellent flexibility, toughness, and processability [130]; however, its low thermal stability can limit its use in applications requiring high temperatures [131]. In marine environments, PBA's compostability is limited, but some studies have explored its potential to degrade in specific conditions [132]. Generally, PBA requires more time and conditions promoting microbial degradation, such as elevated temperatures and nutrient presence, to break down effectively.

Marine Compostable Polymers

Recent developments in marine compostable polymers include next-generation materials specifically designed to degrade in seawater. These polymers, such as PHA-derived copolymers or bio-polyesters modified for marine environments, are engineered to break down within weeks or months after exposure to seawater [114]. They exhibit flexibility and strength similar to PBAT, while maintaining rapid biodegradability in marine conditions [133]. These new polymers can be used for a wide range of nonwoven applications, including marine-based

hygiene products (such as wipes and diapers intended for use on ships or in coastal areas), disposable fishing gear, or nonwovens used in marine biology applications like biodegradable sample collection nets or ocean cleanup technologies [134].

Table 2-2 Melt processable and Compostable Polymers

Polymer	Compostability	Typical Applications	Reference
PLA	Industrial compostable	Masks, single-use filters, packaging	[135]
PHA	Marine and landfill compostable	Biodegradable masks, packaging, textiles	[136]
PBAT	Industrial compostable	Blend with PLA for flexible films, bags	[137]
PBS	Industrial compostable	Packaging films, agricultural mulch, bags	[105, 123]
PBA	Limited	Biodegradable packaging, agricultural films	[138]

2.2.5.3. Requirements for Compostability and Marine Compostability

Fiber Compostability Requirements

Compostability of fibers refers to their ability to decompose into natural substances under specific conditions in a composting environment. Key criteria include a biodegradation rate similar to that of organic materials, typically requiring 90% biodegradation within 90 to 180 days, and complete disintegration into small fragments (less than 2 mm) within 12 weeks [139]. Additionally, the final compost must be ecotoxicity-free, ensuring it poses no harmful effects on plant growth or soil ecosystems, with tests demonstrating that germination rates of plants grown in the compost are at least 90% of those grown in standard soil [140]. Standards such as ASTM D6400 and EN 13432 outline these requirements [141], evaluating factors like

organic content (at least 70% of the final product) and physical characteristics to ensure materials do not interfere with the composting process [142].

Marine Compostability Requirements

Marine compostability, on the other hand, focuses on the degradation of materials in marine environments, requiring them to break down rapidly within approximately six months, with some studies indicating a complete biodegradation rate of 90% within 180 days when subjected to specific marine conditions [143]. The disintegration must leave no harmful residues, and the breakdown products should be non-toxic to marine life, with studies showing that mortality rates for marine organisms exposed to leachate from degraded materials should be below 10%. Standards for marine compostability, such as ASTM D6691, are evolving to assess these criteria, considering factors like biodegradation rates (ideally over 90% in less than six months), microbial activity, and environmental conditions unique to the ocean [144]. The incorporation of these materials into nonwoven production offers a sustainable alternative to conventional petrochemical-based nonwovens, which contribute significantly to environmental pollution [145]. However, challenges remain, including cost, mechanical performance, processing challenges, and the need for proper composting infrastructure to maximize the environmental benefits of these materials [146].

2.2.5.4. Process Safety and Environmental Considerations

Ensuring safety and environmental protection during fiber manufacturing is paramount. Each production method presents unique safety challenges that must be addressed to minimize risks to workers and the environment [147]. For instance, electrospinning processes may involve the

use of solvents and high-voltage equipment, necessitating stringent safety protocols to prevent chemical exposure and electrical hazards [139, 140]. Research by Kumar et al. emphasized the importance of implementing comprehensive safety training and risk assessment strategies in electrospinning facilities to mitigate potential hazards [149]. In contrast, melt blowing and solution blowing processes typically require high temperatures and pressures, which pose thermal and mechanical risks [150]. Manufacturers are increasingly adopting measures to minimize emissions and effluents, incorporating advanced filtration systems to capture particulates and volatile organic compounds (VOCs) generated during production [151]. Research study demonstrated that integrating air and water treatment systems in fiber production facilities could significantly reduce the environmental impact and enhance sustainability [152]. In conclusion, the transition toward sustainable practices in fiber manufacturing, the development of compostable formulations, and robust safety protocols are critical for minimizing environmental impacts and promoting responsible production [153].

2.3 Nonwovens as Air Filters

The properties of nonwoven materials produced from the melt blowing process have been extensively studied due to their diverse applications in filtration, medical textiles, and hygiene products [154]. Melt-blown nonwovens have gained significant attention in recent advancements, particularly in air filtration applications, due to their fine fiber diameter and porosity [155].

2.3.1 Properties of Melt-blown Nonwovens

One of the most notable features of melt-blown nonwovens is the fine diameter of the fibers they consist of, typically ranging between 1 to 5 micrometers [155]. This fine fiber diameter is achieved through the high-velocity hot air used in the process, which stretches the molten polymer into ultrathin fibers [156]. As a result, melt-blown nonwovens have a high surface area-to-volume ratio, which is especially useful in filtration applications, as it allows for effective particle capture. Porosity is another defining characteristic of nonwovens produced through melt blowing. Due to the random arrangement of fibers, melt-blown nonwovens exhibit a high level of porosity, with a wide distribution of pore sizes [157]. This high porosity is particularly beneficial for applications that require a balance between airflow permeability and particle filtration. In air filtration, for instance, this allows melt-blown nonwovens to offer high filtration efficiency while maintaining a low pressure drop, which is a critical factor in applications like HVAC filters or face masks, where both effective filtration and breathability are essential [149, 150]. Despite these benefits, the mechanical strength of melt-blown nonwovens is generally lower compared to other nonwoven materials, such as those produced through spun bonding. The fine fibers in melt-blown nonwovens contribute to this reduced strength. However, the softness and flexibility that result from the low tensile strength make melt-blown nonwovens particularly suitable for certain applications, such as medical gowns, disposable wipes, and surgical masks [160]. Melt-blown nonwovens also demonstrate beneficial surface energy and chemical resistance properties, largely because they are often made from polymers like PP. The low surface energy of polypropylene renders these fibers hydrophobic, which makes them suitable for water-repellent applications [161]. Additionally,

melt-blown nonwovens exhibit excellent resistance to chemical degradation, further expanding their applicability in industrial and medical settings where exposure to harsh chemicals is common [162].

2.3.2 Melt-blown Nonwovens as Air Filters

In terms of air filtration, melt-blown nonwovens have emerged as one of the most effective materials, particularly when designed to capture fine particulates, including bacteria, viruses, and submicron dust particles. The filtration efficiency of melt-blown nonwovens is largely attributed to the fine fiber structure and high porosity, which allow them to trap small particles effectively. Moreover, the use of electrostatic charging in the production process further enhances particle capture [163]. For example, by applying a corona charge to the fibers, melt-blown nonwovens gain an electrostatic property that attracts and captures particles, significantly boosting filtration performance. This electrostatic enhancement has become crucial in HEPA filters and N95 respirators, which require high levels of filtration efficiency [164]. In addition to filtration efficiency, maintaining a low pressure drop across the filter is critical, as it ensures that airflow is not overly restricted. Melt-blown nonwovens excel in this aspect, as their porous structure allows air to pass through while capturing particles. Multilayer nonwoven materials, such as those that combine melt-blown and spun bond layers, have been developed to optimize both filtration efficiency and mechanical strength, further enhancing the utility of melt-blown nonwovens in various filtration applications such as surgical masks [165].

Recent advancements in the field have focused on improving the sustainability of melt-blown air filters. For instance, there is growing interest in using biodegradable polymers, such as

polylactic acid (PLA), PHA, Polyhydroxybutyrate (PHB), PBS, PBAT in the melt-blown process to produce more environmentally friendly air filters [166]. Furthermore, surface treatments to impart antibacterial properties have become a topic of significant research, particularly for filters used in medical environments. These treatments help reduce the risk of bacterial contamination and extend the lifespan of the filter, adding another layer of functionality [167].

2.3.3 Melt-blowing Process

The melt-blown process itself, which involves extruding polymer melt through small nozzles and using high-speed hot air jets to attenuate the polymer into fine fibers, has also seen advancements aimed at improving the efficiency of fiber production [168]. One key area of development is in the selection of polymers and the control of processing parameters, such as temperature and airflow. While PP remains the most common polymer used in the melt blowing process due to its low cost and favorable properties, other polymers, including polyesters and biodegradable options like PLA, are increasingly being explored to enhance the material properties for specific applications. Control over temperature and airflow during the melt blowing process is critical, as these parameters directly influence the fiber diameter and uniformity of the final material [169].

In addition to traditional fiber production, researchers have begun exploring ways to produce even finer fibers, including nanofibers, through modified melt blowing techniques [73]. These nanofiber materials are particularly effective in capturing ultrafine particles, making them ideal for air filtration systems designed to protect against viruses or fine dust. Another recent trend

in the melt blowing process is the move toward greater sustainability. Researchers are investigating ways to reduce the energy consumption of the process and exploring options for recycling melt-blown nonwovens [170]. For example, the use of renewable polymers are making melt blowing more environmentally friendly. Sustainability considerations have become especially relevant in the wake of global health crises, where the demand for PPE surged, leading to concerns about the environmental impact of disposable nonwoven products [171].

In addition to sustainability, there have been innovations aimed at adding functionality to melt-blown nonwovens. By incorporating additives, surface treatments, or coatings, these materials can be tailored for specific uses, such as adding antimicrobial properties for medical textiles or flame retardancy for industrial applications. Multilayer and hybrid structures have also become increasingly popular. For instance, the combination of melt-blown and spun bond layers (known as SMS structures) offers a balance between filtration performance, mechanical strength, and cost-effectiveness. Researchers are investigating "smart" filters made from melt-blown nonwovens. These smart filters are designed to respond to environmental changes, such as fluctuations in humidity or particulate concentration. By embedding sensors or using smart materials, these filters can provide real-time feedback on air quality or filter performance, offering exciting possibilities for future air filtration systems [172].

2.3.3.1 Recent Applications of Porous Melt-blown Nonwovens

The integration of smart technologies into melt-blown nonwovens has led to the development of materials with the ability to sense, respond, and adapt to environmental stimuli such as

temperature, humidity, pressure, and particulate concentration. These innovations have widespread implications, particularly in fields such as air filtration, medical textiles, and environmental monitoring [173].

Functionalization with Sensors and Smart Fibrous Materials

Melt-blown nonwovens have been functionalized with electronic sensors that can monitor real-time changes in air quality or filter performance. These sensors detect particles or pollutants in the air and send signals that allow for automated adjustments in filtration systems [174]. Smart melt-blown air filters with embedded sensors are particularly useful in industrial environments, hospitals, and public transportation systems, where maintaining clean air is crucial. Recent research has focused on flexible electronics that can be integrated into the porous structure of melt-blown fibers without compromising the material's filtration efficiency or breathability [175]. Moreover, smart textiles that incorporate electrospun nanofibers with melt-blown substrates are capable of improving filtration performance while offering functionalities like self-cleaning and antimicrobial properties. Self-cleaning filters, for example, can reduce maintenance and extend the lifespan of the material, particularly in harsh environments where dust accumulation is a major issue [176].

Temperature and Humidity Responsive Fibrous Textiles

Another exciting development in smart melt-blown textiles involves materials that respond to changes in temperature and humidity [177]. Researchers have explored melt-blown nonwovens embedded with shape memory polymers (SMPs), which can change shape in response to heat [178, 179]. These materials are ideal for adaptive air filtration systems that

adjust airflow and filtration efficiency based on temperature variations. Such smart nonwovens could be highly effective in environments where climate control is critical, such as HVAC systems in buildings, hospitals, and laboratories. Similarly, melt-blown nonwovens have been designed to react to changes in humidity. For instance, the use of hydrophilic polymer coatings on fibers allows the material to adjust its permeability in response to moisture in the air [180]. These smart humidity-responsive materials can be applied in fields such as wound care, where moisture management is crucial for healing [181]. Researchers are also investigating these smart materials for packaging that responds to humidity levels to preserve the freshness of perishable good [180].

Antibacterial and Antiviral Functionalities

The integration of antibacterial and antiviral properties into melt-blown fibers is another key area of research, particularly given the heightened focus on public health and hygiene following global health crises such as the COVID-19 pandemic. Smart melt-blown nonwovens have been developed with surfaces that can actively kill or deactivate pathogens upon contact [182]. Several studies have focused on applying nanoparticles, such as silver, copper, or zinc oxide, **(Table 2-3)** to the surface of melt-blown fibers to provide continuous antimicrobial action [183]. Silver nanoparticles, for instance, have been shown to disrupt bacterial cell membranes, providing long-lasting protection in medical masks, gowns, and filters [62, 158]. In combination with melt-blown nonwovens, these materials create a multifunctional filter that not only captures pathogens but also neutralizes them. Another approach involves incorporating photoactive coatings into melt-blown nonwovens, where exposure to light

triggers the generation of reactive oxygen species (ROS) that degrade viral and bacterial particles [184]. These types of smart textiles are particularly valuable for applications in healthcare settings, where PPE and air filtration systems can benefit from enhanced protection against pathogens [185].

Table 2-3 Melt Processable and Antimicrobial Materials Incorporated into Fibers

Antimicrobial agents	Description	Mechanism of Action	Applications
Silver Nanoparticles [186]	Nanoscale particles of silver with broad-spectrum antimicrobial properties	Disrupts bacterial cell membrane and DNA	Medical textiles, sportswear, wound dressings
Copper Nanoparticles [187]	Copper-based particles with effective antibacterial and antiviral activity	Generates reactive oxygen species (ROS)	Hospital fabrics, wound care products
Zinc Oxide Nanoparticles [41]	White pigment with antibacterial, antifungal, and UV-protective properties	Disrupts microbial cell wall and membrane	Clothing, UV-protective fabrics, face masks
Graphene Oxide [188]	Graphene-based material with high antibacterial efficiency against a range of pathogens	Mechanical damage and oxidative stress to microbes	Antibacterial coatings, medical garments
N-halamines [189]	Chemical class with long-lasting antimicrobial effect, regenerated after washing with bleach	Oxidizes cell proteins	Hospital textiles, protective clothing
Cationic Polymers [171, 172]	Positively charged polymers that adhere to negatively charged microbial cell walls, causing cell rupture	Cell membrane disruption	Medical and industrial textiles

A study by Kim [192] is highlighting the antifungal effectiveness of photosensitizers RB (rose bengal), PB (phthalocyanine blue), TBO (toluidine blue O), and AA (acid orange 7) grafted onto nanofiber-based fabrics and microfiber-based fabrics. Nanofiber-based fabrics consistently demonstrated higher inhibition rates compared to their microfiber counterparts, largely due to their significantly larger surface area (29 m^2/g vs. 1.4 m^2/g). Among the photosensitizers, RB exhibited the highest antifungal activity, followed by PB, TBO, and AA in decreasing order. RB-treated nanofiber fabrics achieved the highest inhibition rates, with up to 92% growth reduction and maximum inhibition rates of 3.7×10^{-2} L/μmol·min against P. cinnamomi (Phytophthora cinnamomi) and 3.5×10^{-2} L/μmol·min against T. viride (Trichoderma viride) [193]. In contrast, M. grisea (Magnaporthe grisea), with its larger spore size and ergosterol-dominated membrane, showed the highest resistance, requiring a multi-hit process by singlet oxygen ($^1O_2$) to achieve inhibition. The mode of action involves singlet oxygen ($^1O_2$) produced by the photosensitizers, which primarily targets lipids in fungal membranes. Pathogens with high levels of polyunsaturated fatty acids, such as P. cinnamomi (rich in arachidonic acid and eicosapentaenoic acid), were highly susceptible due to photooxidation of these lipids. In contrast, fungi with larger spore sizes or ergosterol-dominated membranes, such as M. grisea, were less affected [194]. A direct relationship between spore surface area and inhibition percentage was observed, with larger spores exhibiting greater resistance. Overall, nanofiber-based fabrics treated with RB demonstrated the highest inhibition rates across all tested fungi, indicating its superior photodynamic efficiency and grafting performance. These results underscore the importance of surface area, lipid composition, and photosensitizer properties in enhancing antifungal activity, suggesting

the potential for tailored antimicrobial applications using photosensitizer-functionalized fabrics [195].

In another study by Safaa Abd Zaid Abd Ali [196], the filters were loaded with organic particles derived from micronized rice. The particle size distribution of the micronized rice was designed to be representative of PM10 particles, with the intent of providing nutrients to support microbial growth. The loading of filters with micronized rice particles was done in a vertical filtration column, utilizing a rotating brush particle generator (RBG 1000, Palas) at a rate of 5 m^3/h for 2 minutes. The average particle concentration generated during this process was around 1.5 g/h. The micronized rice naturally contained the fungus Penicillium chrysogenum (P. chrysogenum), with a concentration of 2250 ± 850 CFU/g of rice. The size distribution of the particles was characterized using an optical particle counter (WELAS 2100), with a mass median diameter of 7.4 µm and a number median diameter of 0.6 µm. After the particles were loaded, the filters were further contaminated with the microbial consortium (containing P. chrysogenum and two bacterial species) in the filtration device [197]. The quantity of P. chrysogenum contributed by the micronized rice during the 2-minute loading was estimated to be a maximum of 10^2 CFU. This was considered negligible compared to the larger quantities coming from the microbial suspension nebulized upstream of the filters, which amounted to 10^{12} CFU.

Once contaminated with the microbial consortium, the filters (whether new or loaded with particles) were incubated in airtight containers for 8–10 days at 25°C and either 50% or 90% relative humidity (RH) to promote microbial growth. The two humidity conditions were

selected to reflect typical conditions in HVAC systems (50% RH) and to ensure significant microbial growth (90% RH). The incubation period simulated a common scenario in HVAC systems where ventilation might stop during extended periods like nights or vacations, allowing for microbial growth on the filters [198]. During the incubation, the filters were not subjected to airflow, allowing for microbial growth under controlled conditions. After the conditioning period, microbial concentrations on the filters were quantified by colony-forming unit (CFU) counting. The microorganisms were extracted by stirring the filters in a solution of magnesium sulfate ($MgSO_4$) and Tween-20, followed by ultrasonic treatment. This extraction method recovered 80-85% of the microorganisms from the filter media. The extracted solutions were then diluted and plated on agar media specific to the microbial species including P. chrysogenum: Rose Bengal Chloramphenicol agar (incubated at 25°C for 5 days), Staphylococcus epidermidis: Chapman agar (incubated at 37°C for 24 hours), Serratia marcescens: Nutrient agar (incubated at 30°C for 48 hours) [199]. The microbial concentration was expressed as CFU per filter surface area, with a limit of quantification (LQ) set to 10 CFU/cm^2. This study also evaluated the influence of zinc pyrithione (ZPT) on the filtration performance and microbial behavior on the tested filters. The ZPT treatment did not affect the filtration efficiency of the filters, with both new and loaded filters performing similarly in terms of particle collection. The filtration efficiency during the clogging process was similar for both filters, and the antimicrobial treatment did not degrade their performance [200]. Filtration efficiency was consistently above 96% for all particle sizes and throughout the clogging stages. After incubation at 90% RH, the results demonstrated the effectiveness of the ZPT treatment in preventing fungal growth. For new filters, the antimicrobial treatment significantly reduced

the growth of P. chrysogenum, with no growth observed. Bacterial survival was also impacted, with S. epidermidis showing a 99.99% reduction and S. marcescens showing a 90% reduction. However, for the loaded filters, P. chrysogenum growth was not entirely inhibited, although bacterial populations still showed significant reductions, similar to those seen with the new filters. At lower humidity (50% RH), microbial survival was limited across all filters, with most bacteria and fungi showing significant reductions in population, especially for the bacterial strains. The survival of P. chrysogenum was also reduced under these conditions, but not as drastically as with higher humidity levels. In summary, it was demonstrated that filters with zinc pyrithione (PP/ZPT filters) performed similarly to untreated filters in terms of particle filtration efficiency, even when loaded with organic particles [201]. The antimicrobial treatment was effective in limiting fungal growth, especially at high humidity (90% RH), where bacterial survival was significantly reduced, and fungal growth was inhibited. In contrast, at low humidity (50% RH), the survival of microorganisms on both new and loaded filters was significantly limited, with a notable reduction in both bacterial and fungal populations. Additionally, the results indicated that the loading of filters with organic particles, such as micronized rice containing P. chrysogenum, had a minor effect on microbial survival when compared to the antimicrobial treatment. The presence of the organic particles did, however, influence microbial behavior, particularly in the case of fungal growth. The findings suggest that the inclusion of antimicrobial treatments like ZPT can be an effective strategy to prevent microbial contamination in HVAC systems, especially in environments prone to high humidity [202].

Filtration Performance Monitoring

By embedding real-time particulate sensors into melt-blown nonwovens, filters can detect when they are becoming clogged or saturated with particles and signal when they need to be replaced. This advancement has important implications for energy efficiency in HVAC systems and industrial air purifiers, where filters typically need to be replaced based on estimated schedules rather than actual performance data [186, 187]. These sensors can also detect changes in airborne contaminants, such as sudden increases in pollution levels or the presence of harmful chemicals. Smart filters are being designed to respond by adjusting their filtration capacity in real-time, improving air quality while reducing energy consumption [205].

Smart Medical Applications

In the healthcare sector, melt-blown nonwovens are being developed for smart wound dressings that can monitor the healing process and adjust conditions to promote faster recovery [206]. For example, smart dressings can incorporate pH sensors to detect infections in wounds [190, 191]. These dressings may also release antimicrobial agents or adjust moisture levels based on real time data, creating a dynamic and responsive wound healing environment [209]. Additionally, researchers are exploring the use of melt-blown nonwovens in drug delivery systems, where smart textiles can deliver therapeutic agents in response to stimuli such as temperature or moisture [210]. This technology has the potential to revolutionize wound care, bandaging, and drug administration, offering more personalized and efficient treatment methods [211].

Environmental Sensing and Adaptation

Materials that respond to the presence of specific gases, particulates, or hazardous chemicals can be integrated into protective clothing, air filters, and industrial filtration systems. These smart textiles can trigger warnings or initiate protective measures when harmful substances are detected in the air. For example, smart air filters designed for industrial applications can sense when the concentration of a particular chemical exceeds a safe threshold, automatically increasing the filtration capacity or shutting down air intakes. These applications are particularly relevant in industries where worker safety is a priority, such as chemical manufacturing, mining, and construction [212].

Energy Harvesting from Airflow

Another emerging area of research is the integration of energy harvesting capabilities into melt-blown nonwovens [213]. Some studies have focused on using the constant airflow passing through melt-blown filters to generate small amounts of energy. For example, triboelectric nanogenerators (TENGs) can be incorporated into the fiber structure to harvest energy from the mechanical motion caused by airflow. This energy can be used to power sensors embedded in the filter or stored for other purposes. Smart melt-blown textiles with energy-harvesting capabilities have significant potential in self-powered systems, where the filter itself can monitor performance without relying on external power sources. These innovations hold promise for autonomous environmental monitoring systems or remote filtration devices in areas where access to energy is limited [214].

2.4 Case Study

The following case study is based on the work of Liu et al. (2015), exploring the application of polyacrylonitrile (PAN) nanofibrous filters as a promising solution for urban air filtration, highlighting their efficiency in capturing PM 2.5 while maintaining high transparency and low airflow resistance [215]. In recent years, the increasing levels of particulates in urban environments have raised significant health concerns, prompting the need for effective air filtration solutions. Transparent air filters made from advanced nanofibrous materials present a promising alternative to regular filters by providing essential particulate capture while allowing natural light transmission. This study also investigates the performance of various transparent air filters, particularly focusing on their particulate capture efficiency, light transmittance, and airflow characteristics.

2.4.1 Fabrication Method

The fabrication method used in this study was electrospinning, where a 6 wt.% PAN solution in dimethylformamide (DMF) is processed along with additives like Polyvinylpyrrolidone (PVP), Polyvinyl alcohol (PVA), and Polystyrene (PS). The solution was electrospun onto a copper-coated fiberglass wire mesh to form nanofibrous filters with diameters ranging from 100 to 500 nm. Key parameters such as polymer concentration, voltage, and collection distance were controlled to optimize fiber structure for high surface area, porosity, and effective particulate matter filtration.

2.4.2 Performance of Transparent Air Filters

The performance of the transparent air filters was evaluated based on key parameters: capture efficiency, light transmittance, and airflow. The air filters demonstrated varying transmittance levels of approximately 85%, 75%, 55%, 30%, and 10%. Using photographs, it was shown that filters with transmittance above 50% enable sufficient light penetration, enhancing natural lighting and visibility. The PM2.5 capture efficiencies of the different polymer nanofibrous filters were assessed at various transmittance levels. An increase in the thickness of the fibrous filters generally led to enhanced PM2.5 capture efficiencies across all filter types (PAN, PVP, and PVA). The PAN filter achieved remarkable capture efficiencies, with over 95% removal at approximately 90% transmittance and greater than 99% at around 60%. Similarly, PVP and PVA filters demonstrated more than 95% capture efficiency at lower transmittance levels of around 60% and 30%, respectively. In contrast, PS fibers, commonly used in commercial filters, did not show significant improvements in PM2.5 capture efficiency with increased thickness. For larger particles (PM10–2.5), all polymer air filters exhibited higher removal efficiencies than PM2.5, often exceeding the 95% efficiency standard, with PAN maintaining the highest performance relative to the other materials. The airflow through the PAN filter was demonstrated using an electric fan at a wind velocity of 3 m/s. The setup showed that the transparent filter facilitated efficient air exchange. A quantitative analysis of pressure drop across the filters highlighted that at a face velocity of 0.21 m/s, the pressure drops for the 85% and 75% transmittance filters were only 133 Pa and 206 Pa, respectively, which is a minor fraction (<0.2%) of atmospheric pressure, comparable to that of a blank window screen. The pressure drop increased with greater filter thickness and lower transmittance, but the overall

performance, measured by the quality factor (QF), indicated that the PAN filter outperformed commercial alternatives by significant margins.

To further investigate the dynamics of PM capture, in situ optical microscopy (OM) and scanning electron microscopy (SEM) were utilized on a PAN nanofibrous filter with a fiber diameter of approximately 200 nm. The study depicted the filter's performance over time (5, 120, and 600 seconds) in capturing PM, illustrating a progressive accumulation of particles. Initially, PM particles adhered tightly to the fibers, subsequently aggregating to form larger clusters. The SEM images revealed that the PM particles wrapped around the nanofibers, deforming and stabilizing into spherical shapes, demonstrating a strong affinity between the PM and PAN fibers. In explaining the differential performance of various fibrous filters, the composition and surface chemistry of smoke PM were characterized. X-ray photoelectron spectroscopy (XPS) revealed that carbon (C), oxygen (O), and nitrogen (N) comprised the primary components of smoke PM. The functional groups present included C–C, C–O, C=O, and C–N, with ratios indicating a predominance of C–C and C–O bonds. Fourier transform infrared spectroscopy (FTIR) further confirmed the presence of various functional groups associated with organic carbon in the PM. Transmission electron microscopy (TEM) and electron energy loss spectroscopy (EELS) were also utilized to visualize the morphology of PM on PAN fibers and analyze the chemical distribution. EELS demonstrated that polar functional groups (C–O, C=O, and C–N) were concentrated on the PM surface, enhancing the filter's dipole interactions, which likely contributed to its higher capture efficiencies. The long-term efficacy of the PAN filter with approximately 75% transmittance was evaluated under

hazardous conditions (PM2.5 index >300). After 100 hours, the filter maintained high removal efficiencies of 95–100% for PM2.5 and PM10–2.5, with minimal pressure drop increases (from ~2 to ~5 Pa), indicating robust long-term performance. Post-test SEM images depicted aggregated PM particles forming larger domains (20–50 μm), without any noticeable detachment during cleaning attempts, affirming the filter's stability.

A field test conducted in Beijing under hazardous PM conditions aimed to assess the real-world performance of the filters. PAN filters with varying transmittances (~77%, ~54%, ~40%) achieved PM2.5 removal efficiencies of 98.69%, 99.42%, and 99.88%, respectively. For PM10–2.5, efficiencies were similarly high. In contrast, PS filters exhibited significantly lower efficiencies, and commercial masks with PP fibers performed poorly, highlighting PAN's superior performance as a transparent air filter. Additionally, the study examined how environmental factors influenced filter performance under different wind forces and humidity levels. PAN filters maintained high removal efficiencies (>96%) across all wind speeds, demonstrating an increasing trend in efficiency with wind velocity. Humidity levels also improved PM capture, particularly for PS filters.

2.4.3 Conclusion and Future Direction of the Case Study

PAN nanofiber filters are highly effective as transparent air filters, offering high PM removal efficiency, low pressure drop, and long-term durability. They can be used in applications where both filtration and transparency are needed, such as on windows, providing an efficient solution for reducing indoor air pollution. One primary direction for future research would be enhancing the lifespan and durability of the filters, especially under extreme environmental conditions

such as high humidity or heavy pollution levels, possibly by applying coatings or treatments that increase resistance to environmental damage. Since materials like PVP and PVA suffered degradation under humid conditions, it would be beneficial to explore methods to prevent such issues and enhance the overall durability of PAN filters. Another important area for improvement is optimizing the electrospinning process itself. Fine-tuning parameters such as polymer concentration, voltage, and fiber diameter can significantly influence the performance and structural integrity of the filters. Additional research could explore the impact of these parameters on the efficiency of PM filtration under varying airflow conditions. Additionally, testing different polymer blends or composite materials could lead to improvements in specific properties like hydrophobicity, mechanical strength, or flexibility, further improving the filters' performance in real-world applications. Exploring the use of biodegradable polymers or natural fibers could also be a promising direction for future work and might offer similar or superior performance. Research into hybrid materials or nanocomposites, incorporating elements like carbon nanotubes or graphene, could also enhance the electrostatic properties of the filters and further improve their ability to capture fine particulate matter. Incorporating self-cleaning technologies into the filters could be another area of development. Approaches such as photothermal, photochemical, or electrostatic regeneration could allow the filters to maintain high efficiency over time by removing accumulated particles without the need for manual cleaning or replacement. This could drastically improve the convenience and longevity of the filters, making them more suitable for long-term use in real-world environments. Partnerships with industries such as HVAC systems, automotive, and personal protective equipment manufacturers could facilitate the integration of transparent PAN filters into various

consumer products like air purifiers, windows, and face masks, broadening their potential applications. Additionally, understanding the long-term effects of exposure to various pollutants, including VOCs and ozone, on filter performance and degradation would be crucial for refining their effectiveness in diverse settings. Finally, quantifying the health benefits of using transparent PAN filters in indoor environments could provide valuable evidence for their widespread adoption. Research that directly measures improvements in air quality and health outcomes for vulnerable populations (such as children, the elderly, or those with respiratory conditions) would provide compelling data to support the integration of these filters into public health strategies.

2.5 Conclusion and Future Direction

Among the three methods evaluated—electrospinning, solution blowing, and melt blowing—melt blowing emerges as the most feasible and practical choice for air filtration applications. It offers significant advantages in terms of cost-efficiency, production speed, ease of operation, adaptability to existing technologies, scalability, sustainability, filtration performance and safety. These factors make melt blowing a highly competitive method for large-scale fiber production in air filtration. The primary limitation of melt blowing lies in its ability to produce ultrafine fibers. However, advancements in nozzle technology have shown promise in overcoming this challenge. Improved nozzle mechanics and innovative designs are enabling the production of fine fibers comparable to those achieved through electrospinning, without the associated safety concerns and complexities of the electrospinning process. Further enhancements to melt blowing could focus on expanding its compatibility with a broader range

of polymers, particularly those with lower melt flow indices (MFI). As polymer manufacturing evolves, specially toward the production of sustainable polymers, incorporating high-performance polymers into the melt blowing process will be crucial for advancing the functionality and performance of fiber-based filtration materials. Additionally, integrating melt blowing with complementary methods like solution blowing could unlock new possibilities for producing high-performance fibers with diverse functionalities. Such hybrid approaches may address specific challenges in air filtration, leading to innovative solutions that combine the strengths of multiple fabrication techniques.

Chapter 3

Nano-porous melt-blown poly (lactic acid) fiber mat air filters for high efficiency particulate capture

This chapter introduces a two-step technique for developing nano-porous, compostable melt-blown nonwovens with high porosity, specifically engineered for high-performance particulate capture in air filter applications. The first step entails creating a high melt flow index (MFI) material by melt-blending low-viscosity polylactic acid (PLA) with a sacrificial additive, polyethylene glycol (PEG), of varying molecular weights. Rheological, compatibility, and thermal analyses are conducted on the sample blends. The MFI of the resulting blends ranges from 56 g/10 min (baseline PLA) to 238 g/10 min (PLA/PEG 400 – 10%), confirming their suitability for the melt-blowing process. These blends are then formed into nonwoven mats using a twin-screw extruder, producing microfibers with diameters between 1.05 and 2.64 µm. The second step involves boiling water etching to remove PEG, creating nanopores within the fibers. This etching process leaves a network of nanopores (50 to 200 nm in size), distributed throughout the microfiber structure. The PLA/PEG 2000 sample exhibits optimal properties, achieving approximately 85% particulate capture efficiency for 0.3 µm NaCl particulates during air filtration testing. This study represents an innovative and eco-friendly approach for creating nano-porous nonwoven mats with potential applications in air filtration, water filtration, and battery separators, where high porosity is beneficial.

3.1 Introduction

Particulate matter filtration typically involves the employment of porous materials, including nonwovens that are engineered with specific properties like pore size, fiber structure, and mechanical behavior [216]. This customization enables them to achieve characteristics such as high porosity, hydrophilicity, hydrophobicity [217], and antimicrobial activity [218]; making them ideal for applications including air filtration. Other applications of fibrous porous materials include battery separators, medical dressings, hygiene products [40], spill mitigation materials [219]. Electrospinning and melt-blowing are the leading techniques for producing porous nonwovens. Electrospinning is renowned for generating nonwovens with fine fibers but is constrained by low throughput and limited polymer compatibility which restricts its suitability for large-scale commercial production [220]. Additionally, electrospun nonwovens often exhibit reduced mechanical strength and durability, which can limit their practical applications [155].

Contrary to electrospinning, melt-blowing offers enhanced structural integrity, higher and more efficient production rates, and is a more cost-effective method for large-scale manufacturing [221]. While electrospinning typically employs organic solvent media's that makes it less eco-friendly, melt-blowing is inherently safer and avoids the use toxic and/or organic solvents [222, 223]. Melt-blown nonwovens, with their enhanced structural integrity often bestows superior mechanical properties and durability onto the final product [224, 225]. This makes them highly customizable for demanding applications such as air filtration [226], water filtration [227], battery separators, and geotextiles [228]. Previously, the melt-blown process was limited to polypropylene (PP) due to its high melt flow index (MFI) and low

viscosity [229]. However, recent improvements within the polymer industry, particularly toward high MFI and advanced polymer production, have broadened the selection of melt-processable materials for the melt-blown process [230, 231]. This helps in enabling more advanced and diverse applications for melt-blown products. Among these polymers, poly(lactic acid)(PLA) has notably gained significant attention for its renewability and compostability [232]. The growth in demand for air filters for surgical masks, as the environmental impact of discarded masks and single use residential air purifiers becomes a more pressing global issue, especially during and following the COVID-19 pandemic [233] and driven innovation in new material options. The discovery and employment of sustainable produced and biodegradable material alternatives for single-use applications is an important area of research and aligns well with the United Nations (UN) sustainable development goals (SDG) associated with sustainable communities, consumption and production (SDGs 11, 12). High porosity nonwovens offer superior properties across various industries, including air and water filtration for usage in high efficiency particulate air (HEPA) filters [219] and wastewater treatment [234, 235] as well as within the medical [236], food packaging [237] and electronics industries [38]. Specifically for air filtration, high porous nonwovens work to efficiently capture fine particulate matter (i.e. dust, pollen, and airborne pathogens) across diverse settings, including hospitals, laboratories, industrial facilities, and residential spaces [237]. These filtration systems provide critical protection for the end users and patients all the while maintaining breathability and comfortability through a low pressure drop during prolonged usage [38]. However, filtration systems like HEPA filters have a major limitation which is their finite particle capture capacity, necessitating costly, frequent, and inconvenient maintenance

or replacement due to their significant efficiency drop with particles smaller or larger than 0.3 microns [238]. Additionally, many HEPA filters are also made from non-biodegradable materials, contributing to non-degradable plastic waste generation. To overcome these key issues, increasing the filter's surface area by decreasing the fiber dimension or incorporating porosity within the fibrous structure significantly boosts particles capture and enhances filter capacity [227].

Therefore, this study aims to address the current demands for advanced air filtration by introducing a novel approach for generating nanopores within a low molecular weight PLA (high melt flow rate) based- melt-blown fibrous network. In this approach, polyethylene glycol (PEG), a water-soluble additive, was selected as a sacrificial blend additive for its compatibility with PLA, excellent phase change properties, non-toxicity, low cost, and chemical stability. The PEG was later etched via a simple washing process to leave behind a porous structure. The effects of the PEG additive were examined at three different molecular weights (400 g/mol, 2000 g/mol, 4000 g/mol) and two weight concentrations (5 and 10 wt.%) to determine how these parameters influence the size and distribution of the generated pores. The morphology of the non-woven mats was analyzed in detail, before and after etching. The approach employed in this study is notable for its effectiveness, sustainability, and safety, offering a practical solution for industries such as air filtration that require high-porosity materials while upholding environmental responsibility.

3.2 Materials and processing methods

3.2.1 Materials

The primary substrate used in this study was compostable PLA grade 040, supplied by Total Corbion, with an MFI of 56 g/10 min at 190 °C/0.325 kg. Three different molecular weights of polyethylene glycol (PEG) with 400 g/mol (liquid), 2000 g/mol (flakes), 4000 g/mol (flakes) were procured form Sigma-Aldrich (Oakville, ON, Canada) were used in this study as a sacrificial agent and plasticizer.

3.2.2 Melt blending and injection molding

To develop highly porous and compostable melt-blown nonwovens, PLA was selected as the primary substrate. PEG was employed as both a pore-forming sacrificial agent and plasticizer. To evaluate the effect of PEG's molecular weight on its compatibility with PLA and the resulting porosity of the fibers, six distinct PLA/PEG formulations were prepared (see **Table 3-1)**. These formulations incorporated three different PEG molecular weights (400, 2000, and 4000 g/mol) at two concentrations (5 and 10 wt.%); all the while, maintaining a consistent PLA composition across all samples. After dry-mixing the individual components, the composition was melt-blended using via Rheomix a torque mixer from (HAAKE PolyLab QC). The mixing was conducted at 190 °C and 100 rpm for four minutes. The processed samples were then cooled, dried (80 °C overnight), and pelletized. Injection molding was conducted using a HAAKE Mini-Jet Pro from Thermo-Fisher Scientific, set to 190 °C with an injection pressure of 750 bar and a packing time of 1 second, to produce rheology discs for rotational rheometry experiments.

Table 3-1 Formulation breakdown for the processed blends

Formulations	PLA wt.%	PEG 400-wt.%	PEG 2000-wt.%	PEG 4000-wt.%
PLA	100	-	-	-
PEG 400-5%	95	5	-	-
PEG 400-10%	90	10	-	-
PEG 2000-5%	95	-	5	-
PEG 2000-10%	90	-	10	-
PEG 4000-5%	95	-	-	5
PEG 4000-10%	90	-	-	10

3.2.3 Melt-blowing

The pelletized PLA/PEG polymer blends were processed with a twin-screw extruder equipped with a melt-blowing die (diameter 1 mm), in which the temperature, pressure, and airflow rates, were optimized [219]. The employed temperature profile in the seven heating zones was (Die) 195-195-195-195-195-185-110 (Feeder) with an extrusion speed of 100 rpm. This process parameters optimization aimed to ensure a consistent melt flow from the nozzle and achieve high-quality fiber formation. Other parameters included a motor voltage of 95 V (equivalent to 273 °C air temperature) to produce heated air for the extruded polymer, an air pressure of 6.8 psi, a rotating material collector with speed of 39 rpm, and a die-to-collector distance of 40 cm. The set up ensured uniform dispersion of the melt-blown fibers generating a uniform nonwoven, porous, PLA fibrous mat.

3.2.4 Etching process

To enhance pores within the melt-blown fibrous network and generate nanopores along fiber strands, PEG was removed from the PLA/PEG blend nonwoven mats through an etching process using boiling water. For this, the nonwoven mats were encased in a meshed fabric and immersed in boiling water for 30 min to dissolve and remove PEG, and the process was repeated three times with the use of clean water. This treatment effectively removed PEG from the fiber matrix, leaving behind nanopores on the melt-blown fibers. To meshed encasing maintained the structural integrity of the nonwoven samples, prevent fiber breakage, and eased the nonwoven separation post etching. After the etching was completed, the mats were dried in a convection oven (60 °C for 24 h) to ensure thorough drying. Fourier transform infrared spectroscopy (FTIR) analysis was employed to ensure complete removal of PEG from the PLA nonwovens.

3.2.5 Characterizations

3.2.5.1 Compatibility analysis

The compatibility of PLA with PEG was evaluated at two concentrations (5% and 10%) and with different molecular weights of PEG (400 g/mol, 2000 g/mol, and 4000 g/mol). This analysis employed Gibbs free energy calculations for mixing using **Eq.1** to determine the interactions between the polymer components [239, 240].

$$\Delta G_m = \Delta H_m - T\Delta S_m \qquad \textbf{(Eq.1)}$$

ΔG_m reflects the stability of the blend, with a negative value indicating favorable mixing between PLA and PEG. The enthalpy of mixing, ΔH_m, was calculated using the relationship in equation (2) [239, 240]:

$$\Delta H_m = (\delta_1 - \delta_2)^2 \Phi_1 \Phi_2 \quad \textbf{(Eq.2)}$$

In **Eq.2**, delta δ represents the solubility parameters, and Φ_1 and Φ_2 denotes the volume fractions of PLA and PEG in the mixture. This equation indicates that the enthalpy of mixing is directly influenced by the difference in solubility parameters and the concentration of each polymer, allowing for an assessment of the thermodynamic favorability of blending. The solubility parameters were further characterized by their relation to density (ρ), group molar attraction constants ($\sum G_m$), and molecular weight of monomer as shown in equation (3) [239, 240]:

$$\delta = \frac{\rho . \sum G_m}{M} \quad \textbf{(Eq.3)}$$

3.2.5.2 Scanning electron microscopy (SEM)

SEM (Phenom Desktop SEM, Thermofisher Scientific USA) was used to examine the size and morphology of the melt-blown nonwovens. Post PEG removal, the fiber morphology, pore size, shape, and distribution of the resulting nanopores within the fibrous structure was evaluated using a high-resolution field-emission SEM (FESEM) (FEI Quanta Feg 250, Oxford Instrument, UK). For the high-resolution SEM, the samples were gold coated prior to the evaluation.

3.2.5.3 Attenuated total reflection - Fourier transform infrared spectroscopy (ATR-FTIR)

FTIR analysis (Nicolet 6700 NEXUS, Thermo-Fisher Scientific) with an attenuated total reflectance (GladiATR from Pike technologies) was used to analyze the chemical structure and functional groups of samples. The FTIR was operated in the transmittance mode, recording spectra from 500 to 4000 cm^{-1} at a resolution of 4 cm^{-1} over 32 scans.

3.2.5.4 Thermal stability analysis

The thermal stability and decomposition behavior of the samples was analyzed using thermogravimetric analysis (TGA) (TGA 550, TA Instrument Co. Ltd., New Castle, USA). The analysis was performed by ramping the temperature from room temperature to 500 °C at a rate of 20 °C/min under a nitrogen atmosphere. The nitrogen gas flow rate was 40 mL/min.

3.2.5.5 Thermal properties

The thermal properties of the samples were investigated using differential scanning calorimetry (DSC) (DSC 2500, TA Instrument Co. Ltd., New Castle, USA). Each sample was first heated from 10 to 200 °C at a rate of 10 °C/min under a nitrogen atmosphere (20 mL/min), followed by cooling to 10 °C at the same rate, and second heating to 200 °C. All analyses were performed using data from the second heating cycle. The information obtained from the 1st heating cycle from the DSC was used to model the glass transition temperature (Tg), as the 1st heating cycle resembles PLA's crystalline state of the blends, by using a linear relationship **(Eq.4)** and the Fox equation **(Eq.5)**.

$$T_g = w_A T_{GA} + w_B T_{GB} \quad \textbf{(Eq.4)}$$

$$\frac{1}{T_{GM}} = \frac{w_A}{T_{GA}} + \frac{w_B}{T_{GB}} \quad \textbf{(Eq.5)}$$

3.2.5.6 Air filtration testing

The filtration performance including the particulate filtration efficiency (PFE) and pressure drop (dp) of the nonwoven samples was evaluated using the TSI 8130A Automated Filter Testing System (TSI Company, Minnesota, USA). The testing was performed using a 0.3 μm NaCl aerosol, at a flow rate of 10.5 fpm which is specifically appropriate for evaluating high-efficiency particulate arresting (HEPA) filter performance.

3.2.5.7 Melt flow index (MFI**)**

The melt flow index (MFI) was measured using a Dynisco Melt-flow indexer model 4002 in accordance with ASTM D1238 at a temperature of 190 °C and a load of 0.325 kg. The half die (1 mm) and piston were heated for 15 minutes at the set temperature prior to testing. For all samples, the material was passed through the MFI machine within approximately 7 min, with sample collection occurring halfway through during laminar flow.

3.2.5.8 Capillary rheometer

A NETZSCH twin-bore ROSAND RH2200 capillary rheometer was used to examine the melt rheology behavior of the polymer blends. For the twin-bore rheometer, two different dies (capillary and orifice) were used simultaneously to compensate for the pressure drop and conduct the Bagley end correction. The capillary die had an L/D (length/diameter) of 16 with a 1 mm inner diameter opening, while the orifice die had an L/D of 0.25 with a 1 mm inner diameter opening. The testing temperature was set to 200 °C to evaluate the desired melt

blowing temperature with shear rates of 100, 300, 1000, and 3200 s^{-1}. The apparent shear stress (τ_{app}) and apparent shear rate (γ'_{app}) are represented in **(Eq.6)** and **(Eq.7)**, respectively [241, 242].

$$\tau_{corr} = \frac{R\Delta P}{2L} \quad \textbf{(Eq.6)}$$

$$\gamma'_{corr} = \frac{4Q}{\pi R^3} \quad \textbf{(Eq.7)}$$

Where the parameter R is denoted as the die's radius, P is ascribed to the die's pressure drop, L is the die's length, and lastly, Q is the volumetric flow rate of the polymer melt. Following this, the values were corrected using the parameters found by applying the Bagley **(Eq.8)** and Rabinowitsch **(Eq.9)** end corrections to obtain the true or corrected shear stress (τ_{corr}) and rate (γ'_{corr}), respectively [241, 242].

$$\tau_{corr} = \frac{\Delta P}{2(\frac{L}{R} + n)} \quad \textbf{(Eq.8)}$$

$$\gamma'_{corr} = \frac{3n' + 1}{4n'}\gamma'_{app} \quad \textbf{(Eq.9)}$$

Where n is assigned to be the Bagley factor; while n' represents τ_{app}'s slope against γ'_{app} when fitted with the Rabinowitch correction. As such, the corrected or true shear viscosity is Where n is assigned to be the Bagley factor; while n' represents τ_{app}'s slope against γ'_{app} when fitted with the Rabinowitch correction. As such, the corrected or true shear viscosity is defined by **(Eq.10)** [241, 242].

$$\eta_{corr} = \frac{\tau_{corr}}{\gamma'_{corr}} \quad \textbf{(Eq.10)}$$

3.2.5.9 Parallel plate rheometer

To measure the flow properties within the molten phase, a HAAKE MARS III rheometer with parallel plate geometry was employed following ASTM D4440, using samples with a thickness and diameter of 2.5 mm and 25 mm, respectively. The rheological analysis involved a frequency sweep, constant strain, constant gap distance, and set temperature parameters of 0.1 to 100 s^{-1} (0.6283 to 628.3 rad/s), 0.01%, 1 mm, and 190 °C, respectively. For further analysis into complex viscosity of the blends, the zero-shear viscosity value was obtained by curve fitting the Cross model (**Eq.11**).

$$\eta = \left(\frac{\eta_0}{(1 + (\tau_0\gamma)^m)}\right) \qquad \textbf{(Eq.11)}$$

3.3 Results and Discussion

3.3.1 Compatibility analysis

Theoretical miscibility analysis between PLA with PEG was carried out to predict the possibility of obtaining fine dispersion of PEG in PLA during the melt blending processes. Since the PLA and PEG are fairly large macromolecules, the entropy of mixing (ΔS_m) was assumed to be negligible, and the primary factor determining miscibility was considered as the enthalpy of mixing (ΔH_m). For miscibility to occur, Gibbs free energy (ΔG_m) must be negative, which implies that ΔH_m should be small or negative. In our case none of the ΔH_m was negative but they were small, as low as 0.7 J/cm^3. The calculations results are tabulated in **Table 3-2.** Based on the **Table 3-2**, as the concentration of PEG increases (from 5% to 10%), ΔH_m values increase slightly, but remain small. This means a higher concentration of PEG still leads to certain level of miscibility, especially for PEG-2000 and PEG-4000. The Hildebrand solubility

parameters indicate that PLA and PEG-400 have a larger gap in their solubility parameters (PLA = 25.12, PEG-400 = 19.83), leading to higher ΔH_m values, and thus less compatibility. On the other hand, PEG-2000 and PEG-4000 have solubility parameters closer to that of PLA, reducing ΔH_m and improving miscibility. Based on the results of the **Table 3-2**, PEG-2000 and PEG-4000 at both 5% and 10% concentrations exhibit better miscibility with PLA due to their closer solubility parameters and lower enthalpy of mixing values. PEG-400 shows less compatibility, especially at higher concentrations.

Table 3-2 Solubility parameters and mixing enthalpies of PLA and PEG variants.

Formulation	δ $J^{1/2}$ $cm^{-3/2}$	ΔH J/cm^3 (5%PEG)	ΔH J/cm^3 (10%PEG)
PLA	25.12	NA	NA
PEG - 400	19.83	1.33	2.52
PEG - 2000	21.23	0.72	1.36
PEG - 4000	21.06	0.79	1.49

3.3.2 Fourier transform infrared spectroscopy (FTIR)

Figure 3-1(**(a)** to **(c)**) presented the ATR-FTIR results for the PLA/PEG nonwoven samples with three different molecular weights of PEG, all at a loading of 10 wt.%, before and after the PEG etching process. From **Figure 3-1** (**a)** to **(c)**, the typical PLA spectra were shown, where the typical assignments of -CH- and CH_2 from 2950 to 3000 cm^{-1}, -C=O at 1750 cm^{-1}, -C-O- at 1180 cm^{-1}, and -C-O-C- at 1050 to 1120 cm^{-1} were identified [243–246]. The general spectrum of PEG was denoted by peaks at 3420, 2866, 1690, 1092, and 900 cm^{-1}, which were

representative of O-H stretching vibrations, C-C stretching and bending vibrations, C-O stretching, C-H stretching, and C-H bending, respectively [243–246]. When examining the spectra of the blend formulations, the spectra followed the dominant phase of PLA, with the generation of a few new peaks from the PEG phase, in addition to the superposition of blend peaks. The most significant shift was observed at the 1690 and 1750 cm^{-1} carbonyl peaks from PEG and PLA, respectively, where the peaks coalesced into a single, more intense peak, indicating interaction between the two components.

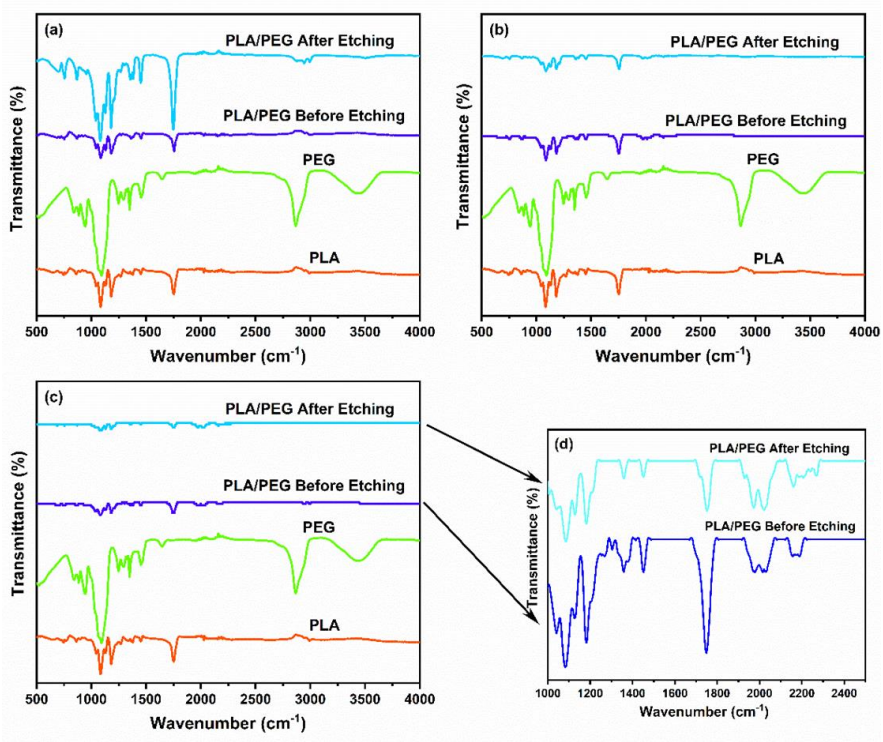


Figure 3-1 ATR-FTIR Spectras of nonwovens; (a) PLA/PEG 400-10%, (b) PLA/PEG 2000-10%, (c) PLA/PEG 4000-10%, prior and after etching of PEG content.

Examining **Figure 3-1(c)**, pronounced changes between the pre- and post-etching process were observed. As shown in **Figure 3-1(c)**, certain functional groups were completely removed,

such as the peak at 1050 cm^{-1} (C-H stretching) and the region from 1150 to 1400 cm^{-1} (C-O-C), along with some partial removal of functional groups around 1700 cm^{-1} (C=O and COO-) and 1950 to 2100 cm^{-1} (C-C). This indicated that the water etching process was mostly effective in removing PEG, however, residual PEG is still lingering on the PLA nonwoven mats [247, 248].

3.3.3 Thermal properties

DSC analysis of the PLA/PEG nonwoven samples before and after PEG removal is shown in **Figure 3-2** and **Table 3-3**. The results illustrate how PEG molecular weights and concentrations influenced the phase transitions and thermal behavior of the samples by shifting the melting temperature (T_M), glass transition temperature (T_G), and cold crystallization temperature (T_{CC}), as well as the heat of fusion (H_F). Before etching (**Figure 3-2b**), the DSC first heating cycle for pristine PLA showed distinct T_G, T_{CC}, and T_M peaks at 59.5, 83.7, and 168 °C, respectively, reflecting its semi-crystalline nature. After the addition of PEG 400, the 5% concentration displayed negligible changes relative to pristine PLA due to its low molecular weight and concentration in the PLA matrix, acting more as impurities rather than as a true blend component. However, the 10% PEG 400 concentration significantly affected the blend's T_G, as the external plasticization of PLA with PEG influenced its crystallization and nucleation abilities, shifting T_G from 59.5 °C (for PLA) to 44.6 °C, a reduction of 28.6%. In general, the 10 wt.% PEG-containing blends, regardless of PEG's molecular weight, showed significant shifts from the pristine PLA sample in T_G and T_{CC} zones due to the high PEG concentrations, while Tm remained minimally affected. This effect resulted from PEG's ability

to plasticize PLA by disrupting its crystalline structure, increasing the amorphous regions [249]. The PEG 2000 and PEG 4000 samples showed similar values due to the proximity of their molecular weights and similar thermal properties (T_M of ~51 and ~61 °C, respectively), in contrast to PEG 400 (T_M ~6 °C) [250, 251].

Table 3-3 Thermal properties of PLA and the PLA+PEG blends obtained from DSC.

Formulation	T_G (°C)	T_{CC} (°C)	T_M (°C)	H_F (J/g)
PLA	59.5	83.7	168.3	51.6
400-5	49.8	70.8	168.1	53.9
400-10	44.6	80.9	170.0	48.4
2000-5	54.7	81.3	169.7	52.3
2000-10	51.7	99.9	171.1	49.9
4000-5	54.8	82.2	169.7	48.9
4000-10	53.0	99.8	170.9	47.7

After etching (**Figure 3-2c**), PLA displayed two melting peaks, attributed to the generation of imperfect crystalline regions (β-crystals) formed through processing and etching operations. This shift resulted in most PLA chains melting at 156 °C instead of the previous 168 °C (7%) [252, 253]. Additionally, the T_{CC} peak of the neat PLA nearly disappeared along with the T_G, further indicating a disruption in crystal formation and content and the formation of new amorphous regions imparted from the PEGs [252, 253]. Across all blended samples, regardless of PEG concentrations and molecular weights, the T_G and T_{CC} information was lost after the

etching of PEG, essentially restoring the blends to a state more closely resembling that of the pristine PLA sample.

Upon examining the model fitting of the blend's T_G to the linear **(Eq.4)** and Fox equation **(Eq.5)**, as shown in **Figure 3-2(d)** and **Table 3-3**, it was evident that the linear equation provided a better fit with the experimental data. In contrast, the Fox equation tended to overestimate the matrix's T_G prediction as noted from the significant differences in the theoretical and experimentally obtained T_G values of the base components. In all cases, the linear model **(Eq.4)** showed an almost exact match with the experimental data; however, the Fox equation demonstrated poor fit accuracy, particularly with the 10 wt.% PEG concentrations, making it a less suitable model.

The thermal stability/degradation of PLA/PEG nonwoven samples was analyzed using TGA, both before and after PEG removal. As can be seen in **Figure 3-3**. the pristine PLA followed typical degradation behavior, displaying a single-step degradation that began around 339 °C through the loss of end groups from the main chain or ester groups [245, 254]. With the inclusion of PEG, the onset degradation temperature has reduced irrespective of the molecular weigh of the PEG, reflecting the low thermal stability of PEGs. As reported in the literature, the onset degradation temperatures of PEG 400, 2000, and 4000 are within 250 to 280 °C range, which is lower than pristine PLA (340 °C) [254–256]. Regarding the loading amount, the 5 wt.% samples tended to be more thermally stable due to the higher PLA content compared to the 10 wt.%. Additionally, plasticization tended to reduce the sample's total crystallinity,

which made the blend much easier to degrade [254–256]. Lastly, regardless of the sample's composition, the residual ash content was negligible as expected.

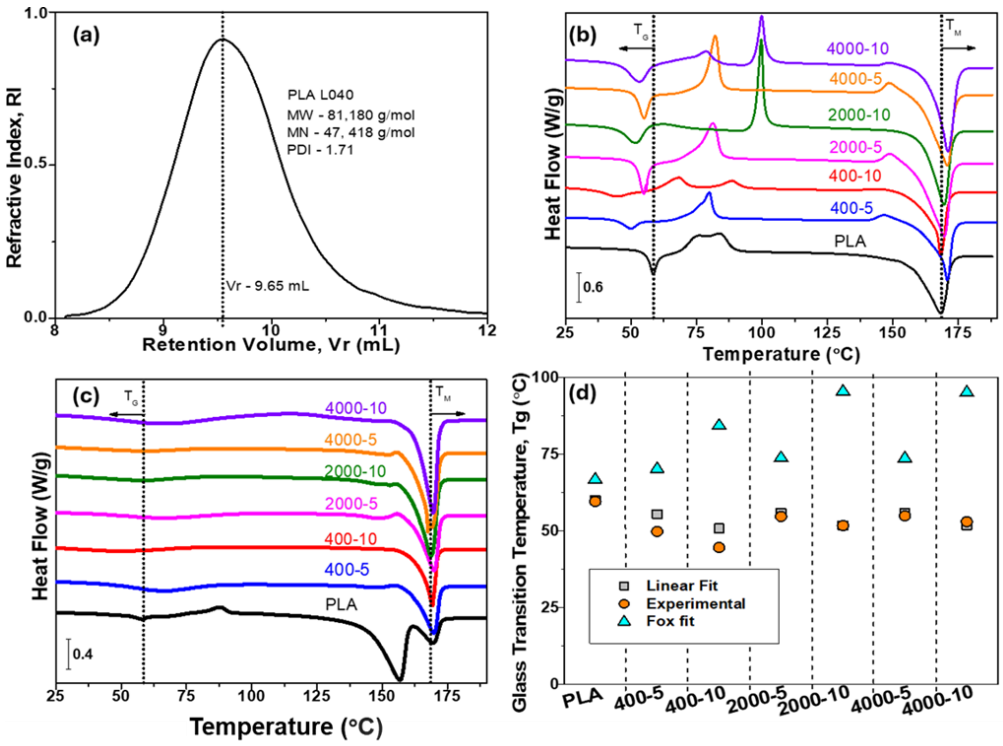


Figure 3-2 (a) GPC for the PLA L040 from Totalenergies corbion, (b) Before etching PEG DSC for the first heating cycle of PLA, PEG 400-5%, PEG 400-10%, PEG 2000-5%, PEG 2000-10%, PEG 4000-5%, PEG 4000-10% nonwoven samples, (c) After etching PEG. As well as (d) model fitting for the changes within the blends TG.

Following the etching of PEG to produce nanopores on the PLA fibers, the resultant samples showed significant deterioration in thermal stability, with reductions ranging from 12 to 35% due to physical and physicochemical changes. After partial or complete PEG etching, as shown in **Figure 3-3**, the reduction in thermal stability was due to three contributing factors. The first was the generated micropores trapping air, which would lead to quicker heat transfer through

the fiber's thickness; the second was the type and amount of PEG used [257, 258]. Thirdly, the generation of more amorphous regions resulted from the blending of PEG into PLA.

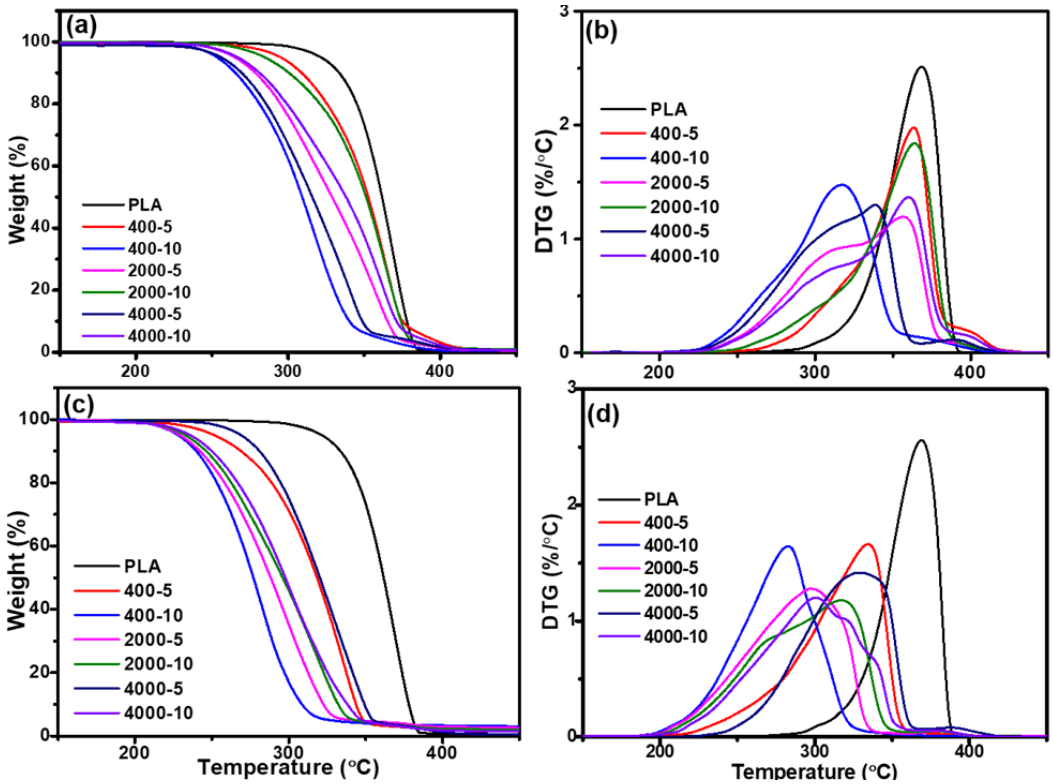


Figure 3-3 (a) TGA prior to etching PEG, (b) Derivative of weight loss prior etching PEG, (c) TGA after etching PEG, (d) Derivative of weight loss after etching PEG.

3.3.4 Physio-chemical properties

The viscosity and hence MFI of polymer resins are critical parameters for their use in melt-blowing operations that requires low viscosity and correspondingly high MFI [230]. As demonstrated in **Figure 3-4(a),** the addition of PEG clearly showed a significant impact on PLA's melt flow ratio or index (MFI), with PEG 400-10% having the most pronounced effect, resulting in a 237% increase from PLA. Although PEG 400 had a significant effect on MFI,

both PEG 2000 and PEG 4000 produced similar results to one another due to their similarity in molecular weights (MW) (e.g. 2000 and 4000 g/mol), which were 5x and 10x greater than PEG 400's MW, respectively; however all of the PEG's MWs are still well below that of the PLA's weight average MW (wMW) of 81.2 kDa with a PDI of 1.71 (see **Figure 3-2a**). When comparing the wMW of the PEGs to that of the PLA's, found by GPC, it is be understood the inclusion of a lower molecular weight compound (PEG) to a higher one (PLA) the amount of will dilute the baseline properties of the PLA such as the blend's T_G, the blend's viscosity, and mechanical properties. Overall, it was noted that the blending of low concentration of PEG with PLA increased the MFI, which is a desirable attribute for melt-blowing process.

Examining the difference between 5 and 10 wt.% PEG loading level, regardless of PEG's MW variability, the 10 wt.% PEG formulations resulted in greater plasticization effects due to the higher inclusion of a high MFI compound, a trend also noted in the literature, resulting in more amorphous regions [259, 260]. Overall, the addition of PEG into the PLA matrix enhances the molecular mobility of the PLA structure, resulting in an increase in MFI, which indicated a reduction in the matrix's viscosity and thus affecting the interactions of molecular chains [259].

Examining the shear viscosity **(Figure 3-4b)**, the viscosity of the PEG-containing blends fell below that of the baseline PLA. Moreover, similar to the MFI tests, the PEG 400-10% system had the lowest shear viscosity. Through examination of the shear viscosity, it is clear that a linear decrease occurred with increasing shear rates in both the baseline PLA and the blends, indicating shear-thinning characteristics. It is typically accepted that a reduction in a system's shear viscosity represents a reduction in chain entanglement as well as orientation along the

flow direction when polymer melts are exposed to increasing shear rates [261]. At exceedingly high shear rates, the disentanglement and orientation phenomenon become more noticeable [261].

The corrected shear stress, shown in **Figure 3-4(c)**, followed the same trend as the shear viscosity and the MFI, with pristine PLA having the highest resistance to flow due to the highest shear stress, and the PEG 400-10% blend displaying the least flow resistance. Additionally, it can be observed that there is a linear relationship between log τ and log γ, indicating that these materials can be described as power law fluids, as shown in **(Eq.12)** and **Table 3-4**, where ***K*** is the consistency of the polymer melt and n is the non-Newtonian index [261]. Since the value of ***K*** is associated with melt viscosity, a high level of ***K*** indicates higher melt viscosity and overall pseudoplasticity. As the overall blend's viscosity decreases, so should the ***K*** parameter [261]. This means that pristine PLA acts more as a pseudoplastic fluid, but after the addition of PEG, its pseudoplasticity decreased.

$$\tau = K\gamma^n \qquad \textbf{(Eq.12)}$$

When examining the relationship between angular frequency and complex viscosity in **Figure 3-4(d)**, all blends exhibited a Newtonian plateau from 0.1 to approximately 100 rad/s, after which they all experienced shear-thinning characteristics [262, 263]. Again, PEG 400-10% had the most severe reduction in complex viscosity compared to the baseline PLA sample. Regardless of the PEG molecular weight, the complex viscosity drastically decreased, which is correlated with changes in the total free volume and chain mobility, as melt viscosity is overly sensitive to macromolecular changes [259, 264]. For the quantitative examination of

the complex viscosity, the zero-shear viscosity was found using the Cross model from **(Eq.10)**. The zero-shear viscosity results align with the previous discussion, indicating that the addition of PEG caused a significant reduction in the material's viscosity due to the plasticization effect, with the most significant drop found in the PEG 400 blends.

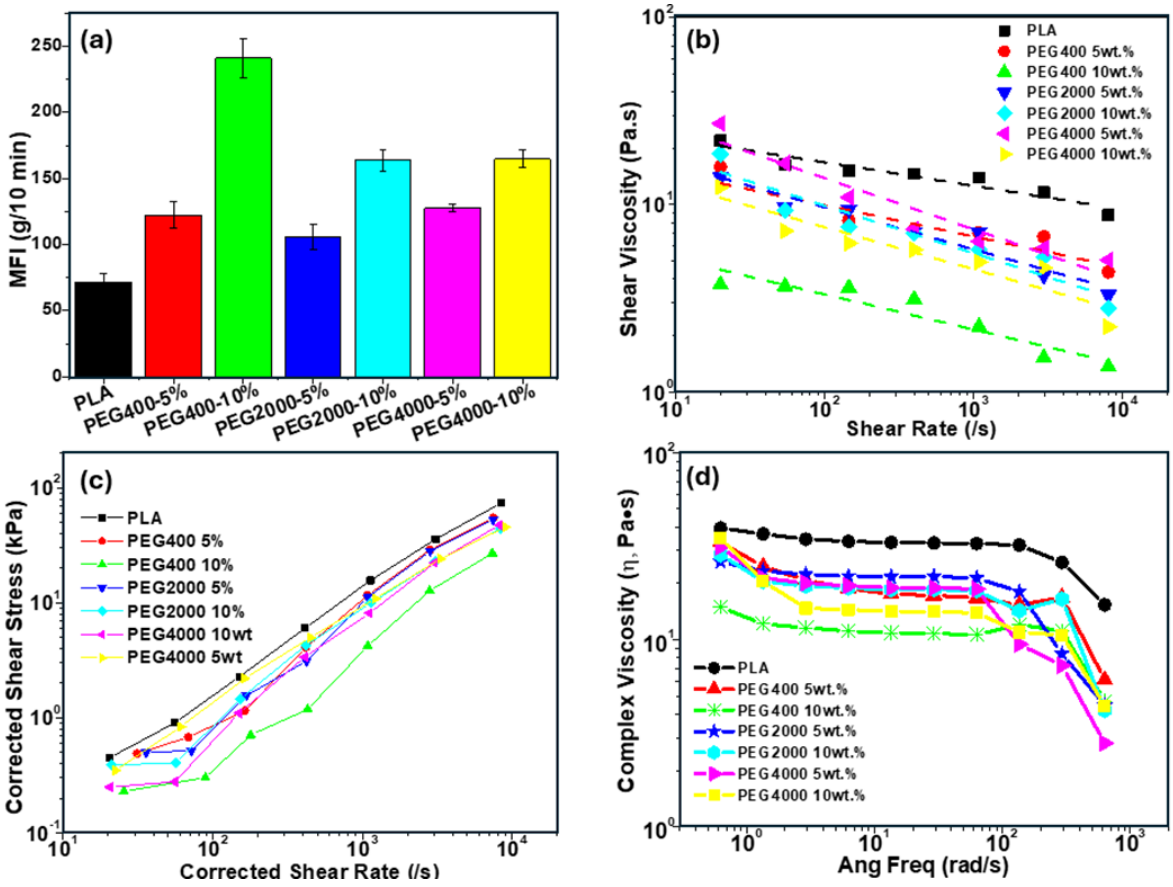


Figure 3-4 (a) MFI for PLA and the various PLA PEG blends, (b) Shear viscosity from capillary rheometry for PLA and the various PLA PEG blends, (c) Shear Stress from capillary rheometry for PLA and the various PLA PEG blends, and (d) Complex viscosity from dynamic rheometry for PLA and the various PLA PEG blends.

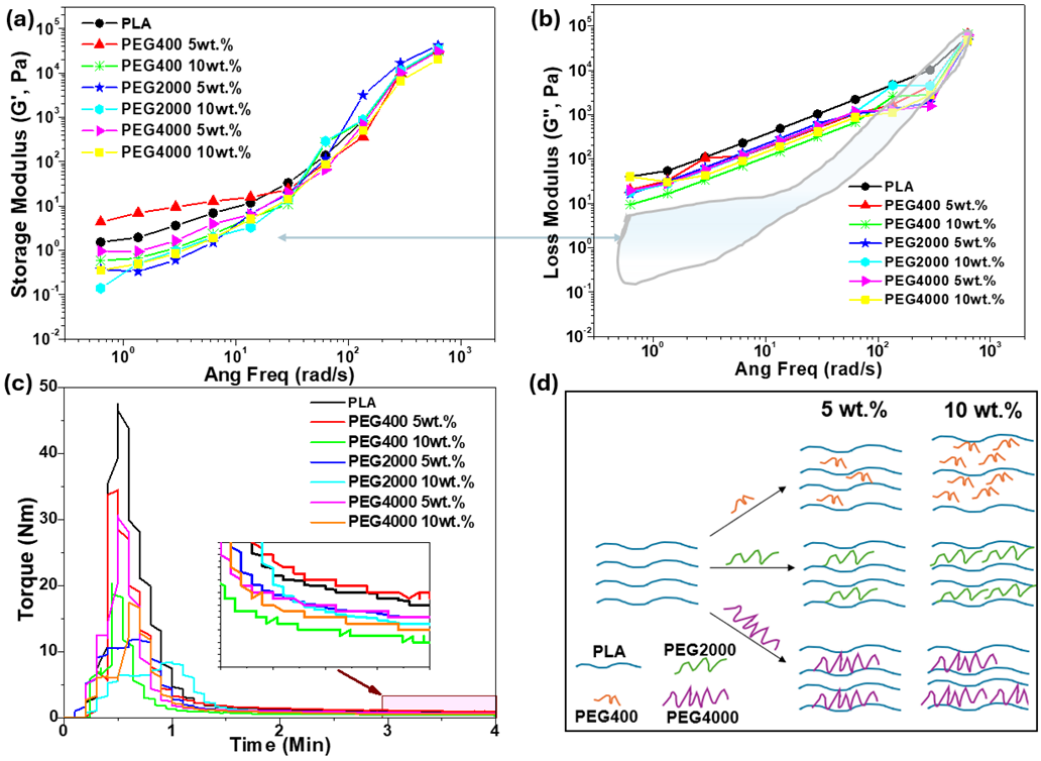


Figure 3-5 (a) Storage modulus curve (G'), from parallel plate, for PLA and its various PEG blends, (b) Loss modulus curve (G"), from parallel plate, for PLA and its various PEG blends, (c) Torque rheometer curves for PLA and its various PEG blends while melt blending, and (d) PLA blending schematic with PEG and different MW contents [263].

As shown in **Figure 3-5(a)**, the storage modulus (G') continuously increased with each subsequent rise in angular frequency, with the majority of the PEG blends falling below that of the pristine PLA. This is due to the reduction in intermolecular forces of the PLA as it is plasticized, decreasing the chain entanglement density of the polymer and resulting in greater free volume [259, 262, 263]. However, it can be seen that PEG only had a pronounced effect at low to intermediate angular frequencies, while at high angular frequencies, the G' values were similar. This non-terminal characteristic behavior is attributed to changes in the shape of

the discrete phase of the polymer system during deformation processes (e.g., shape relaxation) [264]. The low to mid region indicates the material's stress relaxation response and the motion of the polymer as a whole, suggesting that PEG is enabling structural changes [264].

Table 3-4 Calculated K and n values for PLA and its PEG blends at 190 °C.

Formulation	η_0, Zero-shear viscosity (Pa•s)	K (kPa▪s)	n	R^2
PLA	40	21.90	0.0219	0.9616
PEG 400-5%	33	14.18	0.0142	0.9818
PEG 400-10%	14	8.84	0.0088	0.9819
PEG 2000-5%	26	12.51	0.0125	0.9975
PEG 2000-10%	20	16.90	0.0169	0.9985
PEG 4000-5%	21	21.29	0.0213	0.9851
PEG 4000-10%	19	11.07	0.0111	0.9961

As shown by the G' silhouette in the Loss modulus curve (G") in **Figure 3-5(b)**, all samples' loss modulus remained above that of the G', indicating that all samples followed viscous behavior at low frequencies. Note that the silhouette was used to simplify and declutter the graphs for easier and quicker analysis. Similar to the G', but to a lesser extent, all samples' G"

values rose with increasing angular frequency. It should be noted that there were no moduli or frequency crossover points between individual samples' G’ and G”, providing no insight into changes within the systems' MW.

When examining **Figure 3-5(c),** it was found that the PLA had the highest residual torque after four minutes of mixing, with PEG 400-10% having the lowest and the others falling in between. This is better explained by **Figure 3-5(d)**, where a schematic rendering shows how the PEG penetrates the PLA chains to increase its free volume and chain mobility. PEG 400, having a 5 to 10x lower MW, is able to easily penetrate through adjacent PLA chains and increase the space between them, while the larger PEG chains have a comparatively higher difficulty in penetrating the PLA chains [263]. The torque rheometry curves also revealed that at 190 °C and between 1.5 to 4 mins, the torque of both the PLA and the blends decreased slightly from its initial fall, indicating that the blends were well melted under the set processing parameters [265–267]. The PEG blends had significantly lower torque values compared to the pristine PLA due to their lower melt viscosity, indicating better flow and less pseudoplastic behavior, which is consistent with the capillary rheometer results [266].

3.3.5 Fiber morphology

The SEM images in **Figure 3-6** (**a - g**) illustrate the fiber morphology and fiber distributions of PLA and PLA/PEG nonwoven blends before etching. These images collectively demonstrate how varying the PEG MW and content in the PLA matrix influences the fiber structure and integrity, such as mean fiber diameter and distribution. As noted in **Figure 3-6(a - g),** all formulations generated smooth and fairly dense non-wovens, with uniform distribution.

Overall, the melt-blown non-wovens demonstrate fiber diameters in the range of 1.05 – 2.91 μm. The low molecular PLA (Mn 47,418 g/mol, **Figure 3-2**a) with high melt flow rate of 56 g/10 min at 190 °C (**Figure 3-4a**) allowed the generation of fine fibers via the melt blowing process. The incorporation of PEG in the PLA has plasticized the PLA and led to lower viscosity (**Figure 3-4c**) and high MFI (**Figure 3-4a**). Sample with the highest MFI, the PLA/PEG 400-10% (**Figure 3-4a**) provided the finest morphology (**Figure 3-6c**) with average fiber diameter of 1.05 μm. On the other hand, PLA/PEG 400 – 5% with lower MFI showed increased fiber size and broader distribution.

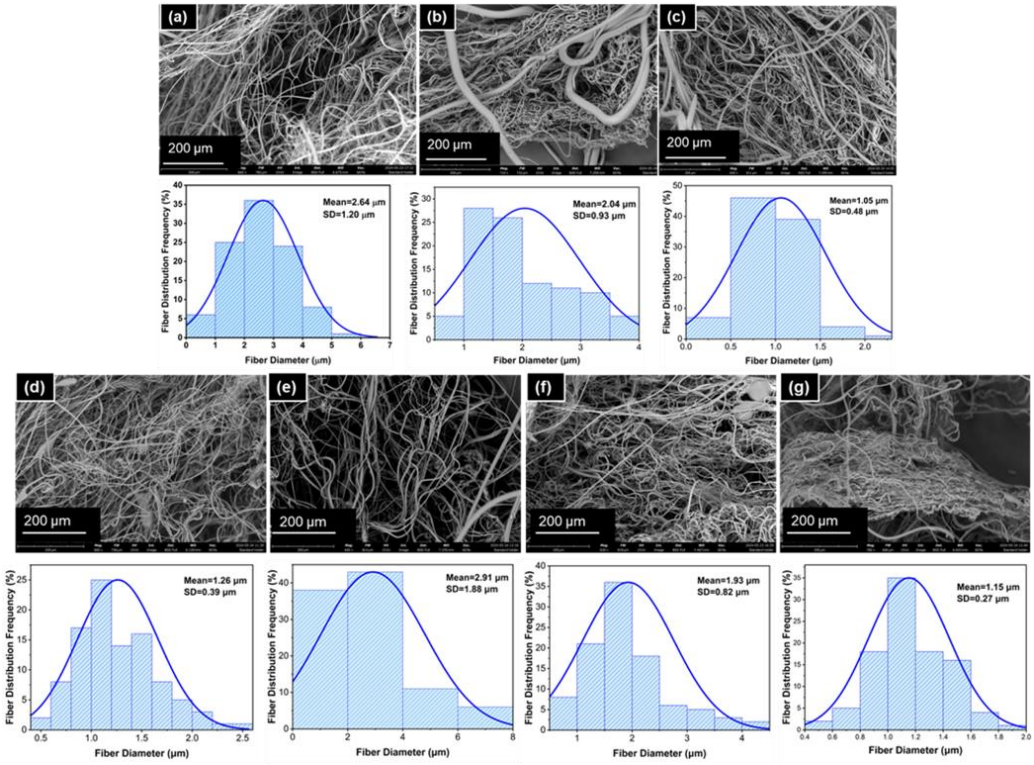


Figure 3-6 SEM images and fiber distributions of non-etched samples (a) Pristine PLA; (b) PLA/PEG 400-5%; (c) PLA/PEG 400-10%; (d) PLA/PEG 2000-5%; (e) PLA/PEG 2000-10%; (f) PLA/PEG 4000-5%; (g) PLA/PEG 4000-10%.

Small fiber diameter attributed to the high MFI of the blend is noticeable in PLA/PEG 400 – 10% and PLA/PEG 4000 – 10% samples. However, during the etching of the PEG to generate porous melt blown non-wovens in the subsequent process led to fiber breakage **(Figure A1 in appendix A)**. The PEG serves as a scarifying agent in the PLA matrix, designed to be removed during the etching process in order to generate pores in the absence of PEG molecules. During the etching process, the PEG is dissolved in water and removed from the structure, leaving behind numerous pores, as depicted in **Figure 3-7** and **3-8**. **Figure 3-7(a-g)** displays the morphology of fibers after the etching removal of PEG. In the low molecular weight loaded PLA melt blown nonwovens, i.e. PLA/PEG 400 – 5% and PLA/PEG 400 – 10%, an increase in the pore size and number was noted. The PEG-2000 based samples displayed a much clearer pore structure (**Figure 3-7c** & **d**). The increase in the PEG content from 5% to 10% lead to a highly porous structure that resembles a crocodile skin. On the other hand, while the PLA/PEG 4000 – 5% melt blown nonwovens displayed rough and porous surface structure, an increase in PEG to 10% led to weak and brittle fibers. This is likely due to the high MFI of the PLA/PEG – 10% formulation (**Figure 3-4a**) in conjunction with the enhanced compatibility **(Table 3-2)**. The enhanced compatibility, which could have led to improved dispersive and distributive mixing of the PEG in the PLA, could have caused weakened fibers upon the leaching out the PEG from the fiber structure.

The SEM micrographs in Figure 8 illustrates a zoomed image of nanopores creation along entire single fiber strand within the PLA/PEG 400-10% fibrous network. **Figure 3-8(a)** shows a single fiber strand of PLA containing PEG 400-10%, demonstrating a solid, non-porous structure within the nonwoven matrix prior to etching. After etching removal of PEG,

numerous pores were generated **(Figure 3-8b)** over the fiber surface. This pore formation was consistent across all formulations **(Figure 3-7)** with a significant increase in the fiber porosity

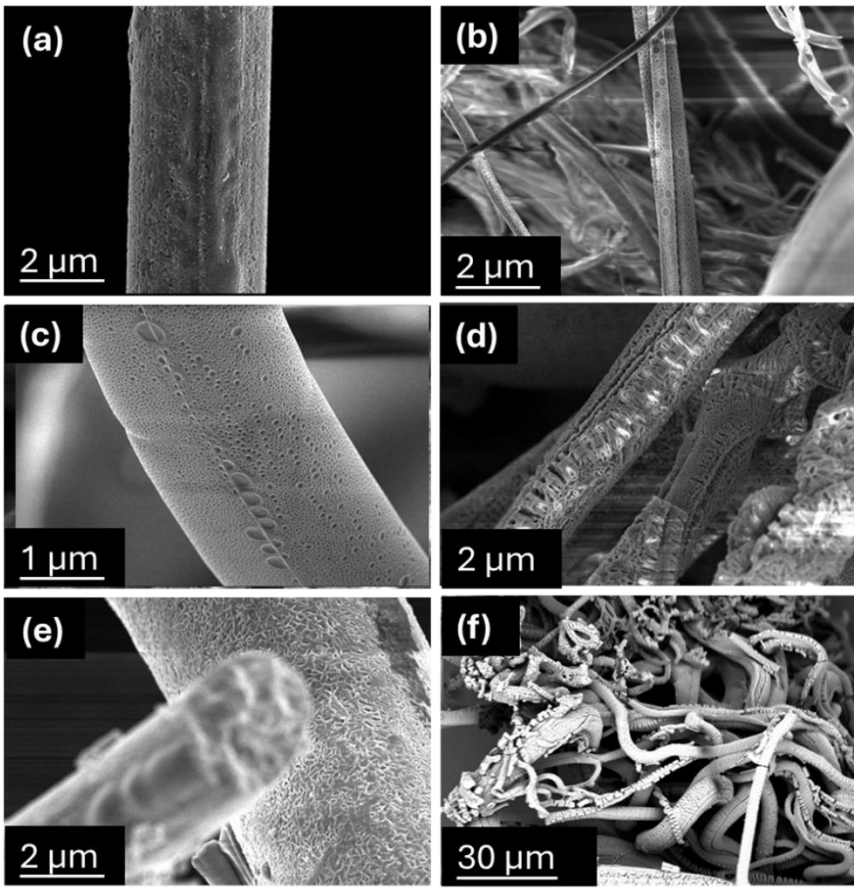


Figure 3-7 Post-etching SEM images and fiber distributions of (a) PLA/PEG 400-5%, (b) PLA/PEG 400-10%, (c) PLA/PEG 2000-5%, (d) PLA/PEG 2000-10%, (e) PLA/PEG 4000-5%, and (g) PLA/PEG 4000-10%.

and likely the surface area making it appealing for practical applications, including air filtration, water filtration, CO_2 capture, etc. To demonstrate its application in practical The SEM micrographs in **Figure 3-8** illustrates a zoomed image of nanopores creation along entire single fiber strand within the PLA/PEG 400-10% fibrous network. **Figure 3-8(a)** shows a

single fiber strand of PLA containing PEG 400-10%, demonstrating a solid, non-porous structure within the nonwoven matrix prior to etching. After etching removal of PEG, numerous pores were generated (**Figure** 3-**8b)** over the fiber surface. This pore formation was consistent across all formulations (**Figure 3-7**) with a significant increase in the fiber porosity and likely the surface area making it appealing for practical applications, including air filtration, water filtration, CO_2 capture, etc. To demonstrate its application in practical materials, the air filtration efficiency of selected non-etched and etched (porous) melt blown fabrics were investigated and presented in the subsequent section.

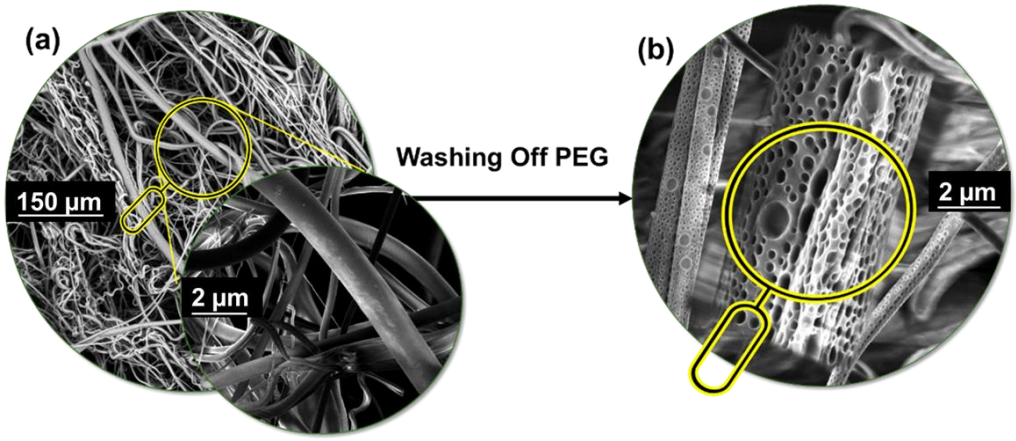


Figure 3-8 The effect of PEG etching process on PLA/PEG 400-10% fibers causing PEG removal from the substrate and resulting in creating nanopores within a single fiber strand. SEM image of PLA/PEG 400-10% (a) Perior etching off the PEG; (b) After etching the PEG.

3.3.6 Air filtration performance and pressure drop

The air filtration performance and pressure drop (filter backpressure) of three selected nonwoven samples, PLA, PLA/PEG 400-10%, and PLA/PEG 2000-10% (before and after etching) was evaluated to assess how generating pores and enhancing porosity affected their

filtration capabilities. The filtration setup and possible mechanism of the aerosol filtration is displayed in **Figure 3-9 (a-c)**. For the non-etched samples, the three selected samples showed filtration efficiency (PFE) of 57.24 – 64% (**Figure 3-9d**). The slightly higher filtration efficiency of the PLA/PEG 400-10% sample (64%) could be attributed to the finer fiber morphology (average fiber diameter 1.05 µm) and compaction of the non-woven mat, which was also noted as a slightly increased pressure drop (**Figure 3-9e**) due to resistance to air flow. As noted in **Figure 3-6c** and **Figure A1a (Appendix A)**, the etching caused substantial fiber breakage to PLA/PEG 400-10%, due to its finer fiber dimension. As a result, the nonwoven mat of the etched PLA/PEG 400-10% presented inferior filtration efficiency (50.44%) and caused very small pressure drop (**Figure 3-9d & e**) despite the observed porosity. On the other hand, the PLA/PEG 2000-10% displayed outstanding particulate filtration efficiency (~85%) without any further surface treatment. This is attributed to the fine and numerous pore formation on the fiber of the resulting nonwoven mats (**Figure 3-7d**). The pore distribution on the individual fibers constituting the nonwoven mats after the PEG etching is presented in a magnified SEM image presented in **Figure 10 (a – b).**

The etched PLA/PEG 2000-10% fibers formed dense, uniformly distributed, and small pores (0.12 ± 0.05 µm) which are capable of capturing the 0.3 µm particulates employed in this study (**Figure 3-10a**). While the etched PLA/PEG 400-10% fibers also displayed appealing pore sizes (0.46 ± 0.2 µm), the relatively inferior filtration efficiency is related to the fiber damage due to the etching process (**Figure 3-10b**) that compromised the nonwoven mats integrity.

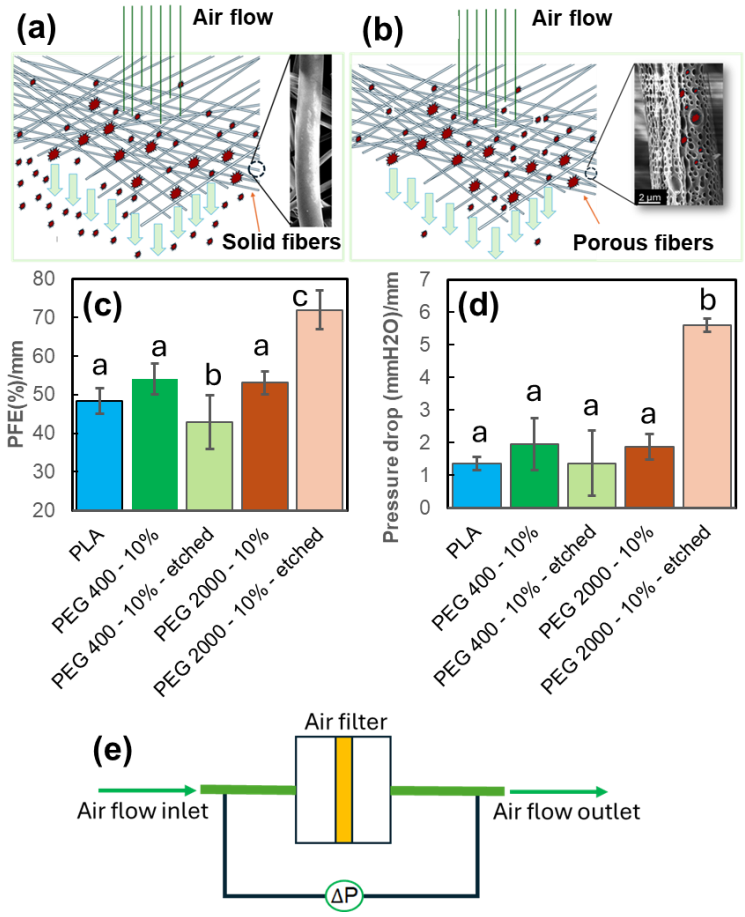


Figure 3-9 Schematics of (a) bulk non-woven mats capturing microparticles, (b) porous non-woven mats capturing microparticles, (c) schematic representation of air filter testing system, (d) particle filtration efficiency of nonwoven mats, and (e) pressure drop.

The rheology variation between the PEG grades (MW) and PLA (**Section 3.1**) is a crucial parameter in determining the phase morphology of the blend that affects the porous structure and PFE of the fibers post etching. The PEG 2000, with its larger MW and viscosity compared to PEG 400, interacts better with the PLA and distributes better in the PLA phase [268, 269]. The enhanced dispersion of the PEG 2000 improves the fibers bulk properties, creating pores

that extend beyond the fiber surface and improve particle capture (**Figure 3-9b**). In contrast, PEG 400, with its lower MW, has inferior compatibility with PLA (**Table 3-2**) and tend to have inferior distribution (and agglomeration) in the PLA phase, leading to catastrophic fiber damage during the etching process. As a result of smaller and deeper pores, the high PFE value of PLA/PEG 2000-10% is accompanied by a significant pressure drop as this will result in higher airflow resistances [270]. In contrast, the pristine PLA and the non-etched samples of PLA/PEG 400-10% and PLA/PEG 2000-10% exhibited a moderate pressure drop. These results underscore the potential of the PLA/PEG 2000-10% formulation in achieving superior particulate filtration performance, making it a promising candidate for HEPA filter applications.

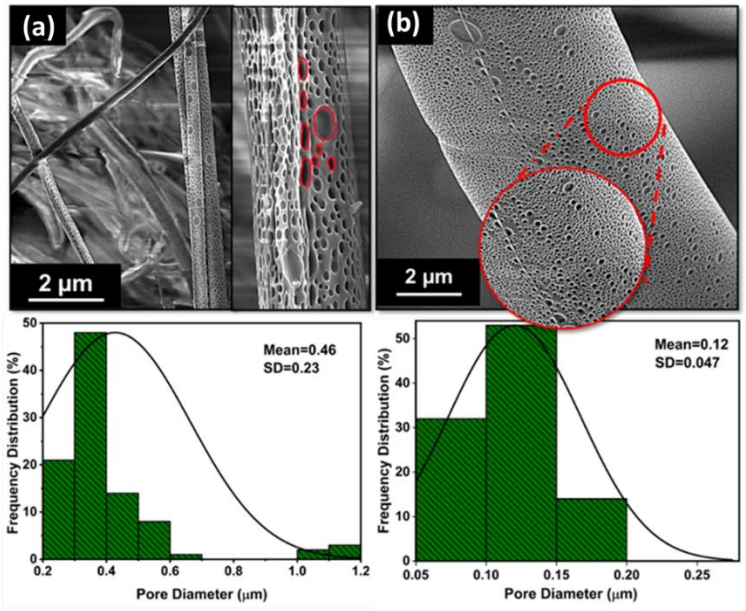


Figure 3-10 Post etching SEM images and histograms of (a) PLA/PEG 400-10% (c) PLA/PEG 2000-10%.

3.4 Conclusions

This study investigated the design of porous nonwoven mats via a scalable melt-blowing process. A water-soluble polymer, PEG, was incorporated into high melt-flow rate PLA as a sacrificial additive through melt blending. Due to the low molecular weight and high MFI of the PEG variants (MW 400 g/mol, 2000 g/mol, and 4000 g/mol), the resulting blends exhibited low viscosity and high MFI, making them well-suited for melt-blowing into nonwoven mats. The melt-blown fibers were subsequently etched with water to remove the sacrificial PEG, generating porous PLA nonwoven mats. The post-etching mat integrity varied depending on the compatibility of each PEG grade with PLA, with PLA/PEG 2000 (5% and 10%) yielding high-quality porous mats due to a balanced compatibility and efficient PEG removal. SEM analysis confirmed that the PEG removal produced numerous nanopores, as small as 50 nm, distributed throughout each fiber strand in the PLA/PEG 2000 – 10% samples. Air filtration tests further validated the success of this approach, showing that the porous PLA/PEG 2000 – 10% nonwoven filters achieved ~85% filtration efficiency for 0.3 μm particles without any surface charging treatment, substantially outperforming baseline PLA and non-etched counterparts. This enhanced filtration efficiency is attributed to the optimized pore structure and increased surface area, facilitating effective particle capture. Overall, this approach represents a significant advancement in creating highly porous, robust, and sustainable nonwovens for particulate air filtration, with promising potential for other applications such as battery separators and water treatment membranes.

Chapter 4

Towards scalable antimicrobial air filters: rose bengal/polypropylene melt-blown nonwoven filters

The COVID-19 pandemic has highlighted the limitations of conventional face masks, which primarily function as aerosol physical filters without inherent antibacterial or antiviral properties. Surgical masks, which depend on electrostatic filtration, lose their efficacy as these charges dissipate within a few hours of use. This study aims to address these shortcomings by developing advanced melt-blown nonwoven filters using polypropylene (PP) and Rose bengal (RB) as a photosensitizer. The impact of varying processing temperatures during the fabrication of melt-blown nonwoven's fiber morphology, filtration efficiency, and antibacterial properties was systematically investigated. The incorporation of RB is intended to enhance antibacterial activity. Results show that processing temperature significantly influences fiber diameter, with optimized filters demonstrating superior antibacterial performance, particulate filtration efficiency (PFE) and breathability compared to conventional masks. These filters with advanced functionality present promising improvements in antimicrobial protection from the ambient environment and durability, contributing to the development of more effective and long-lasting personal protective equipment (PPE).

4.1 Introduction

The urgent need for effective air filtration and infection control technologies has gained significant attention, particularly following the COVID-19 pandemic. While traditional masks and filtration systems primarily target particulate matter, they often lack the ability to actively

deactivate or eliminate pathogens [271]. The pandemic has demonstrated the critical role of face masks in safeguarding public health by preventing the spread of airborne pathogens. Although effective at filtering aerosols, conventional surgical masks do not possess inherent antibacterial and antiviral properties, limiting their capacity to provide comprehensive protection against microbial threats [272]. Enhancing the antimicrobial performance of masks has therefore emerged as a priority, offering an additional layer of defense, especially in high-risk environments, such as hospitals, crowded public spaces, and quarantine facilities. By integrating antimicrobial properties, surgical masks could actively kill or destroy susceptible bacteria and viruses on contact, thereby reducing the risk of cross-contamination and extending the lifespan of the mask [273].

Several methods have been proposed to bolster the antimicrobial capabilities of surgical masks. A common approach involves coating the fibers with antimicrobial agents, such as silver nanoparticles [274], copper ions [275], or natural extracts like chitosan [276]. These materials have been shown to inhibit bacterial growth and provide some degree of antiviral activity. Another strategy focuses on incorporating electrostatic charges to enhance particle capture, indirectly reducing microbial transmission [277]. However, the masks that are reliant on electrostatic charge decreasing effectiveness as these charges dissipate within a few hours of use, particularly in humid conditions [278]. Researchers have also explored embedding photosensitizers, such as RB, which generate reactive oxygen species (ROS) when exposed to light, effectively deactivating pathogens on the mask's surface [279]. Recent advancements in research on new-generation surgical masks have highlighted the usage of various materials and

adoption of different methods [280] to enhance both filtration efficiency and antimicrobial properties on the disposable masks. These innovations not only improve protective equipment but also inform advancements in broader air filtration technologies.

One notable innovation is the fabrication of hybrid hydrophobic composite air filtration membranes that incorporate aluminum oxide nanoparticles alongside silver nanoparticles, achieving high particulate filtration efficiency (PFE) and substantial antibacterial activity [281]. These membranes effectively detoxify chemical contaminants such as volatile organic compounds (VOCs) like formaldehyde and benzene, although a slight increase in resistance occurs with higher Al_2O_3 concentrations [282]. Such developments demonstrate the importance of multifunctional materials in addressing both air quality and health concerns that are developed from particulate virulent pathogens present in the ambient air. Alongside, the development of biodegradable nanofibers and innovative functional nanofibers, embedding the RB dye represents another promising avenue in functional air filtration for masks or air filters [283]. One of the studies reported that the cellulose acetate nanofibers embedding the RB exhibit significant antiviral efficacy against the φx174 virus under visible light irradiation, showcasing the potential of photosensitizers to enhance the base material's performance [283]. Investigation into photosensitized electrospun membranes has demonstrated RB's ability to effectively capture and inactivate airborne viruses, achieving over 97% inactivation of mouse hepatitis virus (MHV-A59) within just 15 minutes of light exposure [284]. This dual-action approach not only enhances filtration capabilities but also addresses the critical need for additive materials that actively disinfect pathogens. As global demand for effective and safe filtration solutions

continues to rise, understanding how functional additives like RB interact with base polymers such as PP is crucial. In this research the synthesis of effective antiviral agents by integrating RB into melt-blown PP nonwoven fabrics is investigated. By incorporating RB as a photosensitizer, the study investigates its effects on material properties, including antibacterial performance, melt flow index (MFI), mechanical strength, thermal stability, and filtration performance. This research provides critical insights into the interactions between functional additives and base polymers, paving the way for more effective and environmentally friendly filtration materials.

4.2 Materials and Processing methods

4.2.1 Materials

The primary substrate utilized in this study was polypropylene (PP), grade PP6936G2, powder, (MFI 1550 g/10 min ASTM D1238) supplied by ExxonMobil. Rose bengal (RB), a photoactive dye with a molecular weight of 1017.64 g/mol, sourced from Sigma-Aldrich (Oakville, ON, Canada) was incorporated in the PP to enhance antibacterial properties of the melt-blown nonwovens. Agar powder (bacteriological grade), phosphate-buffered saline (PBS), and Dulbecco's phosphate buffer saline solution were sourced form Sigma-Aldrich (Oakville, ON, Canada).

4.2.2 Melt-blown processing

PP and PP/RB melt-blown nonwovens were produced using an in-house melt-blown extrusion system. Pristine PP melt-blown nonwoven samples were fabricated and served as the control, establishing a baseline for fiber morphology and structural comparison **(Figure 4-1 (a))**.

Blends of PP with 2% RB were fed into the extruder, where process parameters including melt zone temperatures, nozzle temperatures, air temperature, air pressure, and screw speed were optimized **(Table 4-1)**. Due to the novel nozzle design feature of the meltblown process, we could use higher air temperature (270°C) for fiber attenuation, making the fiber creation feasible by presence/addition of the Rose Bengal. Typically, the operating meltblown air temperature is lower. To evaluate the impact of RB incorporation, the PP/RB nonwovens were produced at three different nozzle temperatures (210 °C, 220 °C, and 240 °C) shown in **Figure 4-1 (b - d)**, while maintaining the other process parameters constant.

Table 4-1 Melt-blown process parameters for the fabrication of PP/RB nonwovens.

Formulations	Melt zones temp (°C)	Nozzle temp (°C)	Air temp (°C)	Distance (in)	Flow rate (SCFM)	Air pressure (psi)
PP (100%)	180 – 190	210	270	5 in	2	100
PP/RB (2%)	180 – 190	210	270	5 in	2	100
PP/RB (2%)	180 – 190	220	270	5 in	2	100
PP/RB (2%)	180 – 190	240	270	5 in	2	100

4.2.3 Characterization

4.2.3.1 Parallel plate rheology

To evaluate the flow properties in the molten phase, a HAAKE MARS III rheometer with parallel plate geometry was used in accordance with ASTM D4440. The samples had a

thickness of 2.5 mm and a diameter of 25 mm. The rheological analysis involved a frequency sweep at constant strain and gap distance, with temperature set at 190 °C and a strain rate ranging from 0.1 to 100 s^{-1} (0.6283 to 628.3 rad/s), applied at a strain of 0.01% and a gap of 1 mm.

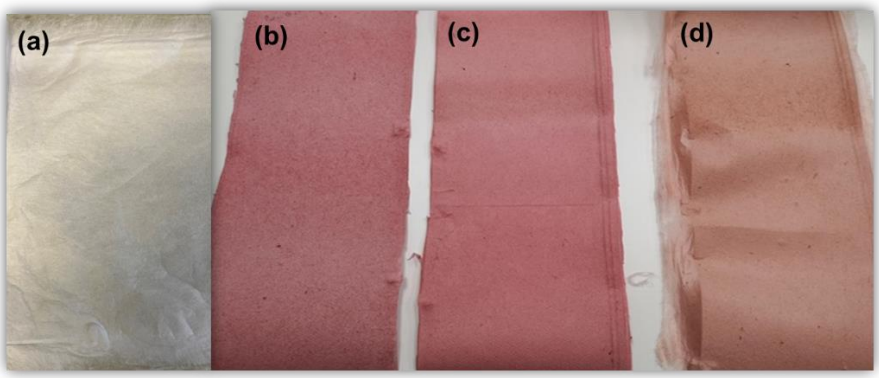


Figure 4-1 Melt-blown nonwovens fabricated at different nozzle temperatures (a) Pristine PP at 210 °C, (b) PP/RB at 210 °C, (c) PP/RB at 220 °C, (d) PP/RB at 240 °C.

4.2.3.2 Melt flow index (MFI)

The MFI was evaluated with a Dynisco Melt flow Indexer model 4002 at a temperature of 230 °C and a load of 2.16 kg. The half die (1 mm) and piston were preheated for 15 minutes at the designated temperature before testing. Each sample was run through the MFI machine in about 7 min, with sample collection taking place during laminar flow, approximately halfway through the process.

4.2.3.3 Thermal properties

The thermal stability of the polymers was evaluated with thermogravimetric analysis (TGA), which was carried out using a TA Instrument 550 (New Castle, DE, USA) to evaluate the

thermal stability and decomposition behavior of the samples. The temperature was ramped from room temperature to 500 °C at a rate of 20 °C per minute in a nitrogen atmosphere. The nitrogen flow rate was adjusted to 60 ml/min, complemented by a balanced flow of 40.03 mL/min.

The thermal transitions were evaluated using a DSC (2500, TA Instrument Co. Ltd., New Castle, DE, USA). Samples were subjected to an initial heating from 10 to 200 °C at a rate of 10 °C/min in a nitrogen atmosphere with a flow rate of 20 mL/min, followed by a cooling phase back to 10 °C at the same rate. The analysis was conducted based on data collected during the second heating cycle.

4.2.3.4 Fourier transform infrared spectroscopy (ATR-FTIR)

FTIR analyze (Nicolet 6700 NEXUS, Thermo-Fisher Scientific) with an attenuated total reflection (GladiATR from Pike technologies) technique was used to analyze the chemical functional groups. The FTIR was operated in transmittance mode, recording spectra from 500 to 4000 cm^{-1} at a resolution of 4 cm^{-1} over 32 scans.

4.2.3.5 Scanning electron microscopy (SEM)

The fiber morphology of the melt-blown nonwovens was analyzed using a Phenom desktop SEM (ThermoFisher Scientific Inc, Waltham, MA, USA). This examination focused on observing the resulting fibrous mat with the RB incorporated into the PP.

4.2.3.6 Tensile testing

The mechanical properties of PP and PP/RB nonwovens, including the tensile strength, tensile modulus, and elongation at break, were assessed using a Universal Testing Machine (UTM, AGS-X series, Shimadzu, Japan). Testing was conducted in the tensile mode at room temperature, with specimens measuring 50 mm in gauge length and 10 mm in width. A 500 N load cell was employed, and the strain rate was set to 100 mm/min. The reported values represent the mean and standard deviation (SD) from a minimum of five tested specimens.

4.2.3.7 Air filtration test

The filtration performance, including particulate filtration efficiency (PFE) and pressure drop (dp), of the nonwoven samples was assessed using the PALAS PMFT 1000 system. Testing was conducted with a 0.3 μm NaCl aerosol at a flow rate of 85 L/min, a widely used condition for evaluating surgical mask filter efficiency.

Antimicrobial tests

The antimicrobial effects of the Rose Bengal (RB) in polypropylene (PP) based nonwoven for mask applications were tested against a Gram-negative *Escherichia coli* (*E. coli*; MG1655) and Gram-positive *Bacillus subtilis* (*B. subtilis*; 168) bacteria. Here, we followed the procedure mentioned in our previous work [285], with minor modifications as necessary. Two modes of antimicrobial tests were conducted to evaluate the nonwovens' antimicrobial efficacy: the dynamic shake flask tests and the static contact surface tests. Regardless of the modes of the utilized tests, overnight cultures of *E. coli* and *B. subtilis* were prepared at first by the addition of starter culture to a 25 mL lysogeny broth (LB), where the LB consisted of 10 g L^{-1} tryptone,

5 g L^{-1} yeast extract, and 10 g L^{-1} NaCl in sterilized distilled water. The agar media for the static contact test consisted of similar ingredients mentioned above but supplemented with 15 g L^{-1} of Agar powder (bacteriological grade, Sigma Aldrich). All culture media, including broth and bacteriological agar solution, buffers, Erlenmeyer flasks, bacterial colony spreader (metal), and pipette tips were sterilized by autoclaving for 20 min at 120°C. Additionally, the transfer of all media and set-up of all experiments were conducted using an aseptic technique under a Class II A2 Biosafety Cabinets (BSC, Labconco®).

4.2.3.8 Dynamic shake flask tests

The PP-based melt-blown nonwovens were precisely cut into optimized squares of 4 cm x 4 cm dimension and sterilized under UV for 30 min at room temperature (RT) within the Class II A2 BSC. The post-sterilized nonwoven samples were then placed into pre-sterilized flasks containing 16 mL of sterilized LB broth to maintain a surface area to volume ratio of 1 cm^2 mL^{-1}. The flasks were then inoculated with 0.64 mL cultures of bacteria (each bacterium in separate sets of experiments) and incubated at 37 °C and 150 rpm for 24h, with light in the Eppendorf Innova® S44i incubator shaker. 1 mL sample of the LB media was withdrawn at every 2 h intervals for the first 8 h followed by a final sample of 1 mL LB media after the 24^{th} h mark, without replenishing the fresh sterilized LB for any withdrawals. The optical density (OD) at 600 nm was observed using a Beckman Coulter DU 530 Life Science UV/Vis spectrophotometer to track the dynamic growth of the bacterium in each withdrawn sample. The experiments were carried out in duplicate for each nonwoven sample on each bacterium,

along with an additional test conducted in parallel, called ‘control’ for each bacterium without the fabric sample.

4.2.3.9 Contact Surface Test

For this mode of antibacterial tests, the PP-based nonwovens were cut into squares of 2 cm x2 cm and sterilized using UV (30 min in a Class II A2 BSC). An arbitrarily small portion of the overnight culture of each bacterium was diluted with the sterile LB broth to result in an OD-600 between 0.07 and 0.08 (Beckman Coulter DU 530 Life Science UV/Vis spectrophotometer). Each of the sterilized nonwoven samples was then placed in a sterile aluminum dish and 0.15 mL (150 µL) of the diluted bacterial culture was pipetted on the surface of the nonwoven. They were then placed in an airtight container at room temperature under light along with an extra aluminum dish containing DI water to prevent evaporation of inoculum. After 24 h, 50 µL of the inoculum was withdrawn from the aluminum dishes and diluted with sterile phosphate-buffered saline (PBS) using dilution factors between 10^{-1} and 10^{-9}. Lastly, 0.1 mL aliquots of the dilutions were seeded onto sterile agar plates prepared using 25 mL agar media and incubated for 24 h at 37°C. The plates were chosen based on the number of evolved colonies in the range of 15 – 250 and the chosen plates were then counted for analysis. All the experiments were performed in duplicate for each nonwoven sample on each bacterium.

4.3 Results and discussion

4.3.1 Parallel Plate Rheology and Melt flow index (MFI)

An amplitude sweep test was performed over a frequency range of 0.1 to 100 Hz to evaluate the viscoelastic behavior of the PP and PP/RB. The complex viscosity (|η*|) **(Figure 4-2 (a))** of the PP/RB decreases as the frequency increases, exhibiting typical shear-thinning behavior. This trend is also observed for PP, though its viscosity remains lower than that of the PP/RB blend across the entire frequency range. The higher viscosity in the PP/RB suggests that RB enhances resistance to deformation [286] potentially due to changes in the internal structure. Based on the rheological data, both PP and PP/RB exhibit shear-thinning behavior (viscosity decreases as frequency increases) but introducing RB to PP matrix leads to a higher overall viscosity. Overall, the incorporation of RB into the PP matrix significantly increases both the elastic and viscous properties, as well as the overall viscosity. This suggests that RB contributes to a more rigid material, through increased polymer entanglement, and modified molecular interactions [287].

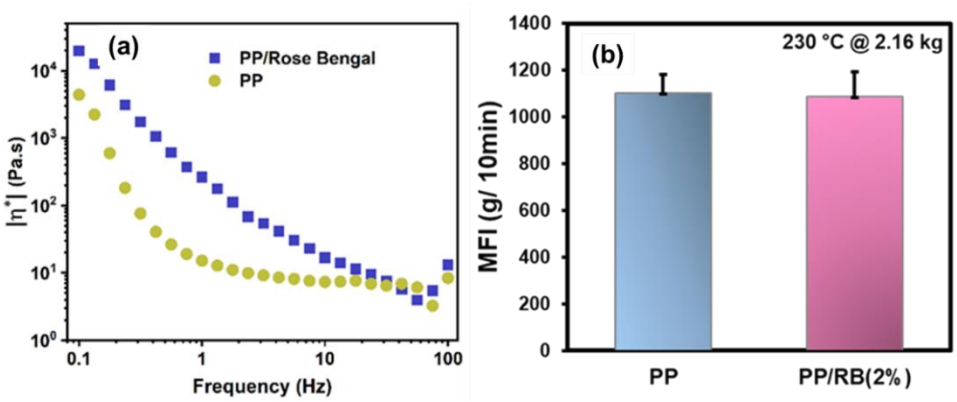


Figure 4-2 Parallel plate rheological analysis (a) complex viscosity as a function of frequency for Pristine PP and PP/RB (b) MFI of the Pristine PP and PP/RB

The MFI analysis (**Figure 4-2 (b)**) reveals that the MFI values for both PP and PP/RB are relatively close, with PP exhibiting an MFI of 1100 g/10 min and PP/RB showing a slightly lower value of 1085 g/10 min. This minor reduction in MFI for the PP/RB blend suggests that the addition of RB has a subtle impact on the flowability of the polymer. The close MFI values align with the observations from the parallel plate rheology, where the viscosity profiles for both materials showed similar behavior, with only slight differences in the lower frequency range. The reduced MFI in the PP/RB blend is due to the modified viscosity and flow characteristics caused by the presence of RB, which appears to slightly increase resistance to flow, as seen in the horizontal trend in the viscosity-frequency curve **(Figure 4-2 (a))** at lower shear rates. As the MFI is a key indicator of polymer processability in the melt-blown system, these results suggest that while the addition of RB modifies the polymer's flow behavior, it The MFI analysis **(Figure 4-2 (b))** reveals that the MFI values for both PP and PP/RB are relatively close, with PP exhibiting an MFI of 1100 g/10 min and PP/RB showing a slightly lower value of 1085 g/10 min. This minor reduction in MFI for the PP/RB blend suggests that the addition of RB has a subtle impact on the flowability of the polymer. The close MFI values align with the observations from the parallel plate rheology, where the viscosity profiles for both materials showed similar behavior, with only slight differences in the lower frequency range. The reduced MFI in the PP/RB blend is due to the modified viscosity and flow characteristics caused by the presence of RB, which appears to slightly increase resistance to flow, as seen in the horizontal trend in the viscosity-frequency curve (**Figure 4-2 (a)**) at lower shear rates. As the MFI is a key indicator of polymer processability in the melt-blown system, these results suggest that while the addition of RB modifies the polymer's flow behavior, it does not

significantly impair processability, maintaining a melt flow comparable to that of pristine PP [18, 19].

Thermal stability

Figure 4-3 presents the TGA **(a),** and DTGA **(b)** analyses of PP nonwoven and PP/RB nonwovens processed at 210°C, 220°C and 240°C, identified as PP/RB@210°C, PP/RB@220°C, and PP/RB@240°C respectively. The PP/RB processed at 240 °C shows the earliest onset of weight loss, suggesting that the higher processing temperature accelerates thermal degradation, due to increased thermal stress on the polymer matrix [290] and its interaction with RB. Additionally, this sample exhibits more pronounced weight loss at lower temperatures indicating more extensive degradation or potential phase separation between PP and RB and also degradation of RB at the processing temperature of 240°C. In contrast, the samples processed at lower temperatures (210°C and 220°C) demonstrate a delayed onset of thermal degradation compared to the PP/RB@240°C sample, reflecting improved thermal stability. These samples also show lower weight loss rates and a more gradual degradation process, which indicates that the blends are more stable when processed at reduced temperatures (210°C and 220°C). As expected, pristine PP follows a single-step [291] thermal degradation mechanism, with an onset temperature higher than any of the PP/RB blends. The weight loss for pristine PP occurs at higher temperatures and follows a more uniform and slower degradation pattern compared to the modified blends.

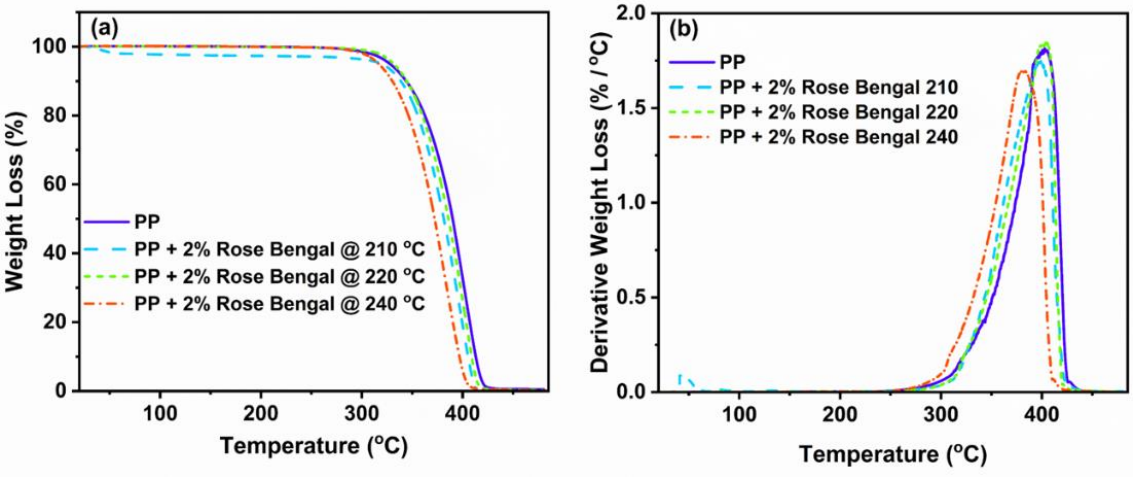


Figure 4-3 (a) TGA (b) DTGA of the PP and PP/RB nonwovens processed at 210°C, 220°C, 240°C

4.3.2 FTIR-DSC

Figure 4-4 (a) displays the FTIR spectra for PP and the PP/RB composites processed at different nozzle temperatures (210°C, 220°C, and 240°C). The PP/RB samples processed at 210°C and 220°C exhibit characteristic peaks at 1453 cm^{-1} and 1375 cm^{-1}, which can be attributed to C–H bonding and C=C stretching vibrations associated with the aromatic structure of RB [292]. Additionally, a peak at 2914 cm^{-1} is observed, corresponding to C–H stretching vibrations typical of the polymer backbone. Interestingly, the PP/RB sample processed at 240°C shows a significant similarity to the spectrum of pristine PP. This observation suggests that the higher processing temperature of 240°C has led to thermal degradation of the RB in the PP/RB matrix, resulting in a diminished presence of its characteristic peaks. The DSC analysis **(Figure 4-4 (b))** reveals slight differences in the thermal behavior of pristine PP and PP/RB composites. The melting peak for PP occurs at the lowest temperature (154°C), indicating that it melts first and demonstrates the typical thermal properties of a pure polymer.

In contrast, the PP/RB composites processed at 210°C and 220°C exhibit higher melting temperatures than pristine PP (158°C). This increase suggests that the incorporation of RB enhances the thermal stability of the material, due to interactions between the PP matrix and the RB dye, which strengthen the overall structure aligning with the rheological analysis, which indicates that the addition of RB improves the elastic properties of the composites, enhancing their ability to store elastic energy.

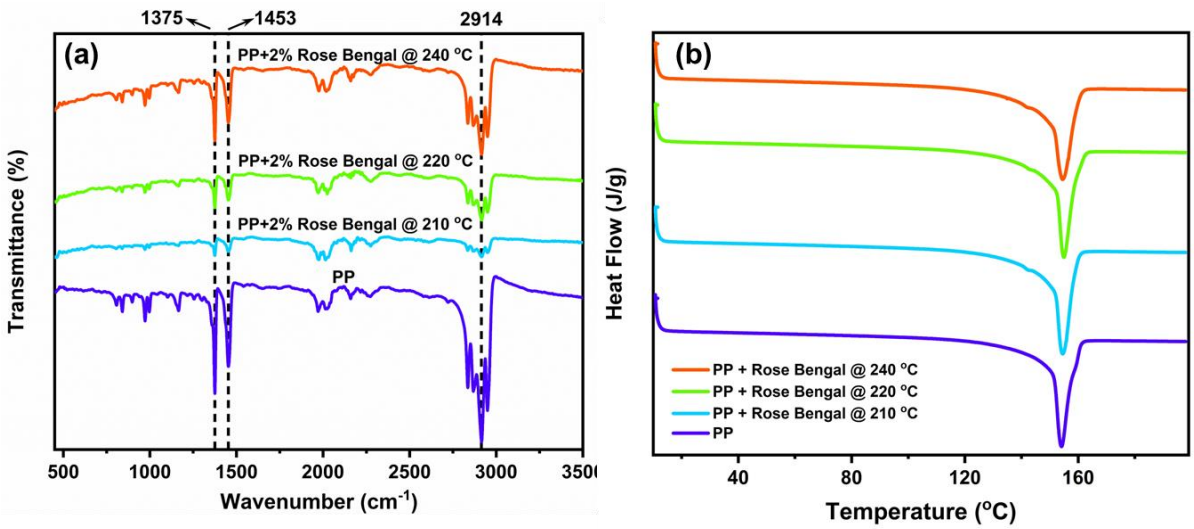


Figure 4-4 (a) FTIR and (b) DSC of the PP and PP/RB nonwovens

4.3.3 Fiber morphology

The SEM results **(Figure 4-5)** reveal a significant impact of RB incorporation on the fiber morphology of PP nonwovens. Pristine PP **(Figure 4-5 (a))** has a mean diameter of 4.36 µm, while the PP/RB samples **(Figure 4-5 (b), (c), (d))** display mean diameters of 12.96 µm, 20.26 µm, and 18.45 µm processed at 210°C, 220°C, and 240°C, respectively. By addition of RB to the PP, the mean fiber diameter notably increases, which correlates with the observed rise in viscosity. The enhanced viscosity arises from the interactions between PP and RB, as supported

by the rheological analysis. Specifically, the samples which containing RB and processed at 210°C and 220°C exhibit a marked increase in fiber size, with mean values of 12.96 µm and 20.26 µm, respectively. This trend does not align with the general principle that higher temperature promotes thinner fibers during the melt-blowing process [293] and as seen in the SEM images (Figure b-d) this increase in diameter is due to the bundling/fusion that has happened during the blowing process. However, the sample processed at the highest temperature of 240°C experiences less fusion compared to Figure b and c, showing a mean diameter of 18.45 µm. This observation can be attributed to the degradation of RB at elevated temperatures (240°C) **(Figure 4-3)**, and as evidenced by the noticeable shift in its natural color from pink to a yellowish hue, which reduces its reinforcing effect in the polymer matrix. Consequently, the influence of PP on fiber formation becomes more pronounced, resulting in a finer fiber diameter compared to the PP/RB@220°C nonwoven sample, as the high MFI of PP contributes more to its fiber attenuation.

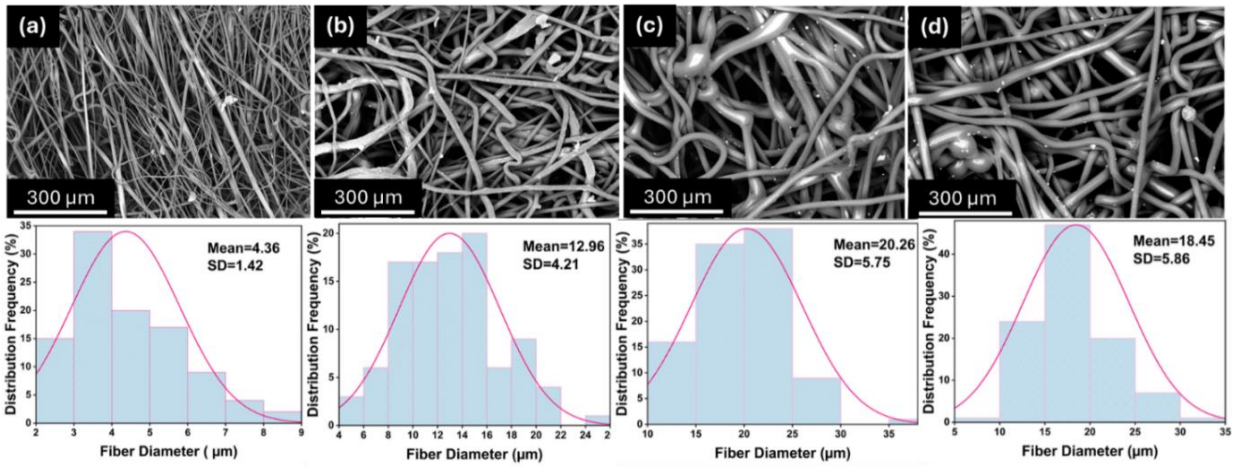


Figure 4-5 Analysis of fiber morphology and histograms of melt-blown nonwovens for (a) Pristine PP, (b) PP/RB@210°C, (c) PP/RB@220°C, (d) PP/RB@240°C

4.3.4 Mechanical properties

The tensile strength analysis **(Figure 4-6 (a))** reveals a clear trend among the tested nonwovens, with PP exhibiting the lowest tensile strength. The PP/RB nonwovens processed at 210°C and 220°C demonstrate increased tensile strength compared to PP. Notably, the tensile strengths of these two samples are quite close, suggesting that the specific processing temperature within this range has a minimal impact on the mechanical properties. The rheological data also indicate that PP/RB composites exhibit higher elastic and viscous properties than that of PP, reinforcing the idea that the addition of RB significantly contributes to structural integrity and significantly enhances the tensile strength of the PP/RB nonwovens. The higher elongation at break **(Figure 4-6 (b))** observed in the PP comparing to the rest of the PP/RBs indicates its ductility, which is compromised in the RB-containing samples. The reduction in elongation at break, particularly in the PP/RB@240°C sample, suggests that while the processing temperature can enhance some mechanical properties, it also leads to brittleness due to thermal degradation and altered fiber morphology. The PP/RB@220°C sample exhibits the highest modulus **(Figure 4-6 (c))**, indicating a stiff structure likely due to proper dispersion and interaction of RB within the PP matrix. The 240°C sample, while also showing a high modulus, reflects a complex interplay between increased stiffness from denser fiber formation and reduced ductility from degradation effects. The lower modulus in the 210°C sample suggests insufficient interaction, leading to a more flexible yet less rigid structure, while pristine PP exhibits the lowest modulus, highlighting the enhancing effect of RB on mechanical properties.

4.3.5 Air Filtration

The particulate filtration efficiency (PFE) results **(Figure 4-7 (a))** reveals a clear trend influenced by the incorporation of RB and the processing temperatures, which subsequently affect the fiber diameter of the nonwoven samples. The pristine PP nonwoven sample exhibits the highest PFE at 75%, demonstrating its effectiveness in capturing particulate (0.3 µm). In contrast, the PFE decreases for the PP/RB samples, with values of 63%, 48%, and 55% for those processed at 210°C, 220°C, and 240°C, respectively. This decline in filtration efficiency of the PP/RB@210^{0}C and the PP/RB@220^{0}C can be attributed to the increased fiber diameters 2.97-4.65 times thicker in the RB-containing samples, which reduces the effective surface area available for filtration. Furthermore, the dp results **(Figure 4-7 (b))** indicate that higher PFE values correspond to increased dp, highlighting a trade-off between filtration efficiency and breathability. Notably, the sample processed at 220°C displays the largest fiber diameter (20.26 µm), corresponding to its lowest PFE (48%) and lowest dp (8.5 mmH2O).

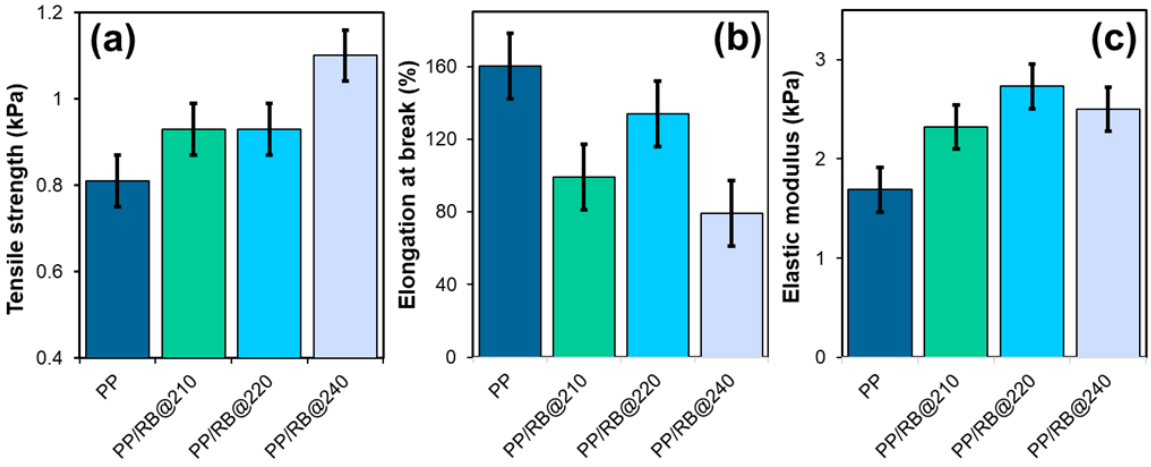


Figure 4-6 Mechanical properties of the PP and PP/RB@210, PP/RB@220, PP/RB@240 nonwovens (a) Tensile strength (b) Elongation at break (c) Elastic modulus

4.3.6 Antibacterial properties

Common use of PP-based melt-blown fabrics includes filtration (air, water, oil), reusable or disposable masks, insulation, and absorption. In this study, the PP polymer was melt-blown along with the Rose Bengal (RB) as a functional additive (photosensitizer), to instill value-added functionality, i.e. antimicrobial effects due to the incorporation of the RB photosensitizer (PS) throughout the microfibers of the nonwoven fabrics. RB is a well-known hydrophobic anionic dye and photosensitizer [283, 284, 294–296]. The US-Food and Drug Agency (FDA) approved RB in 1971 as an injectable drug for use as a diagnostic tool to assess liver function [297]. Additionally, the FDA has designated RB as an orphan drug for the treatment of certain cancers [298]. Recently, it has been extensively used in biomedical applications, such as photodynamic antimicrobial therapy [299–301], tissue repairs[302], and diagnostic imaging.[303] In this study, we evaluated the antimicrobial efficiencies of the PP/RB-based fabrics on two different classes of bacteria, gram-positive (*B. subtilis*) and gram-negative (*E. coli*).

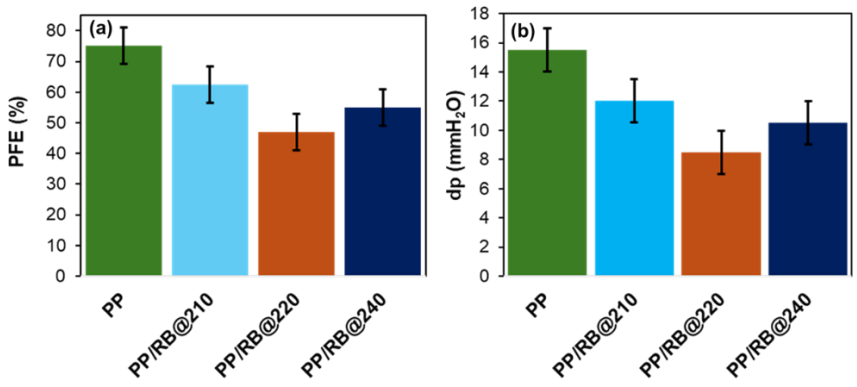


Figure 4-7 (a) Particulate filtration efficiency (b) pressure drop of PP, PP/RB@210°C, @220°C, @240°C nonwovens

Numerous literature [297, 298, 304–312] described that the RB dye, a photosensitizer, predominantly works through the type-II mechanism, which is also schematically shown in **Figure 4-8**. Most Gram-positive and Gram-negative bacteria possess a porous outer layer of the lipid-bilayer cytoplasmic membrane, known as the cell wall, composed of peptidoglycan [294]. In Gram-positive bacteria, the cell wall consists of multiple layers of such peptidoglycan, giving them a rigid and thicker structure, and making them strongly anionic and primarily hydrophobic [294]. Several studies have reported the ease with which anionic photosensitizers (PS), such as rose Bengal (RB), or other neutral PSs can penetrate the relatively porous peptidoglycan layer surrounding the cytoplasmic membrane of Gram-positive bacteria [313]. In Gram-negative bacteria, the cell wall includes an additional outer membrane and several layers of peptidoglycan. These outermost layers are strongly anionic and predominantly hydrophobic, restricting the permeability of bioactive molecules of interest [43, 44]. The results from the antimicrobial tests (**Figures 4-9 and 4-10**) on the nonwoven samples align with literature-reported findings, indicating the ease of RB molecules penetration through Gram-positive bacterial cell walls, resulting in higher bactericidal efficiency. Conversely, the reduced bactericidal efficiency against Gram-negative bacteria is attributed to the limited permeability of RB through their cellular barriers.

The bacterial growth trends over 24 h, obtained from OD-600 data, are presented in **Figure 4-9.** The results clearly demonstrate that the PP/RB@210°C and PP/RB@220°C samples containing the RB photosensitizer, exhibited excellent antibacterial effects against *B. subtilis* as seen from the cessation of growth in the plot **(Figure 4-9)**. A similar cessation trend was

observed for the Gram-negative bacterium (*E. coli*) with these samples. On the other hand, PP/RB@240°C seemed ineffective against both bacterial strains studied bacteria likely due to the degradation of the RB photosensitizer as a result of the elevated processing temperature.

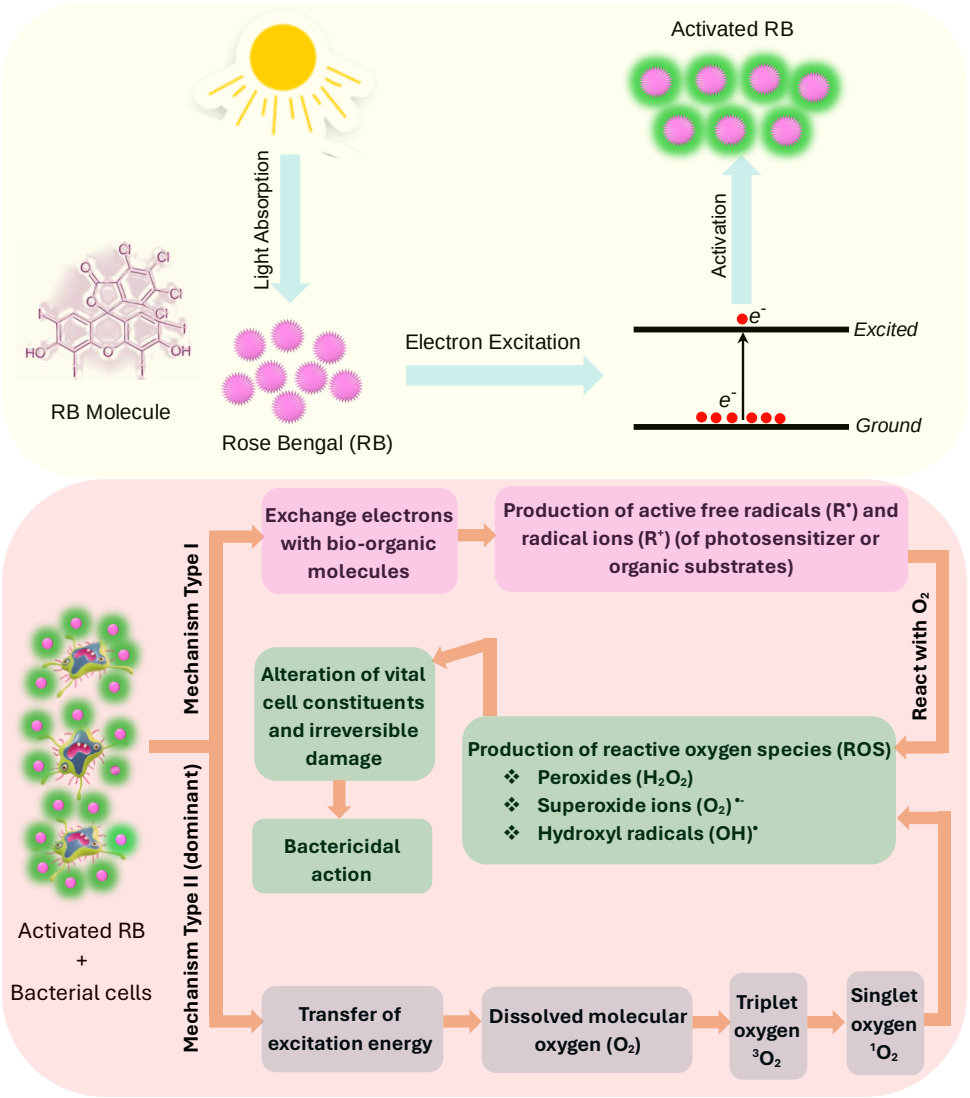


Figure 4-8 Schematic illustrations of the mechanism of action of Rose Bengal (RB), a photosensitizer, for its antibacterial action under light. RB molecules get activated to their excited states under illumination by visible light or near-IR spectral region. The RB molecules

in their excited states (active) then work via two different types of mechanisms to kill the susceptible bacteria [313].

The findings of this study indicate that the growth cessation trends of Gram-positive versus Gram-negative bacteria for the PP/RB@210°C and PP/RB@220°C samples align with the known ease of RB molecule penetration through the relatively porous peptidoglycan layer of Gram-positive bacterial cell walls [313, 314].

The antibacterial actions of the RB, possessing both anionic and hydrophobic properties, is not solely dependent on its cellular entry. Several studies have reported that RB interacts with different bacterial cell walls, such as *Salmonella typhimurium* (*Salmonella enterica*) and *E.coli* through association with the outer membrane rather than intracellular interactions [313]. As a result, RB tends to remain localized at the subcellular surface of the cell walls [313]. **Figure 4-9** (**a** and **c**) shows that the composite melt-blown fabrics (all three PP/RB samples) leach the RB molecules in aqueous media that are loosely bound to the surfaces of the formed fibres during the melt-blown process. This is because the RB was not conjugated to the PP matrix via a chemical bond, and the physical entrapment achieved during the melt-processing was not sufficient to keep the relatively small RB molecule in the PP matrix during soaking. Based on the characterization results (TGA, FTIR, rheology, mechanical properties), it was evident that higher processing temperatures (240°C) degraded the RB additive in the PP. As a result, the antimicrobial properties of the (PP/RB@240°C) were inferior to the samples processed at lower temperatures (PP/RB@210°C and PP/RB@220°C).

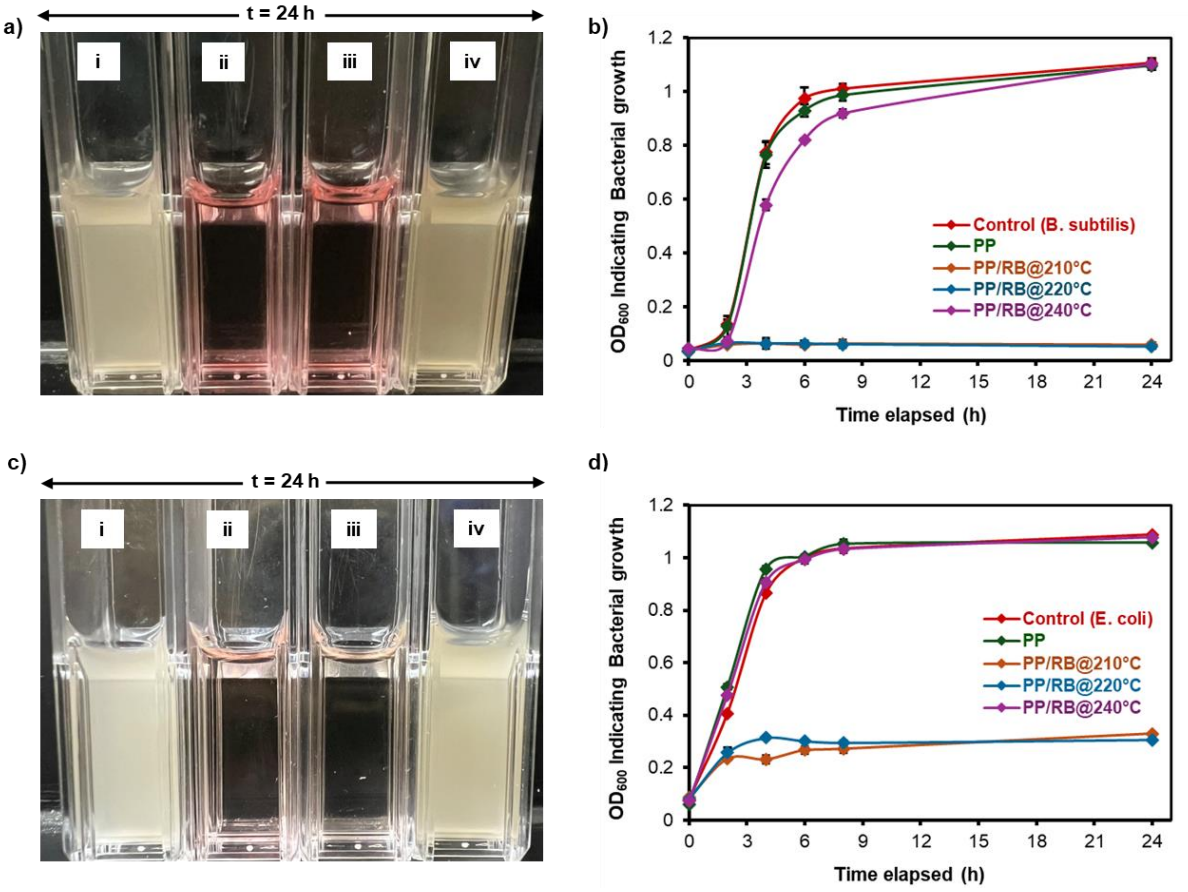


Figure 4-9 Turbidity measurement of bacterial culture media withdrawn after 24 hours in cuvettes forecasting bacterial growth or cessation of growth due to treatment with samples i) PP, ii) PP/RB@210°C, iii) PP/RB@220°C and iv) ii) PP/RB@240°C for a) *Bacillus subtilis* (Gram-positive) and c) *Escherichia coli*. The data of OD-600 are plotted showing the growth trends for all the experimental nonwoven PP/RB samples on b) *B. subtilis* and d) *E. coli*.

Although the PP/RB@220°C nonwoven sample has a smaller diameter than the PP/RB@210°C as shown in the SEM images, the microfibers of the nonwoven sample PP/RB@220°C, exhibited a slightly compacted morphology (as seen in the SEM) formed during the melt-blowing process. This compacted structure could be one of the potential

reasons for the greater leaching of RB from sample PP/RB@210°C compared to PP/RB@220°C. Meanwhile sample PP/RB@240°C showed negligible RB leaching, despite having a smaller mean fiber diameter than PP/RB@210°C. This was likely because the RB was already degraded during the elevated temperature processing in the PP/RB@240°C sample generation. Leaching tests were conducted for all the modified samples (PP/RB@220°C, PP/RB@220°C and PP/RB@220°C) with data provided in the Supplementary information section (**Figure A2 in appendix B**). It appears that the leached RB molecules were primarily responsible for the antimicrobial efficiencies of the PP/RB@210°C and PP/RB@220°C.

Similar results were observed in the static contact plate modes of antimicrobial tests, as shown in **Figure 4-10**. In such agar plate methods, the PP/RB@210°C and PP/RB@220°C samples demonstrated strong antibacterial efficiency against both Gram-positive and Gram-negative bacteria at various specific dilutions of the elute used for seeding. Interestingly, the PP/RB@240°C samples showed fewer colonies on the agar plates compared to the CFUs on the control plates, indicating moderate to strong antimicrobial effects, particularly against Gram-negative *E. coli*. Further studies are needed to better understand the mechanisms underlying the antimicrobial activity exhibited by the PP/RB@240°C samples.

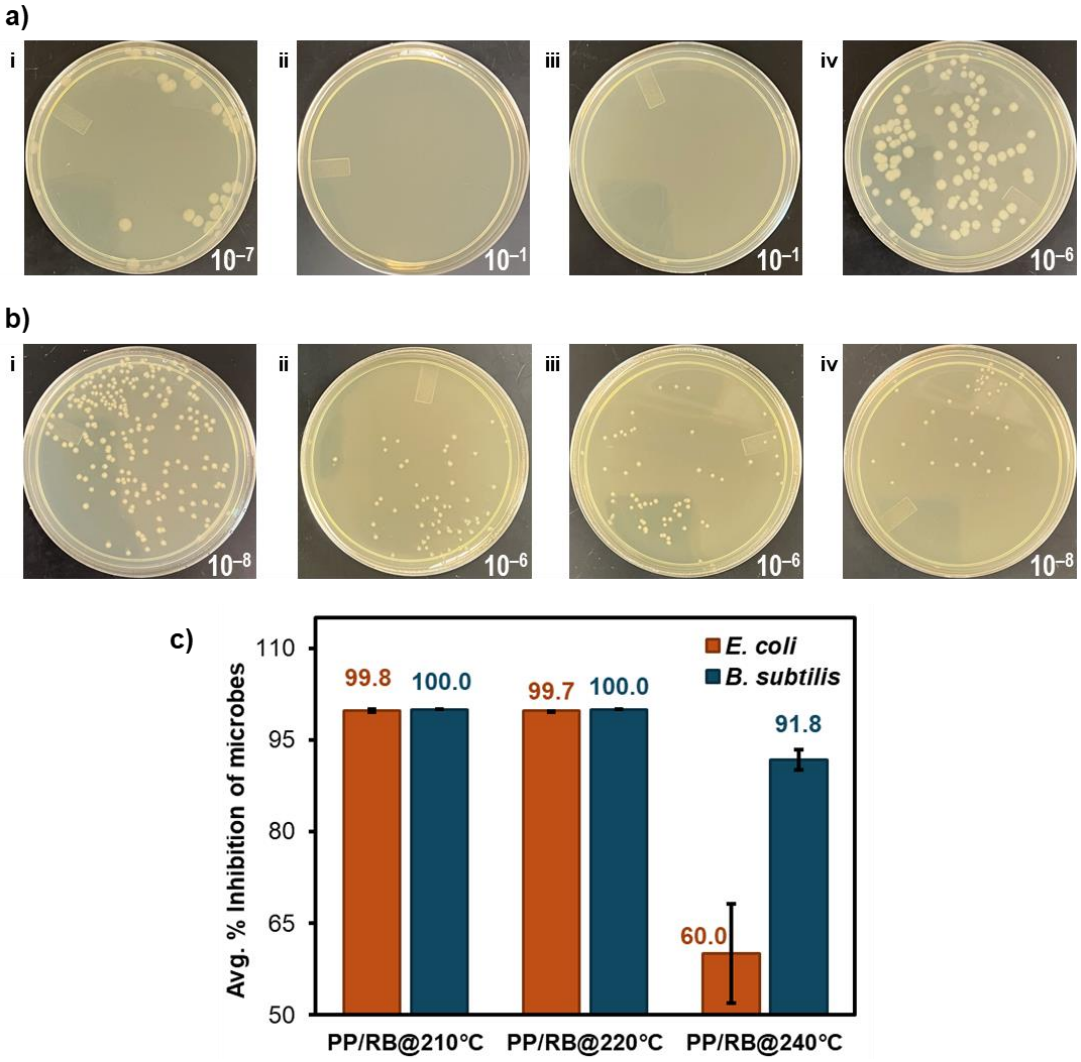


Figure 4-10 Bacterial colony growth tests in agar plates seeded from the bacterial culture media withdrawn from the elute collected after 24 h of contact with fresh diluted culture of each bacterium with the fabrics. The CFU counts on the agar plates (i—iv: PP, PP/RB@210°C, PP/RB@220°C, and PP/RB@240°C respectively) are shown indicating potential antibacterial activities of the RB-modified melt-blown fabrics in a) For Bacillus subtilis (Gram-positive), and in b) For Escherichia coli. c) The corresponding results from the CFU data are plotted showing the antibacterial efficacies for all the experimental fabric samples on both bacteria.

4.4 Conclusion

This study highlights the promising potential of incorporating Rose Bengal into polypropylene melt-blown porous mats with potential air filter applications to significantly enhance their antibacterial properties, achieving an increase in antibacterial efficacy of up to 99%, especially for gram-positive bacteria. The findings reveal that melt-blowing temperatures are one of the crucial parameters in optimizing this effectiveness in terms of filtration efficiencies of MPPS and antimicrobial action. Specifically, samples processed at 210 °C and 220 °C demonstrated superior antibacterial performance, with PFE values of 63% and 48%, respectively, benefiting from the stability of RB. In contrast, the sample processed at 240°C exhibited minimal or no antibacterial activity due to insignificant leaching of RB molecules as well as the possible fractional RB degradation during processing, resulting in a PFE of 55%. The inclusion of RB resulted in reduced melt flow behavior and hence increased fiber diameters, with mean diameters of 12.96 μm for the 210 °C processed sample and 20.26 μm for the 220°C processed sample, which influenced both mechanical properties and filtration efficiency. Despite the increase in fiber diameter, the primary objective of enhancing antibacterial performance was successfully achieved at these lower processing temperatures. This underscores the potential of RB as a valuable additive for the development of advanced air filters that not only provide effective filtration capabilities but also offer antimicrobial protection against airborne pathogens.

Chapter 5
Concluding Marks

This study explored the design and development of porous non-woven mats using a scalable Melt-blowing process, incorporating a water-soluble polymer, PEG, into high melt-flow rate PLA. The low molecular weight and high MFI of the PEG variants (MW 400 g/mol, 2000 g/mol, and 4000 g/mol) allowed for the creation of blends with low viscosity and high MFI, ideal for melt-blowing. The water-etching process successfully removed the sacrificial PEG, generating porous PLA nonwoven mats. Among the different PEG variants, PLA/PEG 2000 (5% and 10%) demonstrated the best compatibility, resulting in high-quality porous mats. SEM analysis revealed nanopores as small as 50 nm within the fibers, with the PLA/PEG 2000 – 10% samples showing a uniform distribution. Air filtration tests confirmed the effectiveness of this method, with the PLA/PEG 2000 – 10% mats achieving approximately 85% filtration efficiency for 0.3 μm particles. This performance surpassed that of both baseline PLA and non-etched filters, attributed to the optimized pore structure and enhanced surface area, which facilitated improved particle capture. The findings highlight the potential of this approach for creating robust, sustainable nonwoven materials for air filtration and extendable applications, including battery separators and water treatment membranes.

In parallel, the other study demonstrates the significant potential of incorporating Rose Bengal (RB) into polypropylene melt-blown air filters to enhance their antibacterial properties. The inclusion of RB resulted in a notable increase in antibacterial efficacy, achieving up to 99% effectiveness, particularly against gram-positive bacteria. The study identified processing

temperature as a critical factor in optimizing both filtration efficiency and antimicrobial action. Samples processed at 210°C and 220°C exhibited superior antibacterial performance, with Particle Filtration Efficiency (PFE) values of 63% and 48%, respectively, benefiting from the stability of RB. In contrast, the sample processed at 240°C showed reduced antibacterial activity due to limited RB leaching and potential degradation during processing, with a PFE of only 55%. Additionally, the incorporation of RB led to an increase in fiber diameter, with mean diameters of 12.96 μm and 20.26 μm for the 210°C and 220°C processed samples, respectively. Although fiber diameter increased, the study successfully met the primary goal of improving antibacterial performance. These findings highlight the potential of RB as a valuable additive for developing advanced air filters that combine effective filtration capabilities with antimicrobial protection against airborne pathogens.

Future work

For the porous PLA fiber mats produced via PEG etching, research could focus on optimizing the compatibility and concentration of PEG variants to fine-tune pore size and distribution, as well as improve the mechanical properties of the mats post-etching. Expanding the application potential, future studies could assess the use of these mats in areas like water treatment and battery separators. Additionally, investigating other sacrificial additives with tailored degradation profiles could enable the production of even more intricate pore structures. For the RB-enhanced polypropylene melt-blown mats, future research could explore strategies to mitigate RB degradation at higher processing temperatures, such as employing thermal stabilizers or alternative encapsulation techniques. Furthermore, optimizing the balance

between fiber diameter and filtration efficiency could yield mats with improved mechanical strength and broader filtration capabilities. Finally, combining the porous PLA approach with RB incorporation for HEPA filter applications could lead to advanced multifunctional nonwovens, merging high filtration efficiency and antibacterial activity.

References

1. Vanangamudi A, Hamzah S, Singh G (2015) Synthesis of hybrid hydrophobic composite air filtration membranes for antibacterial activity and chemical detoxification with high particulate filtration efficiency (PFE). Chemical Engineering Journal 260:801–808. https://doi.org/10.1016/j.cej.2014.08.062
2. Podgórski A, Bałazy A, Gradoń L (2006) Application of nanofibers to improve the filtration efficiency of the most penetrating aerosol particles in fibrous filters. Chem Eng Sci 61:6804–6815. https://doi.org/https://doi.org/10.1016/j.ces.2006.07.022
3. Bian Y, Zhang L, Chen C (2018) Experimental and modeling study of pressure drop across electrospun nanofiber air filters. Build Environ 142:244–251. https://doi.org/https://doi.org/10.1016/j.buildenv.2018.06.021
4. Zaatari M, Novoselac A, Siegel J (2014) The relationship between filter pressure drop, indoor air quality, and energy consumption in rooftop HVAC units. Build Environ 73:151–161. https://doi.org/https://doi.org/10.1016/j.buildenv.2013.12.010
5. Al-Attar IS, Wakeman RJ, Tarleton ES, Husain A (2009) THE EFFECT OF PLEAT COUNT AND AIR VELOCITY ON THE INITIAL PRESSURE DROP AND FRACTIONAL EFFICIENCY OF HEPA FILTERS
6. Kakoria A, Sinha-Ray S (2022) Ultrafine nanofiber-based high efficiency air filter from waste cigarette butts. Polymer (Guildf) 255:125121. https://doi.org/https://doi.org/10.1016/j.polymer.2022.125121
7. Beckman IP, Berry G, Cho H, Riveros G (2023) Alternative High-Performance Fibers for Nonwoven HEPA Filter Media. Aerosol Science and Engineering 7:36–58. https://doi.org/10.1007/s41810-022-00161-6
8. Zhong Z, Xu Z, Sheng T, et al (2015) Unusual Air Filters with Ultrahigh Efficiency and Antibacterial Functionality Enabled by ZnO Nanorods. ACS Appl Mater Interfaces 7:21538–21544. https://doi.org/10.1021/acsami.5b06810

9. Noor MR, Kowal K, Tiernan P, et al Antimicrobial Air Filters. In: Electrically Active Materials for Medical Devices. pp 349–364

10. Bazaka K, Jacob M V., Chrzanowski W, Ostrikov K (2015) Anti-bacterial surfaces: Natural agents, mechanisms of action, and plasma surface modification. RSC Adv 5:48739–48759. https://doi.org/10.1039/c4ra17244b

11. Burko A, Zavatski S, Baturova A, et al (2023) Polymer Membrane Modified with Photocatalytic and Plasmonic Nanoparticles for Self-Cleaning Filters. Polymers (Basel) 15:. https://doi.org/10.3390/polym15030726

12. Borojeni IA, Gajewski G, Riahi RA (2022) Application of Electrospun Nonwoven Fibers in Air Filters. Fibers 10:. https://doi.org/10.3390/fib10020015

13. (2025) ChatGPT. https://chatgpt.com. Accessed 10 Jan 2025

14. Liu H, Zhu Y, Zhang C, et al (2024) Electrospun nanofiber as building blocks for high-performance air filter: A review. Nano Today 55:102161. https://doi.org/https://doi.org/10.1016/j.nantod.2024.102161

15. Liu G, Guan J, Wang X, et al (2024) Large-Scale Preparation of Mechanically High-Performance and Biodegradable PLA/PHBV Melt-Blown Nonwovens with Nanofibers. Engineering 39:244–252. https://doi.org/https://doi.org/10.1016/j.eng.2023.02.021

16. Tadele DT, David D, Yim E, Mekonnen TH (2025) Development and characterization of PVA-zein/α-tocopherol nonwoven mats for functional wound dressing applications. Colloids Surf B Biointerfaces 246:114355. https://doi.org/https://doi.org/10.1016/j.colsurfb.2024.114355

17. Tadele DT, Islam MS, Mekonnen TH (2025) Zein-based nanoparticles and nanofibers: Co-encapsulation, characterization, and application in food and biomedicine. Trends Food Sci Technol 155:104809. https://doi.org/https://doi.org/10.1016/j.tifs.2024.104809

18. Medeiros ES, Glenn GM, Klamczynski AP, et al (2009) Solution blow spinning: A new method to produce micro- and nanofibers from polymer solutions. J Appl Polym Sci 113:2322–2330. https://doi.org/https://doi.org/10.1002/app.30275

19. Zhang X, Liu J, Zhang H, et al (2021) Multi-Layered, Corona Charged Melt Blown Nonwovens as High Performance PM0.3 Air Filters. Polymers (Basel) 13:. https://doi.org/10.3390/polym13040485

20. Jung S, Kim J (2020) Advanced Design of Fiber-Based Particulate Filters: Materials, Morphology, and Construction of Fibrous Assembly. Polymers (Basel) 12:. https://doi.org/10.3390/polym12081714

21. Zhao Z, Li J, Yuan X, et al (2005) Preparation and properties of electrospun poly(vinylidene fluoride) membranes. J Appl Polym Sci 97:466–474. https://doi.org/https://doi.org/10.1002/app.21762

22. Bresee RR, Ko W-C (2003) Fiber Formation during Melt Blowing. International Nonwovens Journal os-12:1558925003os–1200209. https://doi.org/10.1177/1558925003os-1200209

23. Wortmann M, Frese N, Sabantina L, et al (2019) New Polymers for Needleless Electrospinning from Low-Toxic Solvents. Nanomaterials 9:. https://doi.org/10.3390/nano9010052

24. Sathish T, Saravanan R, Sharma K, et al (2023) A novel investigations on medical and non-medical mask performance with influence of marine waste microplastics (polypropylene). Mar Pollut Bull 192:115004. https://doi.org/https://doi.org/10.1016/j.marpolbul.2023.115004

25. Pierpaoli M, Giosuè C, Czerwińska N, et al (2021) Characterization and Filtration Efficiency of Sustainable PLA Fibers Obtained via a Hybrid 3D-Printed/Electrospinning Technique. Materials 14:. https://doi.org/10.3390/ma14226766

26. Nayak R, Kyratzis IL, Truong YB, et al (2012) Fabrication and Characterisation of Nanofibres by Meltblowing and Melt Electrospinning. In: Advanced Manufacturing Technology, ICMSE 2012. Trans Tech Publications Ltd, pp 1294–1299

27. Balogh A, Farkas B, Faragó K, et al (2015) Melt-Blown and Electrospun Drug-Loaded Polymer Fiber Mats for Dissolution Enhancement: A Comparative Study. J Pharm Sci 104:1767–1776. https://doi.org/https://doi.org/10.1002/jps.24399

28. Kakoria A, Sinha-Ray S (2018) A Review on Biopolymer-Based Fibers via Electrospinning and Solution Blowing and Their Applications. Fibers 6:. https://doi.org/10.3390/fib6030045

29. Hiremath N, Bhat G (2015) Melt blown polymeric nanofibers for medical applications-an overview. Nanosci Technol 2:1–9

30. Kara Y, Molnár K (2022) A review of processing strategies to generate melt-blown nano/microfiber mats for high-efficiency filtration applications. Journal of Industrial Textiles 51:137S-180S. https://doi.org/10.1177/15280837211019488

31. Tadele DT, Islam MS, Mekonnen TH (2025) Zein-based nanoparticles and nanofibers: Co-encapsulation, characterization, and application in food and biomedicine. Trends Food Sci Technol 155:104809. https://doi.org/https://doi.org/10.1016/j.tifs.2024.104809

32. Lee H, Trinh BM, Crawford EA, Mekonnen TH (2023) Thermoplastic elastomer melt-blown fiber mats for oil spill remediation: Fabrication, oil uptake, and gel formation studies. Sep Purif Technol 326:124761. https://doi.org/https://doi.org/10.1016/j.seppur.2023.124761

33. Crawford EA, Gupta S, Trinh BM, Mekonnen TH (2024) Styrene-ethylene-butylene-styrene (SEBS) melt-blown fibers for oil spill remediation and oil barrier geotextiles. Polymer (Guildf) 298:126942. https://doi.org/https://doi.org/10.1016/j.polymer.2024.126942

34. Agarwal S, Greiner A (2011) On the way to clean and safe electrospinning—green electrospinning: emulsion and suspension electrospinning. Polym Adv Technol 22:372–378. https://doi.org/https://doi.org/10.1002/pat.1883

35. Rashid TU, Gorga RE, Krause WE (2021) Mechanical Properties of Electrospun Fibers—A Critical Review. Adv Eng Mater 23:2100153. https://doi.org/https://doi.org/10.1002/adem.202100153

36. Jacobs V, Anandjiwala RD, Maaza M (2010) The influence of electrospinning parameters on the structural morphology and diameter of electrospun nanofibers. J Appl Polym Sci 115:3130–3136. https://doi.org/https://doi.org/10.1002/app.31396

37. Bhardwaj N, Kundu SC (2010) Electrospinning: A fascinating fiber fabrication technique. Biotechnol Adv 28:325–347. https://doi.org/https://doi.org/10.1016/j.biotechadv.2010.01.004

38. Kalani S, Kohandani R, Bagherzadeh R (2020) Flexible electrospun PVDF–BaTiO3 hybrid structure pressure sensor with enhanced efficiency. RSC Adv 10:35090–35098. https://doi.org/10.1039/D0RA05675H

39. Cui W, Li X, Zhou S, Weng J (2007) Investigation on process parameters of electrospinning system through orthogonal experimental design. J Appl Polym Sci 103:3105–3112. https://doi.org/https://doi.org/10.1002/app.25464

40. Golkar P, Kalani S, Allafchian AR, et al (2019) Fabrication and characterization of electrospun Plantago major seed mucilage/PVA nanofibers. J Appl Polym Sci 136:47852. https://doi.org/https://doi.org/10.1002/app.47852

41. Nageh H, Emam MH, Ali F, et al (2022) Zinc Oxide Nanoparticle-Loaded Electrospun Polyvinylidene Fluoride Nanofibers as a Potential Face Protector against Respiratory Viral Infections. ACS Omega 7:14887–14896. https://doi.org/10.1021/acsomega.2c00458

42. Medvedev AZh, Bokhonov BB, Kiselev OS, et al (2023) Silver nanoparticle-modified melt-blown polypropylene: Antibacterial and antifungal properties and antiviral activity against SARS-CoV-2. Mater Lett 346:134557. https://doi.org/https://doi.org/10.1016/j.matlet.2023.134557

43. Agarwal S, Greiner A (2011) On the way to clean and safe electrospinning—green electrospinning: emulsion and suspension electrospinning. Polym Adv Technol 22:372–378. https://doi.org/https://doi.org/10.1002/pat.1883

44. Mailley D, Hébraud A, Schlatter G (2021) A Review on the Impact of Humidity during Electrospinning: From the Nanofiber Structure Engineering to the Applications. Macromol Mater Eng 306:2100115. https://doi.org/https://doi.org/10.1002/mame.202100115

45. Wang G, Yu D, Kelkar AD, Zhang L (2017) Electrospun nanofiber: Emerging reinforcing filler in polymer matrix composite materials. Prog Polym Sci 75:73–107. https://doi.org/https://doi.org/10.1016/j.progpolymsci.2017.08.002

46. Kim J, Reneker DH (1999) Mechanical properties of composites using ultrafine electrospun fibers. Polym Compos 20:124–131. https://doi.org/https://doi.org/10.1002/pc.10340

47. Bazilevsky A V, Yarin AL, Megaridis CM (2007) Co-electrospinning of Core−Shell Fibers Using a Single-Nozzle Technique. Langmuir 23:2311–2314. https://doi.org/10.1021/la063194q

48. Scaffaro R, Lopresti F, Botta L (2017) Preparation, characterization and hydrolytic degradation of PLA/PCL co-mingled nanofibrous mats prepared via dual-jet electrospinning. Eur Polym J 96:266–277. https://doi.org/https://doi.org/10.1016/j.eurpolymj.2017.09.016

49. Du Z, Lv H, Wang C, et al (2023) Organic solvent-free starch-based green electrospun nanofiber mats for curcumin encapsulation and delivery. Int J Biol Macromol 232:123497. https://doi.org/https://doi.org/10.1016/j.ijbiomac.2023.123497

50. Nayak R, Padhye R, Arnold L (2017) 2 - Melt-electrospinning of nanofibers. In: Afshari M (ed) Electrospun Nanofibers. Woodhead Publishing, pp 11–40

51. Zhang H-T, Wang Q, Chen Z, Wei F-L (2017) Dynamics and Feedback Control of Electrospinning Processes. IEEE Transactions on Control Systems Technology 25:611–618. https://doi.org/10.1109/TCST.2016.2557224

52. Jiang S, Kang Z, Liu F, Fan J (2023) 2D and 3D Electrospinning of Nanofibrous Structures by Far-Field Jet Writing. ACS Appl Mater Interfaces 15:23777–23782. https://doi.org/10.1021/acsami.3c03145

53. Giannitelli SM, Mozetic P, Trombetta M, Rainer A (2015) Combined additive manufacturing approaches in tissue engineering. Acta Biomater 24:1–11. https://doi.org/https://doi.org/10.1016/j.actbio.2015.06.032

54. Wang Z, Wang Y, Yan J, et al (2021) Pharmaceutical electrospinning and 3D printing scaffold design for bone regeneration. Adv Drug Deliv Rev 174:504–534. https://doi.org/https://doi.org/10.1016/j.addr.2021.05.007

55. Hanna Sofia SalehHudin Edzrol Niza Mohamad WNLM, Afifi AM (2018) Multiple-jet electrospinning methods for nanofiber processing: A review. Materials and Manufacturing Processes 33:479–498. https://doi.org/10.1080/10426914.2017.1388523

56. Wu Y-K, Li Z-J, Fan J, et al (2019) Improved Fiber Uniformity and Jet Number in Multi-spinneret Electrospinning via Auxiliary Electrode. Fibers and Polymers 20:1172–1179. https://doi.org/10.1007/s12221-019-8859-2

57. Jin Q, Fu Y, Zhang G, et al (2022) Nanofiber electrospinning combined with rotary bioprinting for fabricating small-diameter vessels with endothelium and smooth muscle. Compos B Eng 234:109691. https://doi.org/https://doi.org/10.1016/j.compositesb.2022.109691

58. Balogh A, Domokos A, Farkas B, et al (2018) Continuous end-to-end production of solid drug dosage forms: Coupling flow synthesis and formulation by electrospinning. Chemical Engineering Journal 350:290–299. https://doi.org/https://doi.org/10.1016/j.cej.2018.05.188

59. Yiin-Kuen Fuh L-CL, Chen S-Y (2012) High-Throughput Production of Nanofibrous Mats via a Porous Materials Electrospinning Process. Journal of Macromolecular Science, Part B 51:1742–1749. https://doi.org/10.1080/00222348.2012.659628

60. Daristotle JL, Behrens AM, Sandler AD, Kofinas P (2016) A Review of the Fundamental Principles and Applications of Solution Blow Spinning. ACS Appl Mater Interfaces 8:34951–34963. https://doi.org/10.1021/acsami.6b12994

61. Wang S, Zhang P, Li Y, et al (2023) Recent advances and future challenges of the starch-based bio-composites for engineering applications. Carbohydr Polym 307:120627. https://doi.org/https://doi.org/10.1016/j.carbpol.2023.120627

62. Lee JS, Oh Y, Kim H, et al (2022) Performance Study of Composite Air Filters Using Heterogeneous Fibers. Composites Research 35:216–221

63. Wang Y, Liu L, Zhu Y, et al (2023) Tri-Layer Core–Shell Fibers from Coaxial Electrospinning for a Modified Release of Metronidazole. Pharmaceutics 15:. https://doi.org/10.3390/pharmaceutics15112561

64. Teixeira BN, Anaya-Mancipe JM, Thiré RMSM (2023) Evaluation of polycaprolactone nanofibers' spinnability using green solvent systems by solution blow spinning (SBS). Nanotechnology 34:505707. https://doi.org/10.1088/1361-6528/acf8cd

65. An S, Sankaran A, Yarin AL (2018) Natural Biopolymer-Based Triboelectric Nanogenerators via Fast, Facile, Scalable Solution Blowing. ACS Appl Mater Interfaces 10:37749–37759. https://doi.org/10.1021/acsami.8b15597

66. Penconek A, Werner Ł, Moskal A (2024) Combining Solution-Blowing and Melt-Blowing Techniques to Produce an Efficient Non-Woven Filter. Processes 12:. https://doi.org/10.3390/pr12050857

67. da Silva Parize DD, de Oliveira JE, Foschini MM, et al (2016) Poly(lactic acid) fibers obtained by solution blow spinning: Effect of a greener solvent on the fiber diameter. J Appl Polym Sci 133:. https://doi.org/https://doi.org/10.1002/app.43379

68. Carriles J, Nguewa P, González-Gaitano G (2023) Advances in Biomedical Applications of Solution Blow Spinning. Int J Mol Sci 24:. https://doi.org/10.3390/ijms241914757

69. Liu Y, Zhang G, Zhuang X, et al (2019) Solution Blown Nylon 6 Nanofibrous Membrane as Scaffold for Nanofiltration. Polymers (Basel) 11:. https://doi.org/10.3390/polym11020364

70. Rajkishore Nayak Ilias Louis Kyratzis YBTRP, Arnold L (2015) Structural and mechanical properties of polypropylene nanofibres fabricated by meltblowing. The Journal of The Textile Institute 106:629–640. https://doi.org/10.1080/00405000.2014.933512

71. Pu Y, Zheng J, Chen F, et al (2018) Preparation of Polypropylene Micro and Nanofibers by Electrostatic-Assisted Melt Blown and Their Application. Polymers (Basel) 10:. https://doi.org/10.3390/polym10090959

72. Matuana LM, Karkhanis SS, Stark NM, Sabo RC (2016) Cellulose nanocrystals as barrier performance enhancer of extrusion-blown PLA films for food applications. Biotech Biomater Biomed 3:1–4

73. Schmidt J, Shenvi Usgaonkar S, Kumar S, et al (2022) Advances in Melt Blowing Process Simulations. Ind Eng Chem Res 61:65–85. https://doi.org/10.1021/acs.iecr.1c03444

74. Shirwaiker RA, Fisher MB, Anderson B, et al (2020) High-Throughput Manufacture of 3D Fiber Scaffolds for Regenerative Medicine. Tissue Eng Part C Methods 26:364–374. https://doi.org/10.1089/ten.tec.2020.0098

75. Parikh D V, Chen Y, Sun L (2006) Reducing Automotive Interior Noise with Natural Fiber Nonwoven Floor Covering Systems. Textile Research Journal 76:813–820. https://doi.org/10.1177/0040517506063393

76. Van Roey M (1992) Water-resistant breathable fabrics. Journal of Coated Fabrics 22:20–31

77. Yang C, Jiang X, Gao X, et al (2022) Saving 80% Polypropylene in Facemasks by Laser-Assisted Melt-Blown Nanofibers. Nano Lett 22:7212–7219. https://doi.org/10.1021/acs.nanolett.2c02693

78. Müller DH, Krobjilowski A (2001) Meltblown Fabrics from Biodegradable Polymers. International Nonwovens Journal os-10:1558925001os–1000106. https://doi.org/10.1177/1558925001os-1000106

79. Goswami BC (1997) Spunbonding and melt-blowing processes. In: Gupta V. B. and Kothari VK (ed) Manufactured Fibre Technology. Springer Netherlands, Dordrecht, pp 560–594

80. Fedorova N, Pourdeyhimi B (2007) High strength nylon micro- and nanofiber based nonwovens via spunbonding. J Appl Polym Sci 104:3434–3442. https://doi.org/https://doi.org/10.1002/app.25939

81. Gutarowska B, Skora J, Nowak E, et al (2014) Antimicrobial activity and filtration effectiveness of nonwovens with Sanitized for respiratory protective equipment. Fibres & Textiles in Eastern Europe 120–125

82. Hasolli N, Park Y-O, Kim K-D (2021) Multi-layered nonwoven filter media for capture of nanoparticles in HVAC systems. Korean Journal of Chemical Engineering 38:982–988. https://doi.org/10.1007/s11814-021-0773-9

83. Majchrzycka K, Okrasa M, Brochocka A, Urbaniak-Domagała W (2017) Influence of Low-Temperature Plasma Treatment on The Liquid Filtration Efficiency of Melt-Blown PP Nonwovens in The Conditions of Simulated Use of Respiratory Protective Equipment. Chemical and Process Engineering 38:195–207. https://doi.org/10.1515/cpe-2017-0015

84. Haider MdK, Kharaghani D, Sun L, et al (2023) Synthesized bioactive lignin nanoparticles/polycaprolactone nanofibers: A novel nanobiocomposite for bone tissue engineering. Biomaterials Advances 144:213203. https://doi.org/https://doi.org/10.1016/j.bioadv.2022.213203

85. Hu A, Zuo B, Zhang F, et al (2012) Electrospun silk fibroin nanofibers promote Schwann cell adhesion, growth and proliferation. Neural Regen Res 7:

86. Tsai PP, Chen W, Roth JR (2004) Investigation of the Fiber, Bulk, and Surface Properties of Meltblown and Electrospun Polymeric Fabrics. International Nonwovens Journal os-13:1558925004os–1300306. https://doi.org/10.1177/1558925004os-1300306

87. Le B, Omran N, Hassanin AH, et al (2023) Flexible piezoelectric PVDF/TPU nanofibrous membranes produced by solution blow spinning. Journal of Materials Research and Technology 24:5032–5041. https://doi.org/https://doi.org/10.1016/j.jmrt.2023.04.051

88. S Manickam S, McCutcheon JR (2012) Characterization of polymeric nonwovens using porosimetry, porometry and X-ray computed tomography. J Memb Sci 407–408:108–115. https://doi.org/https://doi.org/10.1016/j.memsci.2012.03.022

89. Dong Y, Thomas NL, Lu X (2017) Electrospun dual-layer mats with covalently bonded ZnO nanoparticles for moisture wicking and antibacterial textiles. Mater Des 134:54–63. https://doi.org/https://doi.org/10.1016/j.matdes.2017.08.033

90. Gupta Ashish and Dhakate SR (2021) Cellulose Acetate-Based Nanofibers: Synthesis, Manufacturing, and Applications. In: Patel Jayvadan K. and Pathak Y V (ed)

Emerging Technologies for Nanoparticle Manufacturing. Springer International Publishing, Cham, pp 203–236

91. Olmedo CG, Aragón EQ, Garcia J, et al (2008) Study of porosity and permeability of air filter material in respiratory protection filters. In: Int. Multidiscip. Sci. Geo Conf. SGEM Surv. Geol. Min. Ecol. Manag. p 231

92. Kara Y, Molnár K (2022) A review of processing strategies to generate melt-blown nano/microfiber mats for high-efficiency filtration applications. Journal of Industrial Textiles 51:137S-180S. https://doi.org/10.1177/15280837211019488

93. Nadaf A, Gupta A, Hasan N, et al (2022) Recent update on electrospinning and electrospun nanofibers: current trends and their applications. RSC Adv 12:23808–23828

94. Wojasiński M, Pilarek M, Ciach T (2014) Comparative studies of electrospinning and solution blow spinning processes for the production of nanofibrous poly (L-lactic acid) materials for biomedical engineering. Polish Journal of Chemical Technology 16:43–50

95. Gao Y, Zhang J, Su Y, et al (2021) Recent progress and challenges in solution blow spinning. Mater Horiz 8:426–446

96. Kellie G (2016) Advances in technical nonwovens. Woodhead Publishing

97. Ahmed FE, Lalia BS, Hashaikeh R (2015) A review on electrospinning for membrane fabrication: Challenges and applications. Desalination 356:15–30. https://doi.org/https://doi.org/10.1016/j.desal.2014.09.033

98. Yoon J, Yang H-S, Lee B-S, Yu W-R (2018) Recent Progress in Coaxial Electrospinning: New Parameters, Various Structures, and Wide Applications. Advanced Materials 30:1704765. https://doi.org/https://doi.org/10.1002/adma.201704765

99. Medeiros ES, Glenn GM, Klamczynski AP, et al (2009) Solution blow spinning: A new method to produce micro- and nanofibers from polymer solutions. J Appl Polym Sci 113:2322–2330. https://doi.org/https://doi.org/10.1002/app.30275

100. McCulloch JG (1999) The History of the Development of Melt Blowing Technology. International Nonwovens Journal os-8:1558925099OS–800123. https://doi.org/10.1177/1558925099OS-800123

101. Sonatkar J, Kandasubramanian B (2021) Bioactive glass with biocompatible polymers for bone applications. Eur Polym J 160:110801. https://doi.org/https://doi.org/10.1016/j.eurpolymj.2021.110801

102. Rudnik E (2019) Compostable polymer materials. Newnes

103. Farah S, Anderson DG, Langer R (2016) Physical and mechanical properties of PLA, and their functions in widespread applications — A comprehensive review. Adv Drug Deliv Rev 107:367–392. https://doi.org/https://doi.org/10.1016/j.addr.2016.06.012

104. Wang Y, Jiang F, Ning W, et al (2022) Investigation on the Airflow Fields of New Melt-blown Dies with Rectangular Jets. Fibers and Polymers 23:2732–2739. https://doi.org/10.1007/s12221-022-0043-4

105. Sow PK, Ishita, Singhal R (2020) Sustainable approach to recycle waste polystyrene to high-value submicron fibers using solution blow spinning and application towards oil-water separation. J Environ Chem Eng 8:102786. https://doi.org/https://doi.org/10.1016/j.jece.2018.11.031

106. Muller J, González-Martínez C, Chiralt A (2017) Combination of Poly(lactic) Acid and Starch for Biodegradable Food Packaging. Materials 10:. https://doi.org/10.3390/ma10080952

107. Lv S, Liu X, Gu J, et al (2017) Effect of glycerol introduced into PLA based composites on the UV weathering behavior. Constr Build Mater 144:525–531. https://doi.org/https://doi.org/10.1016/j.conbuildmat.2017.03.209

108. Burns RG (2013) Microbial Extracellular Enzymes and the Degradation of Natural and Synthetic Polymers in Soil. In: Xu Jianming and Sparks DL (ed) Molecular Environmental Soil Science. Springer Netherlands, Dordrecht, pp 27–47

109. Valente BFA, Silvestre AJD, Neto CP, et al (2022) Improving the Processability and Performance of Micronized Fiber-Reinforced Green Composites through the Use of Biobased Additives. Polymers (Basel) 14:. https://doi.org/10.3390/polym14173451

110. Liu G, Wang X, Yu J, Ding B (2024) Earthworm-inspired mechanical toughened biodegradable polylactic acid microfiber for sustainable air filtration. Sep Purif Technol 338:126575. https://doi.org/https://doi.org/10.1016/j.seppur.2024.126575

111. Iwata Tadahisa and Tanaka T (2010) Manufacturing of PHA as Fibers. In: Chen GG-Q (ed) Plastics from Bacteria: Natural Functions and Applications. Springer Berlin Heidelberg, Berlin, Heidelberg, pp 257–282

112. Feijoo P, Samaniego-Aguilar K, Sánchez-Safont E, et al (2022) Development and Characterization of Fully Renewable and Biodegradable Polyhydroxyalkanoate Blends with Improved Thermoformability. Polymers (Basel) 14:. https://doi.org/10.3390/polym14132527

113. Naser AZ, Deiab I, Defersha F, Yang S (2021) Expanding Poly(lactic acid) (PLA) and Polyhydroxyalkanoates (PHAs) Applications: A Review on Modifications and Effects. Polymers (Basel) 13:. https://doi.org/10.3390/polym13234271

114. Kim J, Yun H, Won S, et al (2024) Comparative degradation behavior of polybutylene succinate (PBS), used PBS, and PBS/Polyhydroxyalkanoates (PHA) blend fibers in compost and marine–sediment interfaces. Sustainable Materials and Technologies 41:e01065. https://doi.org/https://doi.org/10.1016/j.susmat.2024.e01065

115. Atasağun HG, Bhat GS (2018) Advancement in flushable wipes: Modern technologies and characterization. Journal of Industrial Textiles 49:722–747. https://doi.org/10.1177/1528083718795910

116. Singh Meenakshi and Unadkat K and KS and EMK and PP and CK (2022) Potential Applications of Biopolymers in Fisheries Industry. In: Nadda Ashok Kumar and Sharma S and BR (ed) Biopolymers: Recent Updates, Challenges and Opportunities. Springer International Publishing, Cham, pp 199–221

117. Kusuma HS, Sabita A, Putri NA, et al (2024) Waste to wealth: Polyhydroxyalkanoates (PHA) production from food waste for a sustainable packaging paradigm. Food Chemistry: Molecular Sciences 9:100225

118. Meereboer KW, Misra M, Mohanty AK (2020) Review of recent advances in the biodegradability of polyhydroxyalkanoate (PHA) bioplastics and their composites. Green Chemistry 22:5519–5558

119. Burford T, Rieg W, Madbouly S (2023) Biodegradable poly (butylene adipate-co-terephthalate)(PBAT). Physical Sciences Reviews 8:1127–1156

120. Ferreira F V, Pinheiro IF, Mariano M, et al (2019) Environmentally friendly polymer composites based on PBAT reinforced with natural fibers from the amazon forest. Polym Compos 40:3351–3360

121. Chinsirikul W, Rojsatean J, Hararak B, et al (2015) Flexible and Tough Poly(lactic acid) Films for Packaging Applications: Property and Processability Improvement by Effective Reactive Blending. Packaging Technology and Science 28:741–759. https://doi.org/https://doi.org/10.1002/pts.2141

122. Schmitz L, Harada J, Ribeiro WB, et al (2023) Toughening of poly(lactic acid) (PLA) with poly(butylene adipate-co-terephthalate) (PBAT): a morphological, thermal, mechanical, and degradation evaluation in a simulated marine environment. Colloid Polym Sci 301:1405–1419. https://doi.org/10.1007/s00396-023-05157-3

123. Vishnu Dorugade Mengistu Taye SAQTABSBA, Komarabathina S (2023) Agrotextiles: Important Characteristics of Fibres and Their Applications – a Review. Journal of Natural Fibers 20:2211290. https://doi.org/10.1080/15440478.2023.2211290

124. Delacuvellerie A, Benali S, Cyriaque V, et al (2021) Microbial biofilm composition and polymer degradation of compostable and non-compostable plastics immersed in the marine environment. J Hazard Mater 419:126526. https://doi.org/https://doi.org/10.1016/j.jhazmat.2021.126526

125. Barletta M, Aversa C, Ayyoob M, et al (2022) Poly(butylene succinate) (PBS): Materials, processing, and industrial applications. Prog Polym Sci 132:101579. https://doi.org/https://doi.org/10.1016/j.progpolymsci.2022.101579

126. Kurkin A, Lipik V, Tan KBL, et al (2021) Correlations Between Precursor Molecular Weight and Dynamic Mechanical Properties of Polyborosiloxane (PBS). Macromol Mater Eng 306:2100360. https://doi.org/https://doi.org/10.1002/mame.202100360

127. Suzuki M, Ishii S, Ota M, et al (2024) Enhancing marine biodegradability of poly(butylene succinate) by blending with 16-hydroxyhexadecanoic acid and poly(ε-caprolactone). Polym Degrad Stab 228:110912. https://doi.org/https://doi.org/10.1016/j.polymdegradstab.2024.110912

128. Pratumpong P, Cholprecha T, Roungpaisan N, et al (2023) Effects of Melt-Blown Processing Conditions on Nonwoven Polylactic Acid and Polybutylene Succinate. Polymers (Basel) 15:. https://doi.org/10.3390/polym15204189

129. Mochane MJ, Magagula SI, Sefadi JS, Mokhena TC (2021) A Review on Green Composites Based on Natural Fiber-Reinforced Polybutylene Succinate (PBS). Polymers (Basel) 13:. https://doi.org/10.3390/polym13081200

130. Xue H, Mi Z, Shi L, et al (2023) A high-toughness, tailorable, wearable multifunctional sensor based on multisynergistic fabric-hydrogel constructed via dual-function boric acid bridge. Mater Today Chem 33:101696. https://doi.org/https://doi.org/10.1016/j.mtchem.2023.101696

131. Wang YR, Tou ZQ, Ravikumar R, et al (2019) Reflection-based thin-core modal interferometry optical fiber functionalized with PAA-PBA/PVA for glucose detection under physiological pH. Journal of Lightwave Technology 37:2773–2777

132. Kijchavengkul T, Auras R (2008) Compostability of polymers. Polym Int 57:793–804. https://doi.org/https://doi.org/10.1002/pi.2420

133. Fernandes MÂC, de Oliveira Vicente AAM, Salvador AFF (2023) Biodegradation Of PHA/PBAT Packaging Materials by Soil Microorganisms

134. Manfra L, Marengo V, Libralato G, et al (2021) Biodegradable polymers: A real opportunity to solve marine plastic pollution? J Hazard Mater 416:125763

135. Pradhan R, Misra M, Erickson L, Mohanty A (2010) Compostability and biodegradation study of PLA–wheat straw and PLA–soy straw based green composites in simulated composting bioreactor. Bioresour Technol 101:8489–8491. https://doi.org/https://doi.org/10.1016/j.biortech.2010.06.053

136. Meereboer KW, Misra M, Mohanty AK (2020) Review of recent advances in the biodegradability of polyhydroxyalkanoate (PHA) bioplastics and their composites. Green Chemistry 22:5519–5558

137. Fernandes M, Salvador AF, Vicente AA (2024) Biodegradation of PHB/PBAT films and isolation of novel PBAT biodegraders from soil microbiomes. Chemosphere 362:142696. https://doi.org/https://doi.org/10.1016/j.chemosphere.2024.142696

138. Neng W-B, Xie W-G, Lu B, et al (2021) Biodegradable thermoplastic copolyester elastomers: Methyl branched PBAmT. e-Polymers 21:336–345

139. Delacuvellerie A, Benali S, Cyriaque V, et al (2021) Microbial biofilm composition and polymer degradation of compostable and non-compostable plastics immersed in the marine environment. J Hazard Mater 419:126526. https://doi.org/https://doi.org/10.1016/j.jhazmat.2021.126526

140. Al Hosni AS, Pittman JK, Robson GD (2019) Microbial degradation of four biodegradable polymers in soil and compost demonstrating polycaprolactone as an ideal compostable plastic. Waste Management 97:105–114. https://doi.org/https://doi.org/10.1016/j.wasman.2019.07.042

141. Greene J (2014) Chapter 12 - Degradation and Biodegradation Standards for Starch-Based and Other Polymeric Materials. In: Halley PJ, Avérous L (eds) Starch Polymers. Elsevier, Amsterdam, pp 321–356

142. Schick S, Groten R, Seide GH (2023) Performance Spectrum of Home-Compostable Biopolymer Fibers Compared to a Petrochemical Alternative. Polymers (Basel) 15:1372

143. López-Ibáñez S, Quade J, Wlodarczyk A, et al (2024) Marine degradation and ecotoxicity of conventional, recycled and compostable plastic bags. Environmental Pollution 351:124096. https://doi.org/https://doi.org/10.1016/j.envpol.2024.124096

144. López-Ibáñez S, Beiras R (2022) Is a compostable plastic biodegradable in the sea? A rapid standard protocol to test mineralization in marine conditions. Science of The Total Environment 831:154860. https://doi.org/https://doi.org/10.1016/j.scitotenv.2022.154860

145. Greene J (2012) Marine Biodegradation of PLA, PHA, and Bio-Additive Polyethylene Based on ASTM D7081. ACADEMIA

146. López-Ibáñez S, Beiras R (2022) Is a compostable plastic biodegradable in the sea? A rapid standard protocol to test mineralization in marine conditions. Science of The Total Environment 831:154860. https://doi.org/https://doi.org/10.1016/j.scitotenv.2022.154860

147. Malara A (2024) Environmental concerns on the use of the electrospinning technique for the production of polymeric micro/nanofibers. Sci Rep 14:8293. https://doi.org/10.1038/s41598-024-58936-5

148. Ng C, Ho WT, Li CH (2023) Synthesis of Biocomposite through Electrospinning and Screw Extruder in Smart Laboratory Safety. In: 2023 IEEE International Symposium on Product Compliance Engineering - Asia (ISPCE-ASIA). pp 1–6

149. Bhatt T, Kumar H, Jain R, Jain V (2023) Emerging Applications of Electrospun Nanofibers Using Various Fabrication Techniques. Ind J Pharm Edu Res 57:658–668

150. Eggers R (2012) Industrial high pressure applications: processes, equipment, and safety. John Wiley & Sons

151. Jang M, Yang H, Park S-A, et al (2022) Analysis of volatile organic compounds produced during incineration of non-degradable and biodegradable plastics. Chemosphere 303:134946. https://doi.org/https://doi.org/10.1016/j.chemosphere.2022.134946

152. Rahman NSA, Yhaya MF, Azahari B, Ismail WR (2018) Utilisation of natural cellulose fibres in wastewater treatment. Cellulose 25:4887–4903. https://doi.org/10.1007/s10570-018-1935-8

153. Sivakumar V (2022) Towards environmental protection and process safety in leather processing – A comprehensive analysis and review. Process Safety and Environmental Protection 163:703–726. https://doi.org/https://doi.org/10.1016/j.psep.2022.05.062

154. Srikrishnan MR, Raghunathan K (2013) Application of nonwoven in medical textiles. Asian textile journal 77:

155. Jafari M, Shim E, Joijode A (2021) Fabrication of Poly(lactic acid) filter media via the meltblowing process and their filtration performances: A comparative study with polypropylene meltblown. Sep Purif Technol 260:118185. https://doi.org/https://doi.org/10.1016/j.seppur.2020.118185

156. Mengna Peng Huiying Jia LJYZ, Ma J (2019) Study on structure and property of PP/TPU melt-blown nonwovens. The Journal of The Textile Institute 110:468–475. https://doi.org/10.1080/00405000.2018.1485461

157. Hassan MA, Yeom BY, Wilkie A, et al (2013) Fabrication of nanofiber meltblown membranes and their filtration properties. J Memb Sci 427:336–344. https://doi.org/https://doi.org/10.1016/j.memsci.2012.09.050

158. Morteza H. Bagheri Iman Khalaji AARTLNBSMMLGSMCM, Schiffres SN (2021) Filtration efficiency, breathability, and reusability of improvised materials for face masks. Aerosol Science and Technology 55:817–827. https://doi.org/10.1080/02786826.2021.1898537

159. Shim E, Jang J-P, Moon J-J, Kim Y (2021) Improvement of Polytetrafluoroethylene Membrane High-Efficiency Particulate Air Filter Performance with Melt-Blown Media. Polymers (Basel) 13:. https://doi.org/10.3390/polym13234067

160. Duran D (2012) Investigation of the physical characteristics of polypropylene meltblown nonwovens under varying production parameters. Thermoplastic Elastomers London, UK: InTech Open Publication 243–260

161. Wang W, Feng L, Song B, et al (2022) Fabrication and application of superhydrophobic nonwovens: a review. Mater Today Chem 26:101227. https://doi.org/https://doi.org/10.1016/j.mtchem.2022.101227

162. Ma Y, Wisuthiphaet N, Bolt H, et al (2021) N-Halamine Polypropylene Nonwoven Fabrics with Rechargeable Antibacterial and Antiviral Functions for Medical Applications. ACS Biomater Sci Eng 7:2329–2336. https://doi.org/10.1021/acsbiomaterials.1c00117

163. Peng Z, Li Z, Huang X, et al Electrostatic charge injection for reusing face masks: Mechanisms, performance, and a household alternative. EcoMat n/a:e12497. https://doi.org/https://doi.org/10.1002/eom2.12497

164. Essa WK, Yasin SA, Saeed IA, Ali GAM (2021) Nanofiber-Based Face Masks and Respirators as COVID-19 Protection: A Review. Membranes (Basel) 11:. https://doi.org/10.3390/membranes11040250

165. Gürsel Korkmaz Mehmet Kılınç SARMOSK, Kut YDT (2023) Comparison of the performance properties of spunlaid non-woven fabrics used as face mask. The Journal of The Textile Institute 114:250–256. https://doi.org/10.1080/00405000.2022.2027073

166. Wu R, Shanbhag S, Selvaganapathy PR (2023) Efficient, Breathable, and Compostable Multilayer Air Filter Material Prepared from Plant-Derived Biopolymers. Membranes (Basel) 13:. https://doi.org/10.3390/membranes13040380

167. Benjamin Valdez-Salas Ernesto Beltran-Partida NCJS-CEAV-SMC-A, Ibarra-Wiley R (2021) Promotion of Surgical Masks Antimicrobial Activity by Disinfection and Impregnation with Disinfectant Silver Nanoparticles. Int J Nanomedicine 16:2689–2702. https://doi.org/10.2147/IJN.S301212

168. Dutton KC (2009) Overview and analysis of the meltblown process and parameters. Journal of Textile and Apparel, Technology and Management 6:

169. Hao X, Zeng Y (2019) A Review on the Studies of Air Flow Field and Fiber Formation Process during Melt Blowing. Ind Eng Chem Res 58:11624–11637. https://doi.org/10.1021/acs.iecr.9b01694

170. Wölfel B, Seefried A, Allen V, et al (2020) Recycling and Reprocessing of Thermoplastic Polyurethane Materials towards Nonwoven Processing. Polymers (Basel) 12:. https://doi.org/10.3390/polym12091917

171. Walsh LJ (2024) Reusable Personal Protective Equipment Viewed Through the Lens of Sustainability. Int Dent J 74:S446–S454. https://doi.org/https://doi.org/10.1016/j.identj.2024.07.1270

172. Pei C, Chen W, Ou Q, et al (2023) Smart Filter Performance Monitoring System. Aerosol Air Qual Res 23:220416

173. Wilson A (2023) 21 - Smart textiles for personal protection equipment (PPE). In: McCann J, Bryson D (eds) Smart Clothes and Wearable Technology (Second Edition), Second Edition. Woodhead Publishing, pp 583–597

174. Mohamadi PS (2023) Innovative air clogging detection system for air filters based on e-textiles. Centrale Lille Institut

175. Luo T, Farooq A, Weng W, et al (2024) Progress in the Preparation and Application of Breathable Membranes. Polymers (Basel) 16:. https://doi.org/10.3390/polym16121686

176. Kim JT, Kwon J, Lee H, et al (2024) Sunlight-Driven Self-Cleaning Ultrafine Particulate Matter Filter with Antibacterial Activity. ACS Nano 18:6387–6397. https://doi.org/10.1021/acsnano.3c11284

177. Liu B, Hu J, Meng Q (2009) Nonwoven supported temperature-sensitive poly(N-isopropylacrylamide)/polyurethane copolymer hydrogel with antibacterial activity. J Biomed Mater Res B Appl Biomater 89B:1–8. https://doi.org/https://doi.org/10.1002/jbm.b.31180

178. Gorji M, Mazinani S, Gharehaghaji AA (2022) A review on emerging developments in thermal and moisture management by membrane-based clothing systems towards personal comfort. J Appl Polym Sci 139:e52416. https://doi.org/https://doi.org/10.1002/app.52416

179. Safranski DL, Griffis JC (2017) Applications of shape-memory polymers. Shape-Memory Polymer Device Design 189–222

180. Aytac Z, Xu J, Raman Pillai SK, et al (2021) Enzyme- and Relative Humidity-Responsive Antimicrobial Fibers for Active Food Packaging. ACS Appl Mater Interfaces 13:50298–50308. https://doi.org/10.1021/acsami.1c12319

181. Liu R, Wang Y, Fan W, et al (2024) Adaptive dynamic smart textiles for personal thermal-moisture management. Eur Polym J 206:112777. https://doi.org/https://doi.org/10.1016/j.eurpolymj.2024.112777

182. He W, Guo Y, Zhao Y-B, et al (2021) Self-supporting smart air filters based on PZT/PVDF electrospun nanofiber composite membrane. Chemical Engineering Journal 423:130247. https://doi.org/https://doi.org/10.1016/j.cej.2021.130247

183. Shahidi S, Wiener J (2012) Antibacterial agents in textile industry. Antimicrobial agents 2012:387–406

184. Sarkar A, Saha A, Bhattacharjee B, et al (2023) Nanozymes Induced Air Purification-A State of the Art Review

185. Asri ARH, Prasetyo A, Sadhana U, et al (2021) Trend Analysis of Superoxide Dismutase 3 (SOD3) and Reactive Oxygen Species (ROS) levels on BioSmart and Safe Bus Passengers. Indian J Sci Technol 14:2751–2760

186. Simončič B, Klemenčič D (2016) Preparation and performance of silver as an antimicrobial agent for textiles: A review. Textile Research Journal 86:210–223. https://doi.org/10.1177/0040517515586157

187. Rafi R, Zulfiqar S, Asad M, et al (2023) Smart wound dressings based on carbon doped copper nanoparticles for selective bacterial detection and eradication for efficient wound healing application. Mater Today Commun 35:105914. https://doi.org/https://doi.org/10.1016/j.mtcomm.2023.105914

188. Bhattacharjee S, Joshi R, Chughtai AA, Macintyre CR (2019) Graphene Modified Multifunctional Personal Protective Clothing. Adv Mater Interfaces 6:1900622. https://doi.org/https://doi.org/10.1002/admi.201900622

189. Ma Y, Wisuthiphaet N, Bolt H, et al (2021) N-Halamine Polypropylene Nonwoven Fabrics with Rechargeable Antibacterial and Antiviral Functions for Medical Applications. ACS Biomater Sci Eng 7:2329–2336. https://doi.org/10.1021/acsbiomaterials.1c00117

190. Jain A, Duvvuri LS, Farah S, et al (2014) Antimicrobial Polymers. Adv Healthc Mater 3:1969–1985. https://doi.org/https://doi.org/10.1002/adhm.201400418

191. Olmos D, González-Benito J (2021) Polymeric Materials with Antibacterial Activity: A Review. Polymers (Basel) 13:. https://doi.org/10.3390/polym13040613

192. Kim JR, Michielsen S (2016) Synthesis of Antifungal Agents from Xanthene and Thiazine Dyes and Analysis of Their Effects. Nanomaterials 6:. https://doi.org/10.3390/nano6120243

193. Moan J (1990) On the diffusion length of singlet oxygen in cells and tissues. J Photochem Photobiol B 6:343–344. https://doi.org/https://doi.org/10.1016/1011-1344(90)85104-5

194. Sánchez-Valdes S, Ramírez-Vargas E, Ortega-Ortiz H, et al (2012) Silver nanoparticle deposition on hydrophilic multilayer film surface and its effect on antimicrobial activity. J Appl Polym Sci 123:2643–2650. https://doi.org/https://doi.org/10.1002/app.34667

195. Kim JR, Michielsen S (2015) Photodynamic antifungal activities of nanostructured fabrics grafted with rose bengal and phloxine B against spergillus fumigatus. J Appl Polym Sci 132:. https://doi.org/https://doi.org/10.1002/app.42114

196. Abd Ali SAZ, Joubert A, Andrès Y (2021) Evaluation of Antimicrobial Effect of Zinc Pyrithione against Airborne Fungi and Bacteria Growth Collected onto New and Loaded HVAC Fibrous Filters. Processes 9:. https://doi.org/10.3390/pr9091528

197. Forthomme A, Joubert A, Andrès Y, et al (2014) Microbial aerosol filtration: Growth and release of a bacteria–fungi consortium collected by fibrous filters in different operating conditions. J Aerosol Sci 72:32–46. https://doi.org/https://doi.org/10.1016/j.jaerosci.2014.02.004

198. Joubert A, Abd Ali SAZ, Frossard M, Andrès Y (2021) Dust and microbial filtration performance of regular and antimicrobial HVAC filters in realistic conditions. Environmental Science and Pollution Research 28:39907–39919. https://doi.org/10.1007/s11356-021-13330-w

199. Burge HP, Solomon WR, Boise JR (1977) Comparative merits of eight popular media in aerometric studies of fungi. Journal of Allergy and Clinical Immunology 60:199–203. https://doi.org/https://doi.org/10.1016/0091-6749(77)90124-5

200. Morisseau K, Joubert A, Le Coq L, Andres Y (2017) Quantification of the fungal fraction released from various preloaded fibrous filters during a simulated ventilation restart. Indoor Air 27:529–538. https://doi.org/https://doi.org/10.1111/ina.12330

201. Seal LA, Paul-Cheadle D (2004) A systems approach to preoperative surgical patient skin preparation. Am J Infect Control 32:57–62. https://doi.org/https://doi.org/10.1016/j.ajic.2003.11.001

202. MacDiarmid CW, Milanick MA, Eide DJ (2002) Biochemical Properties of Vacuolar Zinc Transport Systems ofSaccharomyces cerevisiae *. Journal of Biological Chemistry 277:39187–39194. https://doi.org/10.1074/jbc.M205052200

203. Min KT, Lundrigan P, Sward K, et al (2018) Smart home air filtering system: A randomized controlled trial for performance evaluation. Smart Health 9–10:62–75. https://doi.org/https://doi.org/10.1016/j.smhl.2018.07.009

204. Raman R, Varma R (2024) Next-Gen HVAC Technologies with K-Nearest Neighbors for Cloud-Optimized Allergen Filtration for Healthier Living Spaces. In: 2024 International Conference on Inventive Computation Technologies (ICICT). pp 788–793

205. Walczak J, Sobota M, Chrzanowski M, Krucinska I (2018) Application of the melt-blown technique in the production of shape-memory nonwoven fabrics from a blend of poly(L-lactide) and atactic poly[(R,S)-3-hydroxy butyrate]. Textile Research Journal 88:2141–2152. https://doi.org/10.1177/0040517517716906

206. Hiremath N, Bhat G (2015) Melt blown polymeric nanofibers for medical applications-an overview. Nanosci Technol 2:1–9

207. Mariani F, Serafini M, Gualandi I, et al (2021) Advanced Wound Dressing for Real-Time pH Monitoring. ACS Sens 6:2366–2377. https://doi.org/10.1021/acssensors.1c00552

208. Svensson E, Wahlström E (2017) Monitoring pH in wounds: The possibilities of textiles in healthcare

209. Prakashan D, Kaushik A, Gandhi S (2024) Smart sensors and wound dressings: Artificial intelligence-supported chronic skin monitoring – A review. Chemical

Engineering Journal 497:154371. https://doi.org/https://doi.org/10.1016/j.cej.2024.154371

210. Gupta B, Agarwal R, Alam MS (2010) Textile-based smart wound dressings

211. Brochocka A, Nowak A, Majchrzycka K, et al (2020) Multifunctional Polymer Composites Produced by Melt-Blown Technique to Use in Filtering Respiratory Protective Devices. Materials 13:. https://doi.org/10.3390/ma13030712

212. Kaur M (2024) A Novel Approach to Digital Filter Design for Environmental Monitoring applications. In: 2024 2nd World Conference on Communication & Computing (WCONF). pp 1–7

213. Chung MH, Yoo S, Jung W-N, et al (2023) Self-Powered Airflow Sensor Based on Energy Harvesting of Ventilation Air in Buildings. Advanced Fiber Materials 5:1788–1798. https://doi.org/10.1007/s42765-023-00308-1

214. Wan LY (2018) Nanofibers for smart textiles. Smart Textiles: Wearable Nanotechnology 39–90

215. Liu C, Hsu P-C, Lee H-W, et al (2015) Transparent air filter for high-efficiency PM2. 5 capture. Nat Commun 6:6205

216. Rawal A, Kameswara Rao P V, Russell S, Jeganathan A (2010) Effect of fiber orientation on pore size characteristics of nonwoven structures. J Appl Polym Sci 118:2668–2673. https://doi.org/https://doi.org/10.1002/app.32608

217. Crawford EA, Gupta S, Trinh BM, Mekonnen TH (2024) Styrene-ethylene-butylene-styrene (SEBS) melt-blown fibers for oil spill remediation and oil barrier geotextiles. Polymer (Guildf) 298:126942

218. Nepomuceno NC, Barbosa MA, Bonan RF, et al (2018) Antimicrobial activity of PLA/PEG nanofibers containing terpinen-4-ol against Aggregatibacter actinomycetemcomitans. J Appl Polym Sci 135:45782. https://doi.org/https://doi.org/10.1002/app.45782

219. Lee H, Trinh BM, Crawford EA, Mekonnen TH (2023) Thermoplastic elastomer melt-blown fiber mats for oil spill remediation: Fabrication, oil uptake, and gel formation studies. Sep Purif Technol 326:124761. https://doi.org/https://doi.org/10.1016/j.seppur.2023.124761

220. Ewell N, Lee J, Mulherin K, Rutledge GC (2024) Development of Electrospun Polyacrylonitrile Aerosol Filter Media for Respiratory Personal Protective Equipment. ACS Applied Engineering Materials 2:1082–1093. https://doi.org/10.1021/acsaenm.4c00083

221. Jafari M, Shim E, Joijode A (2021) Fabrication of Poly(lactic acid) filter media via the meltblowing process and their filtration performances: A comparative study with polypropylene meltblown. Sep Purif Technol 260:118185. https://doi.org/https://doi.org/10.1016/j.seppur.2020.118185

222. Li Y, Zhu J, Cheng H, et al (2021) Developments of Advanced Electrospinning Techniques: A Critical Review. Adv Mater Technol 6:2100410. https://doi.org/https://doi.org/10.1002/admt.202100410

223. Agarwal S, Greiner A (2011) On the way to clean and safe electrospinning—green electrospinning: emulsion and suspension electrospinning. Polym Adv Technol 22:372–378. https://doi.org/https://doi.org/10.1002/pat.1883

224. Tsai PP, Chen W, Roth JR (2004) Investigation of the Fiber, Bulk, and Surface Properties of Meltblown and Electrospun Polymeric Fabrics. International Nonwovens Journal os-13:1558925004os–1300306. https://doi.org/10.1177/1558925004os-1300306

225. Liu G, Guan J, Wang X, et al (2023) Polylactic Acid (PLA) Melt-Blown Nonwovens with Superior Mechanical Properties. ACS Sustain Chem Eng 11:4279–4288. https://doi.org/10.1021/acssuschemeng.3c00159

226. Kara Y, Molnár K (2022) A review of processing strategies to generate melt-blown nano/microfiber mats for high-efficiency filtration applications. Journal of Industrial Textiles 51:137S-180S. https://doi.org/10.1177/15280837211019488

227. Podgórski A, Bałazy A, Gradoń L (2006) Application of nanofibers to improve the filtration efficiency of the most penetrating aerosol particles in fibrous filters. Chem Eng Sci 61:6804–6815. https://doi.org/https://doi.org/10.1016/j.ces.2006.07.022

228. Kara Y, Molnár K (2021) A review of processing strategies to generate melt-blown nano/microfiber mats for high-efficiency filtration applications. Journal of Industrial Textiles 51:137S-180S. https://doi.org/10.1177/15280837211019488

229. Wang H, Zhang Y, Gao H, et al (2016) Composite melt-blown nonwoven fabrics with large pore size as Li-ion battery separator. Int J Hydrogen Energy 41:324–330. https://doi.org/https://doi.org/10.1016/j.ijhydene.2015.09.130

230. Binley G, Jubinville D, Prince E, Mekonnen TH (2024) Hydrogen Peroxide-Induced Controlled Degradation of Poly(lactic acid) for Melt-Blown Nonwovens. ACS Appl Polym Mater 6:13427–13438. https://doi.org/10.1021/acsapm.4c02897

231. Yu L, Hu Q, Li T, et al (2023) Ultrahigh Flowability and Excellent Mechanical Performance of Glass Fiber/PA6 Composites Prepared by Hyperbranched Polymers. Macromol Mater Eng 308:2300012. https://doi.org/https://doi.org/10.1002/mame.202300012

232. Wadsworth LC, Hayes DG, Wszelaki AL, et al (2013) Evaluation of Degradable Spun-Melt 100% Polylactic Acid Nonwoven Mulch Materials in a Greenhouse Environment. J Eng Fiber Fabr 8:155892501300800420. https://doi.org/10.1177/155892501300800414

233. Madej-Kiełbik L, Jóźwik-Pruska J, Dziuba R, et al (2024) The Impact of the COVID-19 Pandemic on the Amount of Plastic Waste and Alternative Materials in the Context of the Circular Economy. Sustainability 16:. https://doi.org/10.3390/su16041555

234. Cui J, Li F, Wang Y, et al (2020) Electrospun nanofiber membranes for wastewater treatment applications. Sep Purif Technol 250:117116. https://doi.org/https://doi.org/10.1016/j.seppur.2020.117116

235. Yan F, Yanjin S (2013) Research on preparation and properties of methacrylate grafted meltblown polypropylene nonwovens for oily wastewater treatment. Desalination Water Treat 51:5460–5465. https://doi.org/10.1080/19443994.2012.762330

236. Dzierzkowska E, Scisłowska-Czarnecka A, Kudzin M, et al (2021) Effects of Process Parameters on Structure and Properties of Melt-Blown Poly(Lactic Acid) Nonwovens for Skin Regeneration. J Funct Biomater 12:. https://doi.org/10.3390/jfb12010016

237. Senthil Muthu Kumar T, Senthil Kumar K, Rajini N, et al (2019) A comprehensive review of electrospun nanofibers: Food and packaging perspective. Compos B Eng 175:107074. https://doi.org/https://doi.org/10.1016/j.compositesb.2019.107074

238. Hwang SH, Lee BH (2022) Comparison of melt-blown and glass-fiber HEPA asbestos filters based on ISO filter classes, filtration efficiency, power consumption, and face velocity. J Air Waste Manage Assoc 72:271–280. https://doi.org/10.1080/10962247.2021.1962431

239. Muthuraj R, Hajee M, Horrocks AR, Kandola BK (2019) Biopolymer blends from hardwood lignin and bio-polyamides: Compatibility and miscibility. Int J Biol Macromol 132:439–450. https://doi.org/https://doi.org/10.1016/j.ijbiomac.2019.03.142

240. Shorey R, Mekonnen TH (2024) Oleic acid decorated kraft lignin as a hydrophobic and functional filler of cellulose acetate films. Int J Biol Macromol 268:131672. https://doi.org/https://doi.org/10.1016/j.ijbiomac.2024.131672

241. Kaseem M, Ko YG (2017) Melt Flow Behavior and Processability of Polylactic Acid/Polystyrene (PLA/PS) Polymer Blends. J Polym Environ 25:994–998. https://doi.org/10.1007/s10924-016-0873-5

242. Dangtungee R, Petcharoen K, Pinijsattawong K, Siengchin S (2012) Investigation of the rheological properties and die swell of polylactic acid/nanoclay composites in a capillary rheometer. Mechanics of Composite Materials 47:663–670. https://doi.org/10.1007/s11029-011-9246-2

243. Reddy Polu A, Kumar R (2011) Impedance Spectroscopy and FTIR Studies of PEG - Based Polymer Electrolytes. J Chem 8:347–353. https://doi.org/10.1155/2011/628790

244. Zou H, Yi C, Wang L, et al (2009) Thermal degradation of poly(lactic acid) measured by thermogravimetry coupled to Fourier transform infrared spectroscopy. J Therm Anal Calorim 97:929–935. https://doi.org/10.1007/s10973-009-0121-5

245. Jubinville D, Awad M, Lee H-S, Mekonnen TH (2024) Effect of Compatibilizers on the Physico-mechanical Properties of a Poly(Lactic Acid)/ Poly(Butylene Adipate-co-terephthalate) Matrix with Rice Straw Micro-particle Fillers. J Polym Environ. https://doi.org/10.1007/s10924-024-03314-5

246. Sahu M, Reddy VRM, Kim B, et al (2022) Fabrication of Cu2ZnSnS4 Light Absorber Using a Cost-Effective Mechanochemical Method for Photovoltaic Applications. Materials 15:1708. https://doi.org/10.3390/ma15051708

247. Wang Z, Chang Y, Jia S, Liu F (2024) Preparation and Properties of Polyimide/Polysulfonamide/Polyethylene Glycol (PI/PSA/PEG) Hydrophobic Nanofibrous Membranes. Materials 17:4135. https://doi.org/10.3390/ma17164135

248. Park JY, Daksha P, Lee GH, et al (2008) Highly water-dispersible PEG surface modified ultra small superparamagnetic iron oxide nanoparticles useful for target-specific biomedical applications. Nanotechnology 19:365603. https://doi.org/10.1088/0957-4484/19/36/365603

249. Li F-J, Zhang S-D, Liang J-Z, Wang J-Z (2015) Effect of polyethylene glycol on the crystallization and impact properties of polylactide-based blends. Polym Adv Technol 26:465–475. https://doi.org/https://doi.org/10.1002/pat.3475

250. Johansson P, Paberit R, Rilby E, et al (2020) Cycling stability of poly(ethylene glycol) of six molecular weights: Influence of thermal conditions for energy applications. ACS Appl Energy Mater 3:10578–10589. https://doi.org/10.1021/acsaem.0c01621

251. Zhao H, Liu Z, Park S, et al (2012) Preparation and characterization of PEG/PLA multiblock and triblock copolymer. Bull Korean Chem Soc 33:1638–1642. https://doi.org/dx.doi.org/10.5012/bkcs.012.33.5.1638

252. Hassouna F, Raquez J-M, Addiego F, et al (2011) New approach on the development of plasticized polylactide (PLA): Grafting of poly(ethylene glycol) (PEG) via reactive extrusion. Eur Polym J 47:2134–2144. https://doi.org/10.1016/j.eurpolymj.2011.08.001

253. Jubinville D, Sharifi J, Mekonnen TH, Fayazfar H (2023) A Comparative Study of the Physico-Mechanical Properties of Material Extrusion 3D-Printed and Injection Molded Wood-Polymeric Biocomposites. J Polym Environ 31:3338–3350. https://doi.org/10.1007/s10924-023-02816-y

254. Mohapatra AK, Mohanty S, Nayak SK (2014) Effect of PEG on PLA/PEG blend and its nanocomposites: A study of thermo-mechanical and morphological characterization. Polym Compos 35:283–293. https://doi.org/10.1002/pc.22660

255. Salimi A, Ahmadi S, Faramarzi M, Faghihi J (2023) Reactive blending of polylactic acid/polyethylene glycol toward biodegradable film. Macromol Res 31:873–881. https://doi.org/10.1007/s13233-023-00174-1

256. Li R, Wu Y, Bai Z, et al (2020) Effect of molecular weight of polyethylene glycol on crystallization behaviors, thermal properties and tensile performance of polylactic acid stereocomplexes. RSC Adv 10:42120–42127. https://doi.org/10.1039/D0RA08699A

257. Li R, Pan Y, Chen D, et al (2022) Design, Preparation and In Vitro Evaluation of Core–Shell Fused Deposition Modelling 3D-Printed Verapamil Hydrochloride Pulsatile Tablets. Pharmaceutics 14:437. https://doi.org/10.3390/pharmaceutics14020437

258. Mandal S, Ishak S, Mohd Ariffin MA, et al (2023) Effect of pore structure on the thermal stability of shape-stabilized phase change materials. Journal of Materials Research and Technology 25:465–479. https://doi.org/10.1016/j.jmrt.2023.05.217

259. Zhang J, Wang S, Qiao Y, Li Q (2016) Effect of morphology designing on the structure and properties of PLA/PEG/ABS blends. Colloid Polym Sci 294:1779–1787. https://doi.org/10.1007/s00396-016-3940-5

260. Xue P, Wang K, Jia M, Yang M (2013) Biodegradation and mechanical property of polylactic acid/thermoplastic starch blends with poly (ethylene glycol). Journal of Wuhan University of Technology-Mater Sci Ed 28:157–162. https://doi.org/10.1007/s11595-013-0658-9

261. Li F, Tan L, Zhang S, Zhu B (2016) Compatibility, steady and dynamic rheological behaviors of polylactide/poly(ethylene glycol) blends. J Appl Polym Sci 133:. https://doi.org/10.1002/app.42919

262. Shi W, Chen Z (2023) Mechanical, rheological, and crystallinity properties of polylactic acid/polyethylene <scp>glycol-polydimethylsiloxane</scp> copolymer blends by melt blending. J Appl Polym Sci 140:. https://doi.org/10.1002/app.53346

263. Yu S, Zhang Y, Hu H, et al (2022) Effect of maleic anhydride grafted poly(lactic acid) on rheological behaviors and mechanical performance of poly(lactic acid)/poly(ethylene glycol) (PLA/PEG) blends. RSC Adv 12:31629–31638. https://doi.org/10.1039/D2RA03513H

264. Sungsanit K, Kao N, Bhattacharya SN (2012) Properties of linear poly(lactic acid)/polyethylene glycol blends. Polym Eng Sci 52:108–116. https://doi.org/10.1002/pen.22052

265. Wolf MH, Gil-Castell O, Cea J, et al (2023) Degradation of Plasticised Poly(lactide) Composites with Nanofibrillated Cellulose in Different Hydrothermal Environments. J Polym Environ 31:2055–2072. https://doi.org/10.1007/s10924-022-02711-y

266. Xie D, Zhao Y, Li Y, et al (2019) Rheological, Thermal, and Degradation Properties of PLA/PPG Blends. Materials 12:3519. https://doi.org/10.3390/ma12213519

267. Patti A, Acierno D, Latteri A, et al (2020) Influence of the Processing Conditions on the Mechanical Performance of Sustainable Bio-Based PLA Compounds. Polymers (Basel) 12:2197. https://doi.org/10.3390/polym12102197

268. Azizi N, Mahdavi HR, Isanejad M, Mohammadi T (2017) Effects of low and high molecular mass PEG incorporation into different types of poly(ether-b-amide) copolymers on the permeation properties of CO2 and CH4. Journal of Polymer Research 24:141. https://doi.org/10.1007/s10965-017-1297-1

269. Rostami N, Faridghiasi F, Ghebleh A, et al (2023) Design, Synthesis, and Comparison of PLA-PEG-PLA and PEG-PLA-PEG Copolymers for Curcumin Delivery to Cancer Cells. Polymers (Basel) 15:. https://doi.org/10.3390/polym15143133

270. Wang Z, Zhao C, Pan Z (2015) Porous bead-on-string poly(lactic acid) fibrous membranes for air filtration. J Colloid Interface Sci 441:121–129. https://doi.org/https://doi.org/10.1016/j.jcis.2014.11.041

271. Chen C-C, Willeke K (1992) Aerosol penetration through surgical masks. Am J Infect Control 20:177–184. https://doi.org/https://doi.org/10.1016/S0196-6553(05)80143-9

272. Botequim D, Maia J, Lino MMF, et al (2012) Nanoparticles and Surfaces Presenting Antifungal, Antibacterial and Antiviral Properties. Langmuir 28:7646–7656. https://doi.org/10.1021/la300948n

273. Davison AM Pathogen inactivation and filtration efficacy of a new anti-microbial and anti-viral surgical facemask and N95 against dentistry-associated microorganisms

274. Simončič B, Klemenčič D (2015) Preparation and performance of silver as an antimicrobial agent for textiles: A review. Textile Research Journal 86:210–223. https://doi.org/10.1177/0040517515586157

275. Emam HE, Manian AP, Široká B, et al (2014) Copper(I)oxide surface modified cellulose fibers—Synthesis, characterization and antimicrobial properties. Surf Coat Technol 254:344–351. https://doi.org/https://doi.org/10.1016/j.surfcoat.2014.06.036

276. Li J, Tian X, Hua T, et al (2021) Chitosan Natural Polymer Material for Improving Antibacterial Properties of Textiles. ACS Appl Bio Mater 4:4014–4038. https://doi.org/10.1021/acsabm.1c00078

277. Hwang GB, Park H-S, Bae G-N, Jung JH (2014) Effects of Electric Field Strength on an Antimicrobial Air Filter. Aerosol Air Qual Res 14:1028–1037. https://doi.org/10.4209/aaqr.2013.06.0199

278. Kim J, Park J, Tsai P-J, Yoon C (2024) The Effects of Temperature and Humidity on Electrostatic Changes in Respirators and Their Filtration Efficiency. Indoor Air 2024:5503400. https://doi.org/https://doi.org/10.1155/2024/5503400

279. Seidi F, Deng C, Zhong Y, et al (2021) Functionalized Masks: Powerful Materials against COVID-19 and Future Pandemics. Small 17:2102453. https://doi.org/https://doi.org/10.1002/smll.202102453

280. Rahman MZ, Hoque ME, Alam MR, et al (2022) Face Masks to Combat Coronavirus (COVID-19)—Processing, Roles, Requirements, Efficacy, Risk and Sustainability. Polymers (Basel) 14:. https://doi.org/10.3390/polym14071296

281. Kang L, Huang S, Qin X, et al (2024) Ag Nanoparticles-Decorated PVDF Nanofiber/Net Membranes with Enhanced Filtration and Antibacterial Efficiency for Personal Protective Equipment. ACS Appl Nano Mater 7:9252–9261. https://doi.org/10.1021/acsanm.4c00751

282. Vanangamudi A, Hamzah S, Singh G (2015) Synthesis of hybrid hydrophobic composite air filtration membranes for antibacterial activity and chemical detoxification with high particulate filtration efficiency (PFE). Chemical Engineering Journal 260:801–808. https://doi.org/https://doi.org/10.1016/j.cej.2014.08.062

283. Yoon J, Lee J, Hong SP, et al (2024) Fabrication of biodegradable cellulose acetate nanofibers containing Rose Bengal dye by electrospinning technique and their antiviral efficacy under visible light irradiation. Chemosphere 349:140897. https://doi.org/10.1016/j.chemosphere.2023.140897

284. Balasubramaniam B, Prateek, Ranjan S, et al (2021) Antibacterial and Antiviral Functional Materials: Chemistry and Biological Activity toward Tackling COVID-19-like Pandemics. ACS Pharmacol Transl Sci 4:8–54. https://doi.org/10.1021/acsptsci.0c00174

285. Blanchard R, Jubinville D, Li J, et al (2024) Modified Cellulose Nanocrystals Enabled Antimicrobial Polymeric Films. Adv Sustain Syst 2400033:1–16. https://doi.org/10.1002/adsu.202400033

286. Li Y, Wang J, Yang Y, et al (2021) A rose bengal/graphene oxide/PVA hybrid hydrogel with enhanced mechanical properties and light-triggered antibacterial activity for wound treatment. Materials Science and Engineering: C 118:111447. https://doi.org/https://doi.org/10.1016/j.msec.2020.111447

287. Shen H, Zhou Z, Wang H, et al (2022) Photosensitized Electrospun Nanofibrous Filters for Capturing and Killing Airborne Coronaviruses under Visible Light Irradiation. Environ Sci Technol 56:4295–4304. https://doi.org/10.1021/acs.est.2c00885

288. Doronin F, Rudakova A, Rytikov G, Nazarov V (2023) Simple Determination of the Melt Flow Index of Composite Polymer Filaments Used in Material Extrusion Additive Manufacturing. Coatings 13:1592. https://doi.org/10.3390/coatings13091592

289. Shulga G, Rizhikovs J, Neiberte B, et al (2023) Processing and Properties of Wood-Plastic Composite Containing Alkali-Treated Birch Wood Shavings and Bioadditive Obtained by Biorefinery of Birch Bark. Forests 14:1906. https://doi.org/10.3390/f14091906

290. Ray S, Cooney RP (2018) Chapter 9 - Thermal Degradation of Polymer and Polymer Composites. In: Kutz M (ed) Handbook of Environmental Degradation of Materials (Third Edition), Third Edition. William Andrew Publishing, pp 185–206

291. Gijsman P, Fiorio R (2023) Long term thermo-oxidative degradation and stabilization of polypropylene (PP) and the implications for its recyclability. Polym Degrad Stab 208:110260. https://doi.org/https://doi.org/10.1016/j.polymdegradstab.2023.110260

292. Gupta D (2007) Antimicrobial treatments for textiles

293. Tan DH, Zhou C, Ellison CJ, et al (2010) Meltblown fibers: Influence of viscosity and elasticity on diameter distribution. J Nonnewton Fluid Mech 165:892–900. https://doi.org/https://doi.org/10.1016/j.jnnfm.2010.04.012

294. Silhavy TJ, Kahne D, Walker S (2010) The Bacterial Cell Envelope. Cold Spring Harb Perspect Biol 2:a000414–a000414. https://doi.org/10.1101/cshperspect.a000414

295. Rubekina AA, Kamzeeva PN, Alferova VA, et al (2022) Hydrophobic Rose Bengal Derivatives Exhibit Submicromolar-to-Subnanomolar Activity against Enveloped Viruses. Biomolecules 12:1609. https://doi.org/10.3390/biom12111609

296. Pereira PC de S, Costa PF do A, Pellosi DS, et al (2017) Photophysical properties and interaction studies of Rose Bengal derivatives with biomimetic systems based in micellar aqueous solutions. J Mol Liq 230:674–685. https://doi.org/10.1016/j.molliq.2017.01.055

297. Kurosu M, Mitachi K, Yang J, et al (2022) Antibacterial Activity of Pharmaceutical-Grade Rose Bengal: An Application of a Synthetic Dye in Antibacterial Therapies. Molecules 27:322. https://doi.org/10.3390/molecules27010322

298. Demartis S, Obinu A, Gavini E, et al (2021) Nanotechnology-based rose Bengal: A broad-spectrum biomedical tool. Dyes and Pigments 188:109236. https://doi.org/10.1016/j.dyepig.2021.109236

299. Martinez JD, Arrieta E, Naranjo A, et al (2021) Rose Bengal Photodynamic Antimicrobial Therapy: A Pilot Safety Study. Cornea 40:1036–1043. https://doi.org/10.1097/ICO.0000000000002717

300. Dhaini B, Wagner L, Moinard M, et al (2022) Importance of Rose Bengal Loaded with Nanoparticles for Anti-Cancer Photodynamic Therapy. Pharmaceuticals 15:1093. https://doi.org/10.3390/ph15091093

301. Karthikeyan K, Babu A, Kim S-J, et al (2011) Enhanced photodynamic efficacy and efficient delivery of Rose Bengal using nanostructured poly(amidoamine) dendrimers: potential application in photodynamic therapy of cancer. Cancer Nanotechnol 2:95–103. https://doi.org/10.1007/s12645-011-0019-3

302. Lauto A, Stoodley M, Barton M, et al (2012) Fabrication and application of rose bengal-chitosan films in laser tissue repair. Journal of Visualized Experiments 1–5. https://doi.org/10.3791/4158

303. Kumar S, Meena VK, Hazari PP, et al (2018) Rose Bengal attached and dextran coated gadolinium oxide nanoparticles for potential diagnostic imaging applications. European Journal of Pharmaceutical Sciences 117:362–370. https://doi.org/10.1016/j.ejps.2018.03.008

304. Wei D, Hamblin MR, Wang H, et al (2024) Rose Bengal diacetate-mediated antimicrobial photodynamic inactivation: potentiation by potassium iodide and acceleration of wound healing in MRSA-infected diabetic mice. BMC Microbiol 24:246. https://doi.org/10.1186/s12866-024-03401-6

305. Kurosu M, Mitachi K, Pershing E V., et al (2023) Antibacterial effect of rose bengal against colistin-resistant gram-negative bacteria. Journal of Antibiotics 76:416–424. https://doi.org/10.1038/s41429-023-00622-1

306. Flores J, Blázquez-Moraleja A, Bonet-Aracil M, et al (2023) What is the most effective percentage of Rose Bengal on polyamide fabrics for the visible-light

photoinactivation of Gram-positive bacteria? J Environ Chem Eng 11:1–11. https://doi.org/10.1016/j.jece.2023.110639

307. Gurianov Y, Meistelman M, Albo Y, et al (2022) Antibacterial Activity of Rose Bengal Entrapped in Organically Modified Silica Matrices. Int J Mol Sci 23:3716. https://doi.org/10.3390/ijms23073716

308. Li Y, Wang J, Yang Y, et al (2021) A rose bengal/graphene oxide/PVA hybrid hydrogel with enhanced mechanical properties and light-triggered antibacterial activity for wound treatment. Materials Science and Engineering C 118:111447. https://doi.org/10.1016/j.msec.2020.111447

309. Okamoto I, Miyaji H, Miyata S, et al (2021) Antibacterial and Antibiofilm Photodynamic Activities of Lysozyme-Au Nanoclusters/Rose Bengal Conjugates. ACS Omega 6:9279–9290. https://doi.org/10.1021/acsomega.1c00838

310. Naranjo A, Arboleda A, Martinez JD, et al (2019) Rose Bengal Photodynamic Antimicrobial Therapy for Patients With Progressive Infectious Keratitis: A Pilot Clinical Study. Am J Ophthalmol 208:387–396. https://doi.org/10.1016/j.ajo.2019.08.027

311. Nakonieczna J, Wolnikowska K, Ogonowska P, et al (2018) Rose bengal-mediated photoinactivation of multidrug resistant pseudomonas aeruginosa is enhanced in the presence of antimicrobial peptides. Front Microbiol 9:1–15. https://doi.org/10.3389/fmicb.2018.01949

312. Shrestha A, Hamblin MR, Kishen A (2014) Photoactivated rose bengal functionalized chitosan nanoparticles produce antibacterial/biofilm activity and stabilize dentin-collagen. Nanomedicine 10:491–501. https://doi.org/10.1016/j.nano.2013.10.010

313. Manoil D, Filieri A, Schrenzel J, Bouillaguet S (2016) Rose bengal uptake by E. faecalis and F. nucleatum and light-mediated antibacterial activity measured by flow cytometry. J Photochem Photobiol B 162:258–265. https://doi.org/10.1016/j.jphotobiol.2016.06.042

314. Usacheva MN, Teichert MC, Biel MA (2001) Comparison of the methylene blue and toluidine blue photobactericidal efficacy against gram-positive and gram-negative microorganisms. Lasers Surg Med 29:165–173. https://doi.org/10.1002/lsm.1105

Appendix A

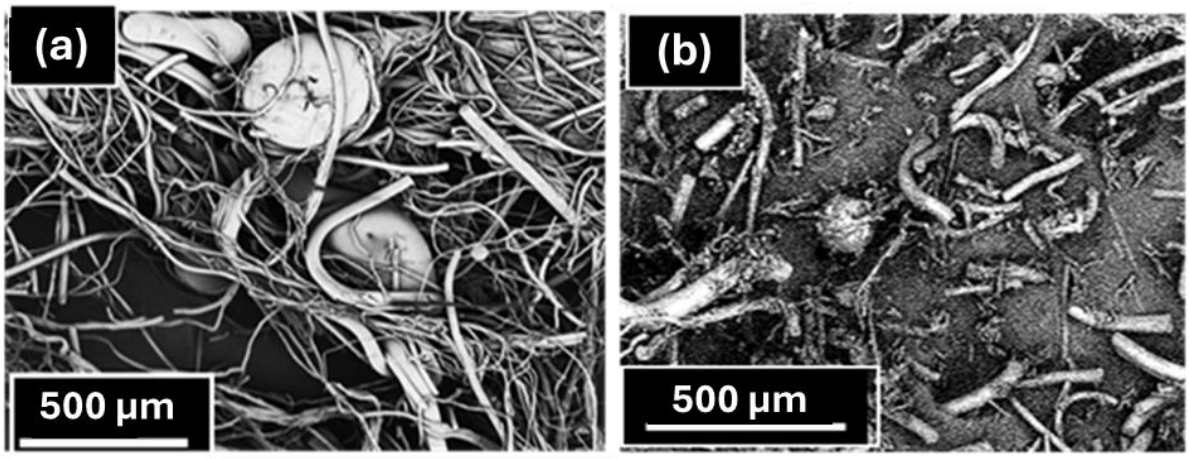
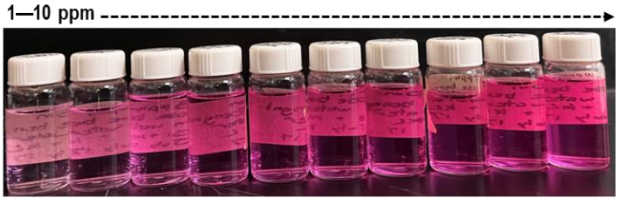
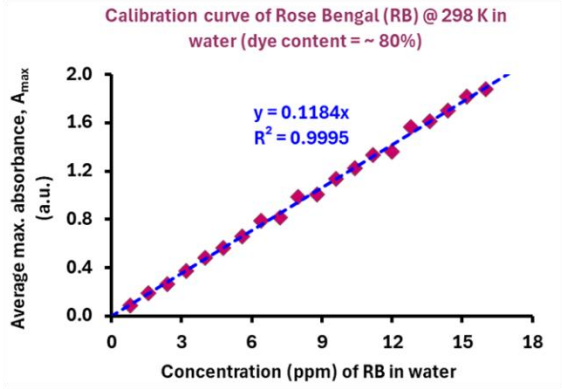
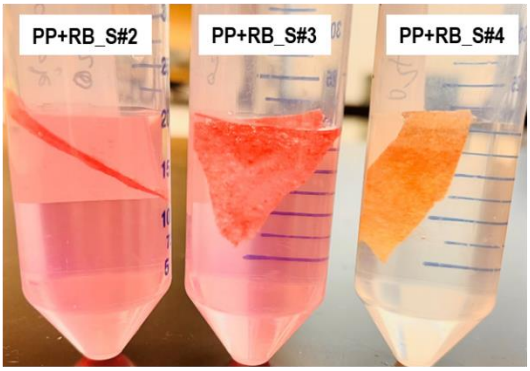


Figure A1: Reference solutions of RB (1 to 20 ppm, 80% w/w dye content) for calibration plot preparation and the constructed calibration plot (left). The leaching of RB dyes from the PP-RB fabrics at room temperature in 25 minutes of dipping in DI water without shaking and the amount of leached RB determined from the constructed calibration curve.

Appendix B







Samples dipped into DI water @ 25^{0}C

*(Image @ ~ **25 mins**; No visible difference @ 24 hrs mark.)*

Sample Name	Conc. (ppm) form calibration curve
PP+RB_S #2 (unknown)	0.30
PP+RB_S #3 (unknown)	0.37
PP+RB_S #4 (unknown)	Non-detectable!

Figure A2